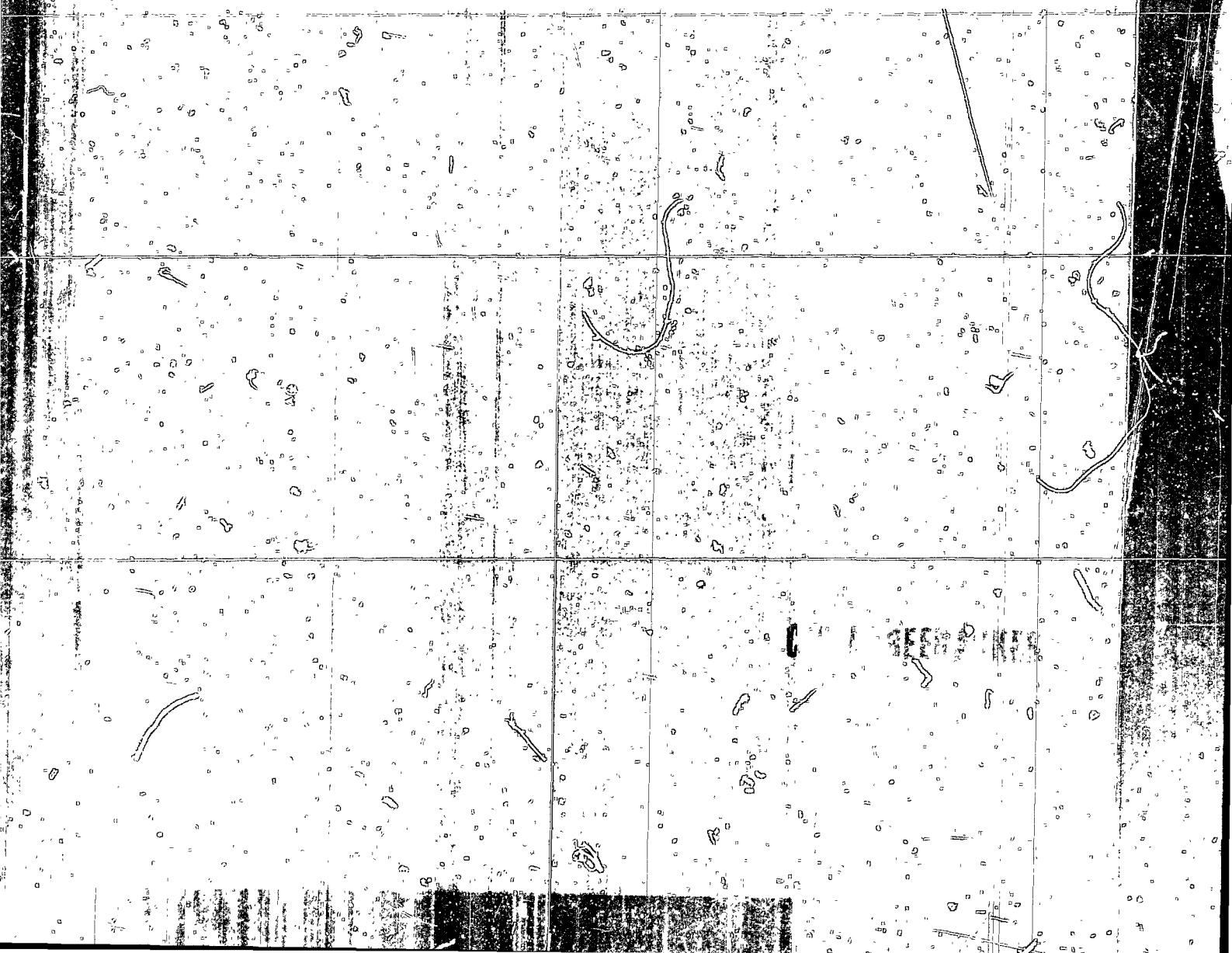


FLUORESCENCE PRODUCED BY ELECTRON IMPACT ON ALIPHATIC HYDROCARBONS, WATER AND BENZENE



**FLUORESCENCE PRODUCED BY ELECTRON
IMPACT ON ALIPHATIC HYDROCARBONS,
WATER AND BENZENE**

FLUORESCENCE PRODUCED BY ELECTRON IMPACT ON ALIPHATIC HYDROCARBONS, WATER AND BENZENE

PROEFSCHRIFT

ter verkrijging van de graad van Doctor in de
Wiskunde en Natuurwetenschappen aan de Rijks-
universiteit te Leiden, op gezag van de
Rector Magnificus Dr. A.E. Cohen, Hoogleraar
in de Faculteit der Letteren, volgens be-
sluit van het college van Dekanen te verdedi-
gen op woensdag 22 mei 1974 te klokke
14.15 uur

door

CORNELIS IGNATIUS MARIA BEENAKKER
geboren te Leiden in 1948

PROMOTOREN: PROFESSOR DR. J. KISTEMAKER
PROFESSOR DR. L.J. OOSTERHOFF

This work has been done under supervision of
Dr. F.J. de Heer

STELLINGEN

1. Uit de resultaten van de in dit proefschrift beschreven metingen kan worden afgeleid, dat 'super-aangeslagen' toestanden voornamelijk dissociëren in brokstukken, die niet electronisch aangeslagen zijn.
2. De fotochemische reactie van overgangsmetaalcarbonylen in aanwezigheid van koolstofdissulfide en trifenylfosfine is waarschijnlijk een efficiënte methode om overgangsmetaalthiocarbonylderivaten te synthetiseren.
G. Jaouen, Tetrahedron Letters 52 (1973) 5159.
3. Resonantie-fluorescentie experimenten, uitgevoerd aan benzeen bij drukken van ongeveer 0.1 Torr, zijn aan bedenkingen onderhevig.
J.M. Blondeau en M. Stockburger, Ber.Bunsenges. 75 (1971) 450.
K.G. Spears en S.A. Rice, J.Chem.Phys. 55 (1971) 5561.
4. Het vermelden van Rf waarden is nutteloos, indien de omstandigheden niet worden genoemd, waarbij de dunne-laag chromatografie is bedreven.
J.W. Meilink, Pharm.Weekblad 109 (1974) 22.

Aan mijn ouders

Aan Gemma

5. De methode van Tully et al. om uit de temperatuurafhankelijkheid van de totale werkzame doorsnede voor botsingsgeïnduceerde dissociatie de specifieke dissociatieve werkzame doorsnede voor een gegeven interne energie te berekenen is mathematisch elegant, maar fysisch niet juist.

F.P. Tully, Y.T. Lee en R.S. Berry, Chem.Phys. Letters 9 (1971) 80.

6. Bij het analyseren van de intensiteiten in emissiespectra dient men rekening te houden met het feit, dat in de theorie de intensiteit in andere eenheden wordt opgegeven dan men experimenteel bepaalt.

T

I. Kovács, Rotational Structure in the Spectra of Diatomic Molecules (Adam Hilger Ltd., London, 1969).

M. Horani, Proefschrift, Universiteit van Parijs (1967).

W. Brennen en T. Carrington, J.Chem.Phys. 46 (1967) 7.

M. Clerc en M. Schmidt, Far.Disc.Chem.Soc. 53 (1972) 217.

7. De verklaring, die W.H. Smith geeft voor het verschil in levensduur van de $\Sigma^+ - \Pi$ overgangen in CO_2^+ , CS_2^+ en N_2O^+ , is aanvechtbaar.

W.H. Smith, J.Chem.Phys. 51 (1969) 3410.

8. Het 'trapped-electron' spectrum van pyridine, zoals bepaald door Pisanias et al., is niet representatief voor dat molecuul.

M.N. Pisanias, L.G. Christophorou, J.G. Carter
en D.L. McCorkle, J.Chem.Phys. 58 (1973) 2110.

J.P. Doering en J.H. Moore, J.Chem.Phys. 56 (1972)
2176.

H.H. Brongersma, Proefschrift, Universiteit van
Leiden (1968).

9. Het bewaren van monsters bloed en urine tussen monsternamen en analyse dient zodanig te geschieden, dat de bewaartijd niet van invloed is op de uitkomsten van de analyse.

I.C. Dijkhuis en G.E.T. Ferguson, Pharm.Week-
blad 109 (1974) 48.

10. De bepaling van de snelheidsconstanten voor processen, waarbij triplet toestanden een rol spelen, door in een ontlading de intensiteit van de fluorescentie en de fosforescentie te meten is onjuist, indien geen rekening wordt gehouden met de directe aanslag van deze triplet toestanden.

M. Stockburger in Organic Molecular Photophysics,
Ed. J.B. Birks, John Wiley & Sons, London,
1973, pages 90 - 93.

Aan mijn ouders

Aan Gemma

11. Het organiseren van politieke cafés kan een belangrijke bijdrage leveren tot het verminderen van de polarisatie in de politiek.

1

Leiden, 22 mei 1974.

C.I.M. Beenakker.

Aan mijn ouders

Aan Gemma

The work described in this thesis is part of the research program of the "Stichting voor Fundamenteel Onderzoek der Materie" (Foundation for Fundamental Research on Matter) and the "Stichting Scheikundig Onderzoek in Nederland" (Netherlands Foundation for Chemical Research) and was made possible by financial support from the "Nederlandse Organisatie voor Zuiver-Wetenschappelijk Onderzoek" (Netherlands Organization for the Advancement of Pure Research).

C O N T E N T S

	page
CHAPTER I : INTRODUCTION	11
1.1. GENERAL	11
1.2. EMISSION CROSS SECTIONS	12
1.3. HIGH ENERGY ELECTRON IMPACT	13
1.4. LOW ENERGY ELECTRON IMPACT	14
CHAPTER II : EXPERIMENTAL	17
2.1. APPARATUS	17
2.1.1. General	17
2.1.2. Vacuum system	18
2.1.3. Electron source and electrode system	18
2.1.4. Optical detection system	19
2.2. EVALUATION OF THE EMISSION CROSS SECTIONS	21
2.3. EVALUATION OF THE THRESHOLDS	21
2.4. DETERMINATION OF THE QUANTUM YIELD	22
2.5. ERROR DISCUSSION	22
2.6. CHECK MEASUREMENTS	23
CHAPTER III : DISSOCIATIVE EXCITATION OF SIMPLE ALIPHATIC HYDROCARBONS	27
3.1. GENERAL INTRODUCTION	27
3.2. ACETYLENE	29
3.2.1. Spectrum	29
3.2.2. Emission of the CH radical	33
3.2.3. Emission of the C ₂ molecule	33
3.2.4. Balmer emission from the hydrogen atom	35
3.2.5. Emission from the carbon atom	35

	page
3.3. METHANE, ETHYLENE, ETHANE AND ACETYLENE	37
3.3.1. Balmer emission	37
3.3.2. Emission from excited carbon atoms	45
3.3.3. Emission from molecular fragments	46
CHAPTER IV : ANALYSIS OF THE INTENSITY DISTRIBUTION OF THE $\text{CH}(A^2\Delta - X^2\Pi)$ SPECTRUM FROM ACETYLENE	51
4.1. INTRODUCTION	51
4.2. SPECTRUM	52
4.3. EXPERIMENTAL	53
4.4. INTENSITY RELATIONS	53
4.4.1. General	53
4.4.2. Franck-Condon factors	55
4.4.3. Line-strengths	55
4.4.4. Frequencies	55
4.4.5. Distribution functions	61
4.5. RESULTS	61
4.6. DISCUSSION	66
APPENDIX	69
CHAPTER V : DISSOCIATIVE EXCITATION OF WATER	83
5.1. INTRODUCTION	83
5.2. EXPERIMENTAL	83
5.3. SPECTRUM	84
5.4. $\text{OH}(A^2\Sigma^+ - X^2\Pi)$ EMISSION	84
5.5. BALMER EMISSION	90
5.5.1. Results	90
5.5.2. Discussion	95
5.6. OXYGEN EMISSION	97
CHAPTER VI : $^1B_{2u} - ^1A_{1g}$ FLUORESCENCE FROM BENZENE I	103
6.1. INTRODUCTION	103
6.2. EXPERIMENTAL	103
6.3. FLUORESCENCE SPECTRUM	104
6.4. EMISSION CROSS SECTIONS	106

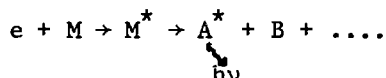
	page
CHAPTER VII : ${}^1B_{2u} - {}^1A_{1g}$ FLUORESCENCE FROM BENZENE	
II	111
7.1. INTRODUCTION	111
7.2. RESULTS	111
7.3. DISCUSSION	114
CHAPTER VIII : DISSOCIATIVE EXCITATION OF BENZENE	119
8.1. INTRODUCTION	119
8.2. BALMER EMISSION	119
8.3. $CH(A^2\Delta - X^2\Pi)$ EMISSION	124
SUMMARY	125
SAMENVATTING	127
CURRICULUM VITAE	129

CHAPTER I

I_N_T_R_O_D_U_C_T_I_O_N

1.1. GENERAL

In this thesis excitation processes caused by electron impact are described which lead to electronically excited states of isolated molecules. In particular those processes are considered which are accompanied by the emission of sufficiently intense radiation. These include radiative decay of the initially excited state and dissociation into excited fragments. The latter process is called dissociative excitation. It can be schematically represented as follows:



A study of the light emission of the fragments provides information on their electronic, vibrational and rotational energies and the cross sections for their formation. These properties are connected with the excited molecular states which are the precursors.

The molecules are excited by a beam of mono-energetic electrons of variable energy (0 - 1000 eV). In comparison with excitation by photoabsorption this method permits one to study molecular states, which can be both optically allowed and optically forbidden with respect to the ground state; also the number of states to be studied is not restricted by a lack of intense light sources emitting radiation of sufficiently high energy. However, the energy spread of the incident electrons (~ 0.5 eV) and the fact that at a given electron impact energy all states of the molecule below that energy are excited simultaneously does not always allow a unique interpretation of the results.

This study seems justified in view of the better understanding that it will give of the fundamental processes, which occur in radiation chemistry.

electric discharges and photochemistry. As a target gas we choose water, benzene and some simple aliphatic hydrocarbons: methane, ethylene, acetylene and ethane. The recent discovery of some of these molecules in the interstellar medium has also lead to the use of cross section data, as presented in this thesis, in the field of astrophysics.

1.2. EMISSION CROSS SECTIONS

The results are expressed in terms of emission cross sections (σ_{em}), which are a measure of the chance that a collision between an electron and a molecule gives rise to the emission of a particular photon. These emission cross sections, which have the dimensions of an area, are related to the excitation cross sections (σ_{exc}) of the state from which radiation is observed.

For excitation of the molecule to a discrete state n with energy E_n above the ground state and probability $\phi_1(E_n)$ that a photon of wavelength λ_1 is emitted from the molecule or fragment this relation is given by:

$$\sigma_{em}^1 = \phi_1(E_n) \sigma_{exc}^n, \quad (1)$$

where $\phi_1(E_n)$ satisfies the rule:

$$\sum_1 \phi_1(E_n) \leq 1. \quad (2)$$

For dissociative excitation the photon is emitted after excitation to a repulsive state. In that case the excitation energy E can take all values above the threshold energy E_n for fluorescence 1 of the fragment. The emission cross section is now given by:

$$\sigma_{em}^1 = \int_{E_n}^{\infty} \phi_1(E) \frac{d\sigma_{exc}(E)}{dE} dE \quad (3)$$

When the state from which the photon is emitted is also populated by cascade from higher states of the molecule a proper allowance for these processes should be made.

1.3. HIGH ENERGY ELECTRON IMPACT

The relation between high energy electron impact data and optical data is given by the Bethe theory [1]. This theory has recently been 'revisited' by Inokuti [2]. According to this theory the excitation cross section of a state n as a function of the energy of the incident electrons can be expressed in the case of optically allowed transitions as:

$$\sigma_{exc}^n = \frac{4\pi a_o^2 R}{E_{el}} M_{n,exc}^2 \ln \frac{c_{exc}^n E_{el}}{R} \quad (4)$$

where a_o is the first Bohr radius, R the Rydberg energy, E_{el} the kinetic energy of the incident electrons corrected for relativistic effects and c_{exc}^n is a constant dependent of the properties of the excited state. For excitation to a discrete state with energy E_n , $M_{n,exc}^2$ is related to the optical oscillator strength f_n by:

$$M_{n,exc}^2 = f_n R/E_n \quad (5)$$

With Formulas (1) and (4) we find for the emission cross sections at sufficiently high energies of the incident electrons:

$$\sigma_{em} = \frac{4\pi a_o^2 R}{E_{el}} M_{1,em}^2 \ln \frac{c_{em}^1 E_{el}}{R} \quad (6)$$

where

$$M_{1,em}^2 = \phi_1(E_n) f_n R/E_n \quad (7)$$

and

$$c_{em}^1 = c_{exc}^n \quad (8)$$

For excitation into a continuum $M_{n,exc}^2$ is given by:

$$M_{n,exc}^2 = \int_{E_n}^{\infty} \frac{R}{E} \frac{df(E)}{dE} dE \quad (9)$$

where $df(E)/dE$ is related to the photoabsorption cross section $\sigma_{p.a.}(E)$ by:

$$\frac{df(E)}{dE} = \frac{mc}{\pi e^2 h} \sigma_{p.a.}(E) = 9.1 \times 10^{-15} \sigma_{p.a.}(E) \quad (10)$$

if E is expressed in eV and $\sigma_{p.a.}$ in cm^2 .

By means of relations (3), (4) and (9) the emission cross section in the case of dissociative excitation can be expressed in the same form as for excitation to a discrete state (Eq. (6)), but now $M_{1,em}^2$ is given by:

$$M_{1,em}^2 = \int_{E_n}^{\infty} \phi_1(E) \frac{df(E)}{dE} \frac{R}{E} dE \quad (11)$$

and

$$M_{1,em}^2 \ln c_{em}^1 = \int_{E_n}^{\infty} \phi_1(E) \frac{df(E)}{dE} \frac{R}{E} \ln c_{exc}^n dE \quad (12)$$

For symmetry forbidden excitation processes Bethe showed that the excitation cross sections and consequently the emission cross sections are inversely proportional to the energy of the incident electrons:

$$\sigma_{em}^1 \propto E_{el}^{-1} \quad (13)$$

Plotting $\sigma_{em}^1 E_{el} / 4\pi a_0^2 R$ versus $\ln E_{el}$ - a so-called Fano plot [3] - will give a straight line at sufficiently high energies with a positive slope in the case of an optically allowed excitation process. From the slope of the Fano plot we derive $M_{1,em}^2$, whereas the intercept with the abscissa of the extrapolated linear portion gives c_{em}^1 . For optically allowed excitation processes we have $c_{em}^1 \sim 1$ and $M_{1,em}^2 > 0$. A horizontal line in the Fano plot will be found in the case of a symmetry forbidden excitation process. We then find $c_{em}^1 \gg 1$ and $M_{1,em}^2 = 0$. If both optically allowed and symmetry forbidden processes give rise to the emission of the photon 1, we obtain $c_{em}^1 \gg 1$ and $M_{1,em}^2 > 0$.

In this work the values of $M_{1,em}^2$ and c_{em}^1 are determined by a least squares analysis.

1.4. LOW ENERGY ELECTRON IMPACT

Thresholds for emission can be determined by varying the energy of the incident electrons from zero to higher energies. These measurements give the excitation energy E_n of the excited state from which the radiation occurs.

In the case of dissociative excitation the knowledge of the threshold for formation of a particular fragment and relevant excitation and dissociation energies permits one to deduce the processes, which occur at the threshold. Frequently it turns out that fragments are formed from neutral states of the parent molecule above the first ionization potential. These neutral states are called, following Platzman [4], super-excited states.

At low impact energies electron exchange processes are relatively important. They can give rise to excited states of the molecule, which have a spin multiplicity different from that of the ground state (see for instance Ref. (5), (6) and (7)). These processes are characterized by a steep increase of the excitation cross section above the threshold, followed by a sharp decrease [8,9]. In view of the proportionality of excitation cross sections and emission cross sections a study of the energy dependence of the emission cross section at low energies may therefore give information about the spin multiplicity of the molecular state from which the emitted photon originates.

REFERENCES

- [1] H.A. Bethe, Ann.Physik 5 (1930) 325.
- [2] M. Inokuti, Rev.Mod.Phys. 43 (1971) 297.
- [3] U. Fano, Phys.Rev. 95 (1954) 1198.
- [4] R.L. Platzman, The Vortex 23 (1962) 372.
- [5] R.N. Compton, R.H. Huebner, P.W. Reinhardt and L.G. Christophorou, J.Chem.Phys. 48 (1968) 901.
- [6] H.H. Brongersma, Thesis, University of Leiden (1968).
- [7] F.W.E. Knoop, Thesis, University of Leiden (1972).
- [8] J.F.M. Aarts and F.J. de Heer, Chem.Phys.Letters 4 (1969) 116.
- [9] V.I. Ochkur, Soviet Phys. JETP 18 (1964) 503.

CHAPTER II

E X P E R I M E N T A L

2.1. APPARATUS

2.1.1. General

The apparatus is shown schematically in Fig. 2.1. It consists of a vacuum chamber containing an electron gun, and of a collision chamber. The electron beam is collimated by an axial magnetic field (~ 300 Gauss) and enters the collision chamber through a collimator consisting of two diaphragms. In the vacuum system the collision chamber and electron gun are also connected by a by-pass. The intensity of the beam is measured at a Faraday cage. The energy of the electrons can be varied between 0 and 1000 eV, while the intensity of the beam is usually kept below 100 μ A.

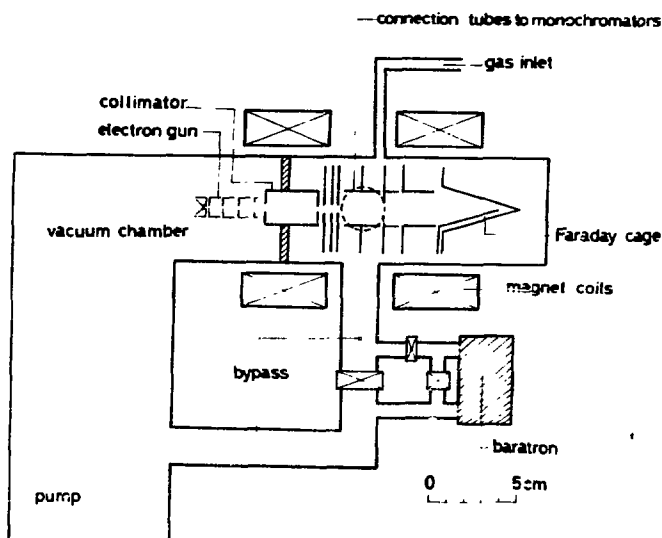


FIGURE 2.1. Schematic representation of the apparatus.

The target gas is admitted into the collision chamber by a variable leak, such that the pressure is in the range 10^{-4} - 10^{-3} Torr. The density of the target gas is measured by a capacitance manometer. The light emission from the target gas is detected at right angles to the electron beam by two monochromators covering the wavelength region 1850 - 9000 Å. These monochromators are positioned at both sides of the collision chamber.

This apparatus was originally designed for measurements below 100 eV electron impact energy [1]. The extension of the measurements to 1000 eV, the introduction of another technique for the determination of the threshold and some special precautions for the measurement of heavier organic molecules lead us to describe the apparatus in some detail.

2.1.2. Vacuum system

With the by-pass valve in open position, the entire system is evacuated by an oil diffusion pump (Edwards EO4), which has a nominal pumping speed of 600 l/sec. This pump is coupled to a rotary pump by a molecular sieve. An ultimate pressure of about 5×10^{-7} Torr is obtained in the system.

During the measurements the by-pass valve is closed. The collision chamber is then pumped through the collimator body, gas flow being about 0.3 l/sec for air. Next the target gas is introduced into the collision chamber by an all-metal variable leak (Vacuum Generator MD6 or Granville Phillips 203). By this differential pumping system the pressure near the electron gun can be kept below 10^{-6} Torr, whereas the pressure of the target gas measured with a capacitance manometer (MKS Baratron, pressure head 77H-1) is between 10^{-4} and 10^{-3} Torr.

A liquid nitrogen baffle, placed between the diffusion pump and the vacuum chamber, is used in the case of measurements on vapours, which strongly affect the filament of the electron gun.

2.1.3. Electron source and electrode system

For the measurements of the thresholds the electrons are produced by a Philips 6-AW-59 television tube with an oxide cathode. The energy spread of the electrons is about 0.3 eV. The other measurements are performed with a Philips DC-7-32 electron gun in which the oxide cathode is

replaced by a Rhenium filament. This filament has a much longer lifetime in the presence of organic vapours, but the source has a larger energy spread (~ 2 eV).

The electrode system of the collision chamber is shown in Fig. 2.2. The Faraday cage consists of two parts. The total current on the two plates is measured (see also Section 2.6). The energy of the electrons in the viewing region of the monochromators is determined by the negative potential of the oxide cathode (or filament as is the case) with respect to that region. It can be varied between 0 and 1000 eV.

2.1.4. Optical detection system

The light emission in the 1850 - 5500 Å region is detected by a Leiss [2] monochromator, fitted with a grating of 2160 grooves per mm (reciprocal dispersion 15 Å/mm) blazed at 2000 Å, and an EMI 6256S photomultiplier. The grating and mirrors have been coated with magnesium fluoride in order to obtain a high reflectance below 2300 Å. For the region 5500 - 9000 Å we used a Leiss monochromator with a grating of 1200 grooves per mm (reciprocal dispersion 27 Å/mm) blazed at 7500 Å and an RCA 31034 A photomultiplier. Both photomultipliers are thermoelectrically cooled to below -15°C .

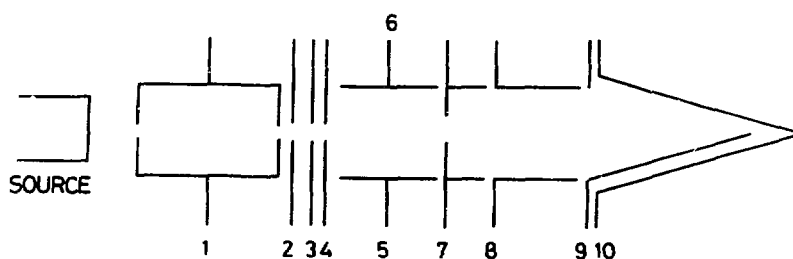


FIGURE 2.2. Cross section of the electrode system parallel to the electron beam. The source is put at the acceleration voltage. The following potentials were applied: 1, collimator : 20 V; 2 : 10 V; 3, 4, 5, 6, 7 and 8 : 0 V; 9 : 30 - 150 V; 10 : 70 - 300 V.

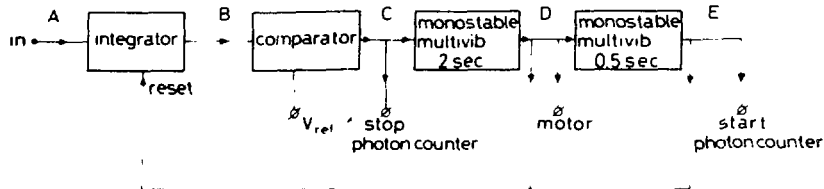


FIGURE 2.3. Block diagram of the circuit used for threshold measurements.

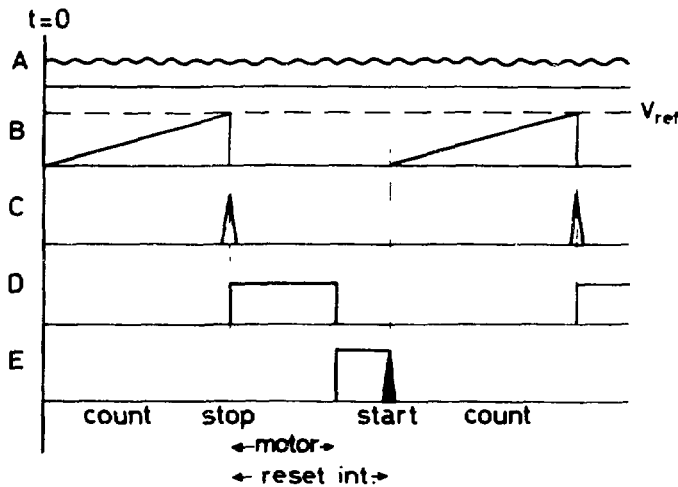


FIGURE 2.4. Time diagram of the system used for threshold measurements. A : electron beam; B : current integrator; C : stop pulse to photon counter; D : motor, coupled to acceleration voltage; E : start pulse to photon counter.

After preamplification and discrimination against dark current counts, the photon pulses are converted to standard height and width and fed into a dual counter (SSR model 1110 Digital Synchronous Computer).

2.2. EVALUATION OF THE EMISSION CROSS SECTIONS

The emission cross sections are evaluated by the relation:

$$\sigma_{em} = \frac{4\pi}{\omega} \frac{S(\omega)}{(I/e) N L k(\lambda)} P$$

In this formula $S(\omega)$ represents the light intensity measured in the solid angle ω , I/e is the number of electrons passing per second through the collision chamber, N is the density of the target gas, L is the observation length along the electron beam and $k(\lambda)$ is the quantum yield of the optical equipment at a wavelength λ . The polarization factor P is a correction factor for the cross section, which accounts for an anisotropic distribution of the emitted radiation and for a different sensitivity of the monochromator for the polarized components of the radiation. The degree of polarization is generally found to be small both for molecular radiation and for radiation from dissociative excitation [1,3,4]. We therefore put $P=1$.

2.3. EVALUATION OF THE THRESHOLDS

Thresholds are determined by a method schematically shown in Figs. 2.3 and 2.4. The electron beam, which is chopped with a frequency of about 70 Hz, is fed into a current integrator. The resulting chopped light signal is measured by the dual photon counter (SSR), which automatically subtracts the dark current signal from the light signal. At a given acceleration voltage the photon counter and the current integrator are started simultaneously. The photon counter is stopped after collection of a certain amount of charge on the Faraday cage. Next a motor, which is coupled to a helipot, runs for two seconds with an adjustable speed changing the acceleration voltage. Thereafter, the cycle is repeated. The photon counts are plotted on an X-Y recorder as a function of the acceleration voltage.

The energy scale is calibrated by simultaneous introduction of the

target gas and a gas which gives radiation of known threshold energy into the collision chamber by two variable leaks. In most cases the $4^3S - 2^3P$ transition of helium with a known threshold at 23.5 eV [5] is used for calibration. In order to avoid space charge effects currents below 10 μA are used. The accuracy of the threshold measurements is limited by the energy spread of the incident electrons (~ 0.3 eV).

2.4. DETERMINATION OF THE QUANTUM YIELD

For the determination of the quantum yield of the optical equipment we made use of a tungsten ribbon lamp as a standard light source. The intensity of the radiation emitted by the tungsten ribbon has been measured as a function of ribbon temperature and wavelength by De Vos [6]. The calibration procedure with this standard has been described in Ref. 7. Below 3000 Å this standard cannot be used because of the sharp decrease of the emission by the hot tungsten filament towards lower wavelength and the relative increase of scattered light. In the wavelength region 1850 - 3000 Å the relative yield as a function of wavelength was determined by means of a deuterium lamp [8] (1850 - 2700 Å) and a quartz-iodine lamp with a coiled-coil tungsten filament [9] (2500 - 4400 Å). This was fitted to an absolute scale by normalization to the quantum yield determined by the tungsten standard.

2.5. ERROR DISCUSSION

The reproducibility of the results is connected to random errors in the measurement of the pressure (3%), the electron beam intensity (2%) and the light signal (1%).

The main systematic error results from the absolute intensity calibration of the monochromators. This error depends on the wavelength and ranges from 10% at 3000 Å to 4% at 9000 Å [7]. Below 3000 Å an iodine lamp and a deuterium lamp are used for the calibration of the relative quantum yield. The systematic errors made by this method are more difficult to evaluate. However, branching ratios for the $B^2\Sigma^+ - X^2\Sigma^+$ system of CO^+ (2100 - 2600 Å), determined experimentally with a deuterium lamp, are within 15% of the theoretically calculated ratios

using Franck-Condon factors [10]. This puts an upper limit of 15% to the error in the relative quantum yield. Together with errors due to normalization we estimate the probable error in the absolute quantum yield below 3000 Å to be 20%. Additional systematic errors occur in the measurement of the electron beam current (2%) and in the determination of the geometrical factors ω and L (2%). The neglect of polarization effects introduces an error probably smaller than 5%. The systematic error in the pressure, determined by the Baratron, is estimated to be 2%. This capacitance manometer has been calibrated against a McLeod manometer, described in Ref. 11. These give probable errors in the emission cross sections ranging from 22% at short wavelengths to 8% at longer wavelengths.

The maximum slit width of our monochromators (3 mm) defines the wavelength region, which can be observed at a fixed position of the grating. In the case of extensive molecular bands we divide the relevant wavelength region into parts. The intensity of the radiation in each part is measured. The emission cross section is determined by adding up the intensities of the different parts. This procedure gives an extra uncertainty of 5%. Larger random errors come into the emission cross sections for weak light signals.

2.6. CHECK MEASUREMENTS

At high energies of the incident electrons errors in the emission cross sections may arise from electrons, which are reflected at the Faraday cage. These give rise to too high apparent emission cross sections. In order to avoid the effect of reflected and secondary electrons we make use of a Faraday cage consisting of two conical parts (Fig. 2.2). At an acceleration voltage of 1000 eV we found the detected electron beam current to be essentially constant, when on the outer plate of the conical detector a voltage larger than 250 V and on the inner plate half this voltage is applied (Fig. 2.5). Under this condition we also checked the dependence of the detected electron beam current on the strength of the magnetic field, used to collimate the beam. No dependence was found within 2%.

To check the apparatus we measured the energy dependence of the

emission cross sections for various systems and compared these with measurements of Aarts *et al.*, performed on an apparatus especially suited for measurements at high electron impact energies. We checked on the following systems: $N_2^+(B^2\Sigma_u^+ - X^2\Sigma_g^+)$, $CO^+(B^2\Sigma^+ - X^2\Sigma^+)$, $CH(A^2\Delta - X^2\Pi)$ from methane and the Balmer series of H from methane. Within an average of 2% we found for these the same energy dependence as measured previously [10,12,13].

Partially as a check on the quantum yield of the optical equipment we compared absolute emission cross sections at 100 eV for $N_2^+(B^2\Sigma_u^+ - X^2\Sigma_g^+, 0-0)$ and $CO^+(B^2\Sigma^+ - X^2\Sigma^+, 0-0)$ transitions with previous measurements. We found the emission cross sections to be respectively 4% and 15% larger than the published results [10,13].

During the course of this investigation the reproducibility of the quantum yield was checked repeatedly.

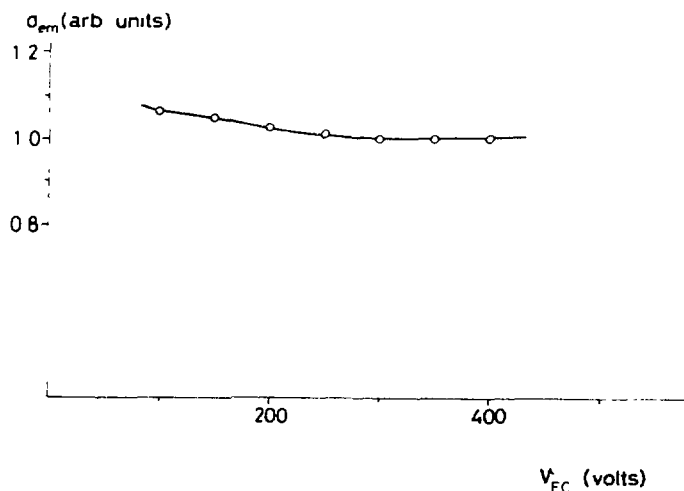


FIGURE 2.5. Dependence of the apparent emission cross section at 1000 eV electron impact energy on the voltage of the outer plate of the Faraday cage. The voltage of the inner plate is half of this.

REFERENCES

- [1] J.F.M. Aarts, Thesis, University of Leiden (1970).
- [2] J. Schutten, P.J. van Deenen, E. de Haas and F.J. de Heer, J.Sci. Instr. 44 (1967) 153.
- [3] R.J. van Brunt and R.N. Zare, J.Chem.Phys. 48 (1968) 4304.
- [4] D.A. Vroom and F.J. de Heer, J.Chem.Phys. 50 (1969) 573.
- [5] C.E. Moore, A Multiplet Table of Astrophysical Interest (Observatory, Princeton, 1945).
- [6] J.C. de Vos, Thesis, University of Amsterdam (1953).
- [7] J. van den Bos, Thesis, University of Amsterdam (1967).
J. van den Bos, G.J. Winter and F.J. de Heer, Physica 40 (1968) 357.
- [8] E. Pitz, Appl.Optics 8 (1969) 255;
W. Böhm, D. Labs, D. Lemke and E. Pitz, Forschungsbericht W 6909, 1969, Bundesministerium für wissenschaftliche Forschung.
- [9] R. Stair, W.E. Schneider and J.K. Jackson, Appl.Optics 2 (1963) 1151.
- [10] J.F.M. Aarts and F.J. de Heer, Physica 49 (1970) 425.
- [11] J. Politiek, Thesis, University of Amsterdam (1970).
- [12] J.F.M. Aarts, C.I.M. Beenakker and F.J. de Heer, Physica 53 (1971) 32.
- [13] J.F.M. Aarts, F.J. de Heer and D.A. Vroom, Physica 40 (1968) 197.

CHAPTER III

D I S S O C I A T I V E E X C I T A T I O N O F S I M P L E A L I P H A T I C H Y D R O C A R B O N S .

3.1. GENERAL INTRODUCTION

Excitation of molecules to states with sufficiently high energy may result in the formation of excited fragments, whose light emission can be studied. A relatively simple method to bring molecules into these states is the excitation by electron impact. This technique is usually applied as a tool to produce fragments in excited states, whose spectral characteristics can then be determined.

Only a few systematic studies on the light emission produced by electron impact on aliphatic hydrocarbons have appeared. Of them the work of Vroom and de Heer [1], who obtained emission cross sections of excited hydrogen atoms from methane, ethylene and ethane, can be mentioned. Sroka [2] studied the light emission from fragments from methane in the vacuum-ultraviolet (900 - 1700 Å). Aarts *et al.* [3] measured the light emission of fragments from methane and ethylene in the wavelength region 1000 - 10000 Å. Balmer emission from propane has been investigated by Kurepa *et al.* [4].

A striking similarity between the results for the measured molecules appears from these studies. The formation of excited hydrogen atoms proceeds via molecular states, which are optically forbidden with respect to the ground state, and the emission cross sections are about the same for all hydrocarbons. Also, no large differences are seen between the cross section data of $\text{CH}(A^2\Delta)$ from methane and ethylene [3], a fragment that is formed via molecular states, which are optically allowed with respect to the ground state.

In Section 3.2. we present measurements on the dissociative excitation of acetylene. These are compared with electron impact data on methane, ethylene and ethane in Section 3.3. A mechanism for the formation of excited hydrogen atoms is also discussed in Section 3.3.

TABLE 3.1.

Emission observed by electron impact on acetylene.		
$\lambda(\text{\AA})$	Transition	Name
1931	$\text{CI } 3s \ ^1P^o \rightarrow 2p^2 \ ^1D$	Mulliken system
2325	$\text{C}_2 \ D^1\Sigma_u^+ \rightarrow X^1\Sigma_g^+$	
2479	$\text{CI } 3s \ ^1P^o \rightarrow 2p^2 \ ^1S$	
3143	$\text{CH } C^2\Sigma^+ \rightarrow X^2\Pi$	3100 \AA system
	$\text{CH}^+ \ ^1\Delta \rightarrow ^1\Pi$	
	$\text{CH}^+ \ ^3\Sigma \rightarrow ^3\Pi$	
	$\text{C}_2 \ C^1\Pi_g \rightarrow A^1\Pi_u$	Deslandres-D'Azambuja system
3900	$\text{CH } B^2\Sigma^- \rightarrow X^2\Pi$	
3900		3900 \AA system
3970	$\text{H } n=7 \rightarrow n=2$	Balmer ϵ
4101	$\text{H } n=6 \rightarrow n=2$	Balmer δ
4314	$\text{CH } A^2\Delta \rightarrow X^2\Pi$	4300 \AA system
4340	$\text{H } n=5 \rightarrow n=3$	Balmer γ
	$\text{C}_2 \ d^3\Pi_g \rightarrow a^3\Pi_u$	Swan system
4861	$\text{H } n=4 \rightarrow n=2$	
4861		Balmer β
6563	$\text{H } n=3 \rightarrow n=2$	Balmer α

3.2. ACETYLENE

3.2.1. Spectrum

In the emission spectrum between 1850 and 9000 Å, obtained by electron impact on acetylene, radiation due to various fragments could be identified (Table 3.1) [5,6,7]. For reasons of intensity and overlap of band systems the threshold and cross section measurements were confined to CI radiation, the Balmer series of hydrogen, the Mulliken system of C_2 and the 4300 Å system of CH. In the case of the 3100 Å system of CH an estimate of the emission cross section could be given.

3.2.2. Emission of the CH radical

Radiation is observed from CH in the three lowest excited doublet states $A^2\Delta$, $B^2\Sigma^-$ and $C^2\Sigma^+$, which decay by radiation only to the $X^2\Pi$ ground state. The $A^2\Delta - X^2\Pi$ emission shows its presence by intense bands in the 4150 - 4400 Å region, which are attributed to the 0-0, 1-1 and 2-2 vibrational transitions [5]. In this experiment we did not observe emission from other vibrational transitions. Calculations on Franck-Condon factors [8] show that these contribute less than 1% to the total $A^2\Delta - X^2\Pi$ emission. Cascade from higher states to the $A^2\Delta$ state has not been found [9]. The emission cross section, evaluated from the light signal between 4150 and 4400 Å, is therefore equal to the cross section for formation of CH in the $A^2\Delta$ state.

The emission cross sections have been determined by means of the same procedure as described in Ref. 3. This procedure excludes errors in the emission cross section by possible contamination from other excited species like CH^+ and H, which also radiate in the 4150 - 4400 Å region. The $CH(A^2\Delta - X^2\Pi)$ emission cross sections are collected in Table 3.2. The error in them is estimated to be 12% (see Section 2.5.).

In Fig. 3.1 the emission cross sections are presented in a Fano plot (see Section 1.3). From the straight line portion follows $M_{em}^2 = 0.049$ and $c_{em} = 1.25$. This low value of c_{em} and the positive slope indicate that optically allowed excitation processes are of major importance in the formation of $CH(A^2\Delta)$. Emission cross sections for $CH(A^2\Delta - X^2\Pi)$ radiation for proton impact on acetylene have been measured by Carré [10]. In the

TABLE 3.2.

Emission cross sections in units of 10^{-19} cm^2 for electron impact on acetylene.				
$E_{\text{el}} (\text{eV})$	CI $1P^o \rightarrow 1S$ 1931 Å	H $n=4 \rightarrow 2$ 4861 Å	CH $A^2\Delta \rightarrow X^2\Pi$ 4300 Å	$C_2 D^1\Sigma_u^+ \rightarrow X^1\Sigma_g^+$ 2325 Å
20	-	-	30.5	1.07
40	4.35	3.20	44.4	1.33
60	8.43	5.71	49.4	1.67
80	10.0	6.45	48.8	1.65
100	10.3	6.68	46.6	1.55
120	10.1	6.34	43.8	1.44
140	9.31	5.74	40.6	1.35
170	8.23	5.03	37.1	1.22
200	7.34	4.64	34.2	1.10
250	5.90	3.67	29.8	0.932
300	5.04	3.05	25.7	0.826
350	4.28	2.67	22.9	0.708
400	3.73	2.38	20.9	0.642
450	3.25	2.09	19.0	0.594
500	2.99	1.81	17.8	0.541
600	2.50	1.52	15.6	0.470
700	2.17	1.30	13.7	0.409
800	1.83	1.09	12.3	0.381
900	1.66	1.02	11.5	0.336
1000	1.44	0.908	10.7	0.304
M_{em}^2 *			0.049±0.002	0.00114±0.00005
c_{em}			1.25	3.97

* errors refer to standard deviation in slope only.

theory of Bethe [11,12] these should become equal to the electron impact cross sections at sufficiently high and equal velocities of the incident particles. A direct comparison between electron and proton impact can therefore be made by scaling the proton energies by the ratio of the electron and proton rest masses. Figure 3.1 shows that, within the framework of the Bethe theory, the agreement between the proton impact data of Carré [10] and the present electron impact data is rather poor. This has also been shown to be the case for $\text{CH}(A^2\Delta - X^2\Pi)$ emission from methane and ethylene [3].

The $\text{B}^2\Sigma^- - \text{X}^2\Pi$ and $\text{C}^2\Sigma^+ - \text{X}^2\Pi$ band systems of CH are contaminated by radiation from background gas in the collision chamber, namely by the first negative band system of $\text{N}_2(\text{B}^2\Sigma_u^+ - \text{X}^2\Sigma_g^+)$ and by the second positive group of $\text{N}_2(\text{C}^3\Pi_u - \text{B}^3\Pi_g)$. For that reason the B - X emission cross sections of CH could not be measured. In the case of C - X emission the contribution of nitrogen radiation to the total light signal at 100 eV could be estimated from the light signal at 14 eV, at which energy the

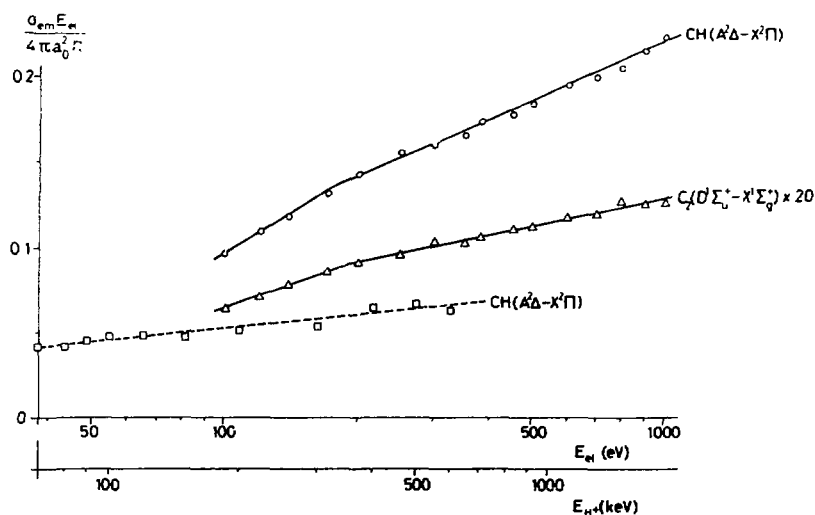


FIGURE 3.1. Emission cross sections for CH and C_2 radiation presented in the form of a Fano plot for electron and proton impact on acetylene; solid lines refer to electrons; dashed line refers to protons [10]. The emission cross sections for C_2 radiation have been multiplied by 20.

TABLE 3.3.

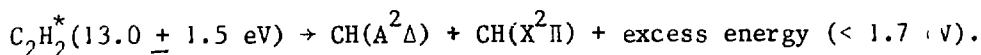
Calculated minimum energies ^{a,b} for formation of excited fragments by dissociative excitation of acetylene.		
	Dissociation products	E(eV)
C_2H_2	$\rightarrow CH(A^2\Delta) + CH(X^2\Pi)$	12.8
	$\rightarrow CH(A^2\Delta) + CH(A^2\Delta)$	15.7
	$\rightarrow CH(A^2\Delta) + C(^3P) + H(n=1)$	16.2
	$\rightarrow CH(A^2\Delta) + CH^+(X^1\Sigma^+)$	23.9
	$\rightarrow C_2(d^3\Pi_g) + H_2(X^1\Sigma_g^+)$	8.6
	$\rightarrow C_2(d^3\Pi_g) + H(n=1) + H(n=1)$	13.1
	$\rightarrow C_2(C^1\Pi_g) + H_2(X^1\Sigma_g^+)$	10.4
	$\rightarrow C_2(C^1\Pi_g) + H(n=1) + H(n=1)$	14.9
	$\rightarrow C_2(D^1\Sigma_u^+) + H_2(X^1\Sigma_g^+)$	11.5
	$\rightarrow C_2(D^1\Sigma_u^+) + H(n=1) + H(n=1)$	16.0
	$\rightarrow C_2H(\tilde{X}) + H(n=4)$	18.1
	$\rightarrow C_2(X^1\Sigma_g^+) + H(n=1) + H(n=4)$	23.3
	$\rightarrow C_2H^+(\tilde{X}) + H(n=4)$	30.0
	$\rightarrow C(^1P) + C(^3P) + H_2(X^1\Sigma_g^+)$	20.0
	$\rightarrow C(^1P) + CH(X^2\Pi) + H(n=1)$	21.0
	$\rightarrow C(^1P) + C(^3P) + H(n=1) + H(n=1)$	24.5

^a $D(HC-CH)=9.89$ eV [19], $D(C-H)=3.47$ eV [20], $D(C-C)=6.2\pm0.2$ eV [7],
 $D(H-H)=4.48$ eV [20], $D(HCC-H)=5.38\pm0.05$ eV [21], $IP(CH)=11.1$ eV [20],
 $IP(C_2H)=11.96\pm0.05$ eV [21].

^b Excitation energies have been taken from Refs. 7, 22 and 23.

radiation can only be due to the strong emission of the second positive group of nitrogen, and from the ratio of the emission cross sections for the second positive group at 14 eV and at 100 eV [13]. We determined $\sigma_{\text{em}}(\text{CH}, \text{C}^2\Sigma^+ - \text{X}^2\Pi) = (8.9 \pm 4.5) \times 10^{-20} \text{ cm}^2$ at 100 eV. Hence $\sigma_{\text{em}}(\text{C} - \text{X})/\sigma_{\text{em}}(\text{A} - \text{X}) = 0.02 \pm 0.01$. Carré [10] found for this ratio 0.01. His value could be more accurate, because in the case of proton impact triplet states cannot be excited when the effect of secondary electrons is avoided. Consequently radiation from the second positive group of nitrogen may not be present.

The energy dependence of $\sigma_{\text{em}}(\text{A}^2\Delta - \text{X}^2\Pi)$ below 100 eV is depicted in Fig. 3.2. The threshold for $\text{CH}(\text{A}^2\Delta)$ radiation is found at 13.0 ± 1.5 eV. Another onset is observed at 32.5 ± 1.5 eV. Table 3.3 shows minimum excitation energies for formation of excited fragments formed by dissociative excitation of acetylene, calculated from known dissociation energies and excitation energies of the fragments. It follows from a comparison of the observed threshold and the calculated energies, that, near threshold, $\text{CH}(\text{A}^2\Delta)$ is formed by:



This excess energy is released as internal and kinetic energy of the fragments. From the energy balance it follows that at the first observed threshold for $\text{CH}(\text{A}^2\Delta)$ the second fragment cannot be an ion (Table 3.3). This indicates that these fragments are formed via super-excited states of acetylene (see Section 1.4). At the second threshold $\text{CH}(\text{A}^2\Delta)$ can also be formed from ion states.

3.2.3. Emission of the C_2 molecule

Electron impact on acetylene produces the Swan, Deslandres-d'Azambuja and Mulliken systems of C_2 . These systems correspond respectively to the $d^3\Pi_g - a^3\Pi_u$, $\text{C}^1\Pi_g - \text{A}^1\Pi_u$ and $\text{D}^1\Sigma_u^+ - \text{X}^1\Sigma_g^+$ transitions. The emission cross sections for Mulliken radiation are collected in Table 3.2. The error in σ_{em} is estimated to be 25%. Since cascade from higher states to the D state has not been observed and only emission from this state to the ground state is known [7], the cross section for C_2 Mulliken radiation is equal to the cross section for formation of C_2 in the $\text{D}^1\Sigma_u^+$ state by dissociative excitation of acetylene. In Fig. 3.1 these cross sections are presented in

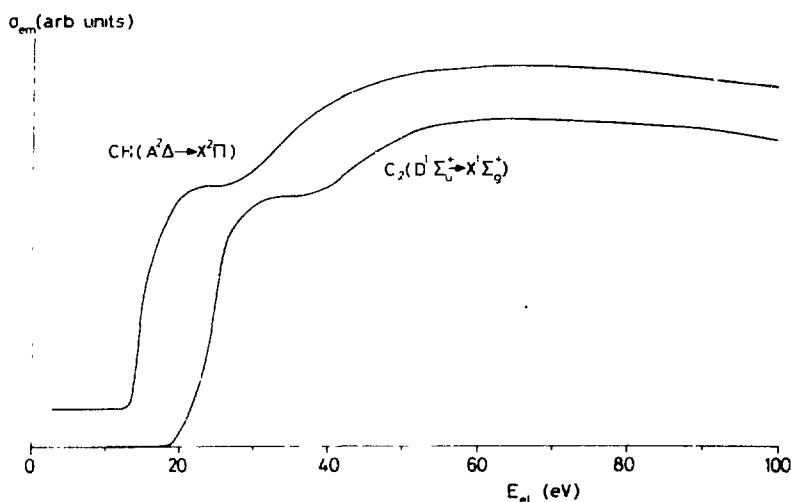
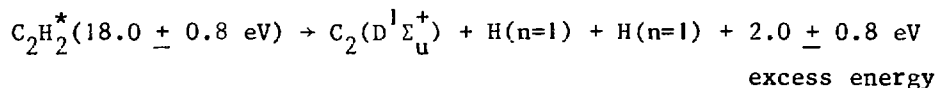
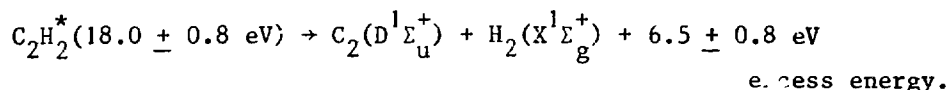


FIGURE 3.2. Energy dependence below 100 eV of the emission cross sections for CH and C_2 radiation for electron impact on acetylene. The ordinate of the $CH(A^2\Delta - X^2\Pi)$ emission cross section is displaced to avoid confusion.

the form of a Fano plot. From the slope and the intercept of this plot one derives $M_{em}^2 = 0.00114$ and $c_{em} = 3.97$ respectively. This indicates that $C_2(D^1\Sigma_u^+)$, like $CH(A^2\Delta)$, is produced mainly by an optically allowed excitation process or processes. The energy dependence of the emission cross sections below 100 eV is depicted in Fig. 3.2. The threshold is found at 18.0 ± 0.8 eV. It follows from a comparison with Table 3.3 that part of the radiation is formed by the process(es):



and/or



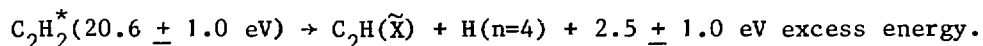
A second onset for Mulliken radiation is observed at 33.5 ± 1.5 eV. At this energy various processes can be operative in the formation of $C_2(D^1\Sigma_u^+)$.

3.2.4. Balmer emission from the hydrogen atom

One of the stronger features in the emission spectrum obtained by electron impact on acetylene is the Balmer series of hydrogen. The emission cross sections for Balmer β radiation are presented in Table 3.2 and in the form of a Fano plot in Fig. 3.3. The same energy dependence is found for Balmer α , γ and δ radiation within 4%. We therefore give for these Balmer lines only the emission cross sections at 100 eV (Table 3.4). Due to the weak light signal, the emission cross section for Balmer ϵ radiation could only be measured at 100 eV. The accuracy of the emission cross sections has been discussed in Section 2.5. It is estimated to be 10% for Balmer γ , γ and δ radiation and 20% for Balmer α and ϵ radiation. For the Balmer δ line an additional error of 10% may arise from contamination with C_2 radiation.

In Fig. 3.3 we also compare our Balmer β data with proton impact data of Carré [10]. As is the case for CH radiation and Balmer β radiation from methane and ethylene [3] the agreement is rather poor. In the asymptotic region the electron impact cross sections are 46% higher than the proton impact cross sections. This is within the stated errors, which are 10% in this experiment and 40% in that of Carré. In addition to Balmer β radiation Carré measured also Balmer γ radiation. The ratio of the emission cross sections of these two lines is 0.34 in agreement with our value of 0.36.

The low energy cross section data for Balmer β radiation are shown in Fig. 3.4. The threshold for production of $H(n=4)$ from acetylene is found at 20.6 ± 1 eV. From Table 3.3 then follows that near threshold $H(n=4)$ is formed by the process:



Because of the absence of structure in the energy dependence of the emission cross sections near threshold (Fig. 3.4) and the zero or nearly zero slope in the Fano plot (Fig. 3.3) we conclude that one or only a few optically forbidden processes are relevant in the formation of excited hydrogen atoms.

3.2.5. Emission from the carbon atom

At 1931 Å and 2479 Å we observed CI emission from the $3s \ ^1P^o$ state to the $2p^2 \ ^1D$ and the $2p^2 \ ^1S$ states respectively. The same energy dependence

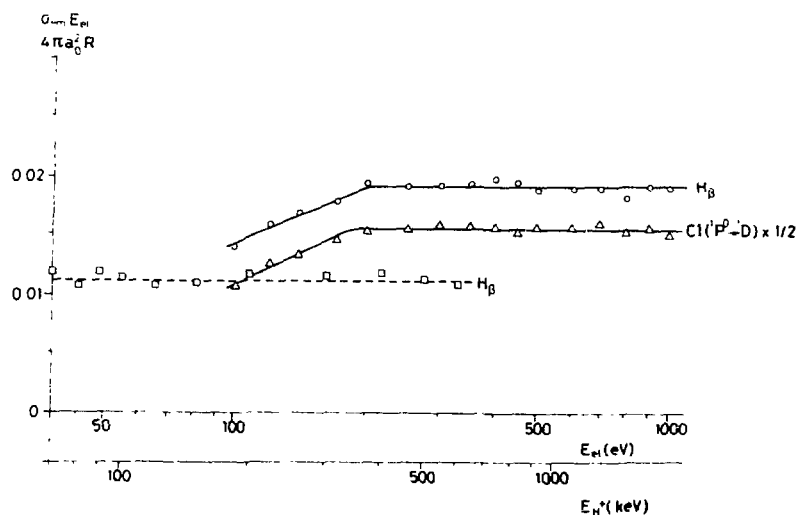


FIGURE 3.3. Emission cross sections for H Balmer β and CI radiation presented in the form of a Fano plot for electron and proton impact on acetylene; solid lines refer to electrons; dashed line refers to protons [10]. The emission cross sections for carbon radiation have been multiplied by 1/2.

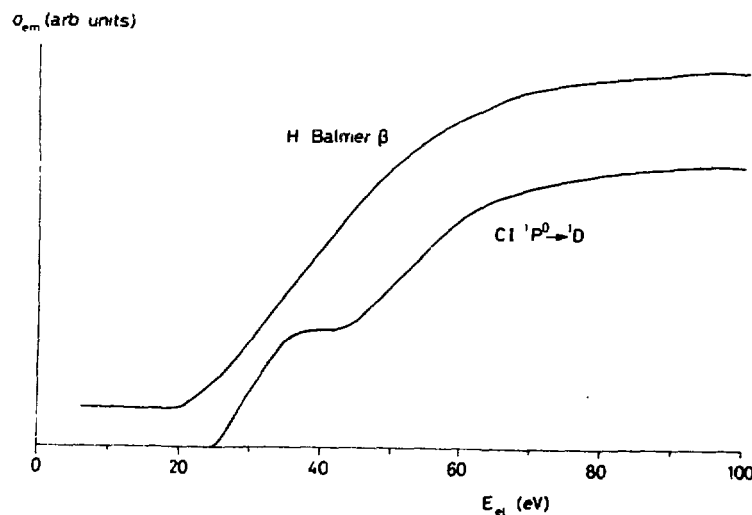


FIGURE 3.4. Energy dependence below 100 eV of the emission cross sections for H and CI radiation for electron impact on acetylene. The ordinate of the H Balmer β emission cross sections is displaced to avoid confusion.

of σ_{em} for both transitions is found, as is expected because the emission originates from the same upper level. Therefore, only the emission cross sections for 1931 Å radiation are presented in Table 3.2. The ratio of $\sigma_{em}(2479 \text{ Å})/\sigma_{em}(1931 \text{ Å})$ was determined to be 0.068 ± 0.024 . The error is mainly due to the uncertainty in the quantum sensitivity of the optical equipment, which is estimated to be 20% at 2479 Å and 30% at 1931 Å (see Section 2.5). Weiss [14] has calculated oscillator strengths for several transitions in CI and CII by the method of superposition of configurations. It is shown that the calculated f -values are generally, although not always, obtainable with an accuracy of about 25%. From the calculated oscillator strengths we derive a theoretical value of $\sigma_{em}(2479 \text{ Å})/\sigma_{em}(1931 \text{ Å})$ of 0.101. This shows that the values obtained from theory and experiment agree with each other within the quoted errors.

From the energy dependence of the emission cross section (Fig. 3.3) it follows that excited carbon atoms in the $3s \text{ } ^1P^o$ state are formed, like excited hydrogen atoms, mainly by optically forbidden excitation processes. The threshold for carbon ($3s \text{ } ^1P^o$) radiation is found at $24.4 \pm 1 \text{ eV}$ (Fig. 3.4). This value allows for a number of processes to be operative in the formation of carbon ($3s \text{ } ^1P^o$) (see Table 3.3). A second onset is observed at 45 eV.

3.3. METHANE, ETHYLENE, ETHANE AND ACETYLENE

3.3.1. Balmer emission

3.3.1.1. Introduction

The dissociative excitation of simple aliphatic hydrocarbons into excited hydrogen atoms has been studied quite extensively by Vroom and de Heer [1]. They measured emission cross sections for Lyman α and Balmer radiation in the case of methane, ethylene and ethane excited by electrons (0.05 - 6 keV). It turns out that the absolute values of the emission cross sections for Lyman α and Balmer radiation are almost independent of the number of hydrogen atoms in the molecule. More recently Aarts *et al.* [3] extended the measurements of Vroom and de Heer in the case of methane and ethylene to low energies. They also measured thresholds for hydrogen radiation. In Section 3.2 we have presented measurements on the hydrogen emission from

TABLE 3.4.

Balmer emission cross sections at 100 eV in units of 10^{-19} cm^2 for electron impact on methane, ethylene, ethane and acetylene					
	Balmer α	Balmer β	Balmer γ	Balmer δ	Balmer ϵ
methane	31.2	6.56	2.38	1.10	
ethylene	31.2	6.12	2.20	1.05	
ethane	28.6	6.29	2.28	1.11	
acetylene	29.8	6.68	2.42	1.34	0.63

TABLE 3.5.

Emission cross sections at 100 eV electron impact energy for Balmer β radiation in units of 10^{-19} cm^2			
	$\sigma_{\text{em}}(\text{H}_\beta)$		
	present	ref. 1	ref. 3
methane	6.56	7.15	6.48
ethylene	6.12	6.80	5.95
ethane	6.29	6.35	-
acetylene	6.68	-	-

TABLE 3.6.

Threshold energies for $\text{H}(n=4)$ and M_{em}^2 for Balmer β radiation.		
	$M_{\text{em}}^2 \times 10^4$ ^a	Threshold (eV)
methane	-0.9 ± 1.3^b	21.8 ± 0.5^b 21.7 ± 0.8^c
acetylene	-1.7 ± 1.0	20.6 ± 1.0
ethylene	-0.6 ± 1.5^b	23.2 ± 1.0^b

^a Errors refer to standard deviation in the slope of the Fano plot.

^b Ref. 3.

^c Ref. 2.

acetylene in the energy range 0 - 1000 eV. We compare the results with those of methane, ethylene and ethane. Previous measurements [1,3] have been repeated at 100 eV.

3.3.1.2. Experimental procedure and error discussion

In order to make a direct and accurate comparison of the Balmer emission cross sections possible we set side by side the light signal, normalized with respect to the pressure and electron beam intensity, of the successive Balmer lines from the various hydrocarbons. This procedure allows us to use the same geometrical factors and the same quantum sensitivity in the evaluation of the emission cross sections for corresponding Balmer lines (see Section 2.2). The error in the ratio of the emission cross sections of one Balmer line for different hydrocarbons is then determined only by uncertainties in the pressure and electron beam intensity. These add up to a probable error of 5% in the ratios (see Section 2.5). The error in the ratio of the absolute emission cross section of one Balmer line and that of another Balmer line from the same hydrocarbon is mainly determined by the uncertainty in the relative quantum sensitivity of the optical equipment as a function of wavelength. Together with random errors in the measurement of the light signal, electron beam intensity and pressure this leads to a probable error in the ratios with respect to the Balmer β line of 12% for the Balmer α and ϵ lines and of 7% for the Balmer γ and δ lines.

In the case of molecules containing two carbon atoms the H_δ emission cross sections might be somewhat higher due to contamination with C_2 radiation. For H_ϵ contamination by N_2^+ radiation from background gas in the collision chamber is possible.

3.3.1.3. Results

The emission cross sections for Balmer radiation from methane, ethylene, ethane and acetylene at 100 eV electron impact energy are collected in Table 3.4. In that table it can be seen that the Balmer emission cross sections of these hydrocarbons have the same value within 10%. This also

applies to the Balmer β and Balmer γ emission cross sections. The Balmer δ emission cross sections are more difficult to compare, because of contamination by C_2 radiation for the molecules containing two carbon atoms.

In Table 3.5 the present results for Balmer β emission are compared with those of Vroom and de Heer [1] and of Aarts *et al.* [3]. Within the experimental errors the absolute emission cross sections agree with those measured previously.

In Fig. 3.5 we compare the energy dependence of the Balmer β emission cross sections of acetylene with earlier measurements on methane and ethylene [3]. The values of M_{em}^2 derived from the Fano plots are collected in Table 3.6. Negative values of M_{em}^2 are probably due to random scatter in the relative cross sections. The Fano plots therefore indicate a zero or very small positive value of M_{em}^2 . In Table 3.6 we also compare threshold energies for Balmer β production.

The ratios of the Balmer α , β , γ , δ and ϵ emission cross sections and the Balmer β emission cross section for methane, ethylene and acetylene are given in Table 3.7. Within the accuracy as given in Section 3.3.1.2. the present values agree with the proton impact experiments of Carré [10], who measured Balmer α , β and γ radiation from methane and Balmer β and γ radiation from ethylene, ethane and acetylene. The present results are also in agreement with those of Vroom and de Heer [1], except in the case of Balmer γ emission from ethane and Balmer δ emission from all hydrocarbons.

The following similarities in the Balmer emission cross sections therefore arise from the above mentioned results:

- The thresholds for Balmer β production are found to be in the 19.6 - 24.2 eV energy range (Table 3.6). The energy dependence of the emission cross section of the Balmer β line does not indicate other onsets for that Balmer line at higher energies (see Fig. 3.4 and Ref. 3). This applies also to the other Balmer lines (see Section 3.2 and Ref. 3).
- The values of the emission cross sections for one Balmer line are the same or only slightly different in the various hydrocarbons (Table 3.4).
- The main part of the excited hydrogen atoms is formed by optically forbidden transitions (Fig. 3.5 and Table 3.6).

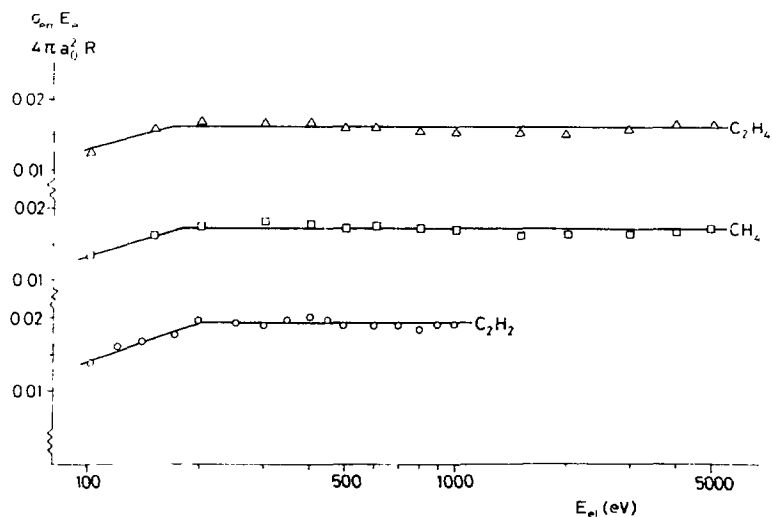


FIGURE 3.5. Emission cross sections for H Balmer β radiation presented in the form of a Fano plot for electron impact on acetylene, methane and ethylene.

3.3.1.4. Comparison with other experiments

The threshold for production of Balmer emission from excited hydrogen atoms by dissociative excitation of methane, ethylene and acetylene is found in the energy range 19 - 25 eV. Because the excitation energy of $H(n=3)$ is 12.0 eV and the dissociation energy of a C-H bond is about 4 eV, only 3 to 9 eV is available for internal energy of the other fragment(s). This is less energy than required for ionization (~ 10 eV). Therefore, at the threshold for Balmer emission, excitation of the molecule is followed by dissociation into neutral fragments. Hence we conclude that the excited hydrogen atoms originate from super-excited states of the parent molecule (Section 1.4). The near-zero value of M_{em}^2 for Balmer radiation (Table 3.6) indicates a small cross section for excitation into these super-excited states by photoabsorption.

Welch and Judge [15] studied fragment emission from methane in the wavelength region 3500 - 8000 Å after excitation of the molecule by monochromatic radiation from 1242 - 555 Å (10.0 - 22.4 eV). Apart from strong $\text{CH}(A^2\Delta)$ emission and a much weaker emission from $\text{CH}(B^2\Sigma^-)$ and $\text{CH}_2(\tilde{b}^1B_1)$

TABLE 3.7.

Emission cross sections for Balmer $\alpha, \beta, \gamma, \delta$ and ϵ radiation at 100 eV relative to the Balmer β emission cross section						
		Balmer α	Balmer β	Balmer γ	Balmer δ	Balmer ϵ
CH ₄	present	4.76	1.00	0.363	0.168	-
	ref. 1	4.03	1.00	0.408	0.236	-
	ref. 5	5.0	1.00	0.35	-	-
C ₂ H ₄	present	5.11	1.00	0.360	0.172	-
	ref. 1	4.00	1.00	0.435	0.253	-
	ref. 5	-	1.00	0.34	-	-
C ₂ H ₆	present	4.55	1.00	0.356	0.176	-
	ref. 1	3.43	1.00	0.458	0.258	-
	ref. 5	-	1.00	0.34	-	-
C ₃ H ₂	present	4.47	1.00	0.363	0.201	0.094
	ref. 1	-	-	-	-	-
	ref. 5	-	1.00	0.35	-	-

they found Balmer α , β and γ radiation with a very small photofluorescence cross section ($\sim 10^{-21}$ cm² at 22.4 eV). This is consistent with the small value of M_{em}^2 derived from the electron impact emission cross sections (Table 3.6).

Backx *et al.* [16] measured photoionization and photoabsorption cross sections for methane in the range 0 - 80 eV. In their experiment a monochromatic photon beam is simulated by a beam of electrons (10 keV) of which the energy loss is measured. They observed that the photoabsorption cross section is equal to the photoionization cross section in the energy-loss region 17 - 23 eV. This also implies that at the threshold for Balmer radiation from methane neutral states of the molecules are not formed by optically allowed excitation processes, consistent with the small value of M_{em}^2 of Balmer radiation found in our experiment.

Considering the production of protons as a limiting case of the production of excited hydrogen atoms, we expect that at least part of the protons are formed by a similar mechanism as excited hydrogen atoms. This would

imply that the appearance potential of H^+ should be close to the threshold for Balmer radiation. The optically forbidden character of the Fano plot for Balmer radiation would mean that in photoionization experiments only very small amounts of protons are formed. Although measurements on the proton production from aliphatic hydrocarbons are rare, a similarity between the formation of protons and excited hydrogen atoms is indicated in the case of methane. Smith [17] measured the appearance potential of H^+ to be 22.7 ± 0.5 eV as compared with the threshold energy at 21.8 ± 0.5 eV for Balmer β radiation [3]. Backx *et al.* [16] studied also the production of protons in the case of electron impact on methane by measuring them in coincidence with the energy loss of those electrons which were scattered at a small angle. Because also the energy of the incident electrons is high (10 keV), this experiment can be compared with photoionization experiments yielding H^+ . Below an electron energy loss of 30 eV they found the proton production to be very small. This means that in the formation of protons below 30 eV probably optically forbidden processes dominate, as is the case for excited hydrogen atoms.

In the case of acetylene Tate *et al.* [18] determined the appearance potential of H^+ to be 21.7 ± 1.0 eV, which is close to the threshold for $H(n=4)$ at 20.6 ± 1.0 eV.

3.3.1.5. Discussion

In this section we wish to discuss the origin of the super-excited states from which the excited hydrogen atoms are formed. In the present state of the art, calculations on molecular states in the region 19 - 25 eV are difficult to do with sufficient accuracy. Yet some insight into the processes leading to excited hydrogen atoms can be gained from a consideration of the electronic configuration and orbital energies in the molecule. These are given in Table 3.8 with the assumption that according to Koopman's theorem the orbital energies are represented by the measured ionization potential. In the case of acetylene the $2\sigma_g$ orbital energy is not known experimentally. Photoelectron spectroscopy places it above 21.4 eV [24], while calculations put an upper limit of 28 eV [27].

If we consider one-electron transitions to be involved in the excitation

process, only the $2a_1$ orbital energy of methane, the $2\sigma_g$ orbital energy of acetylene and the $2a_g$ orbital energy of ethylene are sufficiently large to yield neutral molecular Rydberg states near 20 eV, which may dissociate into excited hydrogen atoms.

In a first approximation the excitation cross section of these Rydberg states can be thought to depend only on the number of relevant electrons and on the orbital energies [28,29]. Because the two factors are the same or almost the same in the three hydrocarbons considered, we expect that the excitation cross sections of the Rydberg states, which produce H^* , will not differ much. In the one-electron model the promoted electron occupies a non-bonding orbital and therefore the potential energy surfaces of these Rydberg states will have the same shape as those of the corresponding ions. Thus the production of excited hydrogen atoms from the neutral molecule could proceed in a similar way as the appearance of protons from the corresponding ions. Apart from the formation of excited hydrogen atoms, also processes like dissociation into heavier fragments, pre-dissociation, pre-ionization and light emission should be considered as possible decay modes. Because the observed threshold for Balmer production is at an energy which is several electronvolts higher than the calculated adiabatic energy, the lifetime of the excited states as far as determined by dissociation yielding hydrogen atoms might be as short as $10^{-15} - 10^{-14}$ seconds. This makes this process by far dominant over the other possible decay processes. In connection with an equal excitation cross section for the H^* -producing Rydberg states (see above) this would explain why the corresponding Balmer emission cross sections are about equal in the various hydrocarbons. In addition the consideration of one-electron transitions also explains why the threshold for Balmer production is always found close to the vertical ionization potential. The observed small value of M_{em}^2 tells us that the absorption oscillator strength for transitions from the ground state to the relevant Rydberg states must be small.

Also excitation processes leading to super-excited states by simultaneous excitation of two electrons should be considered. In the case of proton formation by electron impact on hydrocarbons doubly ionized states certainly play a role [16]. This is concluded from the fact that a fraction of the protons are formed with a large amount of kinetic energy, which can arise from the strong Coulomb repulsion in a doubly ionized state [30,31,32]. These states lie above 30 eV [16,33].

Doubly excited states may already be formed at the threshold for Balmer production. They are probably not important because the excitation cross section for a two-electron transition is relatively small. Moreover, if doubly excited states are important, then they should give rise to discrete structure in the energy dependence of the Balmer emission cross sections. However, only an experiment such as that in which Balmer radiation is measured in coincidence with the energy loss of the incident electrons can establish to what extent higher (doubly excited) states contribute to the formation of excited hydrogen atoms.

Balmer emission from ethane [1] and propane [4] has only been studied at electron impact energies above 50 eV. At these energies the emission cross sections have the same characteristics as for methane, ethylene and acetylene, indicating a similar mechanism for the formation of excited hydrogen atoms.

3.3.2. Emission from excited carbon atoms

In the wavelength region 1850 - 9000 Å electron impact on hydrocarbons produces $\text{CI}(3s\ ^1P^o \rightarrow 2p^2\ ^1D)$ and $\text{CI}(3s\ ^1P^o \rightarrow 2p^2\ ^1S)$ multiplet radiation at 1931 and 2479 Å respectively. Only in the case of acetylene is this emission strong enough to be studied (see Section 3.2). The Fano plot

TABLE 3.8

Electron configuration and ionization potentials for methane, ethylene and acetylene						
methane ^a	:	K	(2a ₁) ²	(1t ₂) ⁶		
I.P. (eV)			23.1	13.6		
ethylene ^{b,c}	:	KK	(2a _g) ²	(2b _{3u}) ²	(1b _{2u}) ²	(3a _g) ² (1b _{1g}) ² (1b _{1u}) ²
I.P. (eV)		~ 23	18.87	15.68	14.47	12.38 10.51
acetylene ^b	:	KK	(2σ _g) ²	(2σ _u) ²	(3σ _g) ²	(1π _u) ⁴
I.P. (eV)		-	18.38	16.36	11.40	

^a Ref. 25.

^b Ref. 24.

^c Ref. 26.

yields a small value of M_{em}^2 , as in the case of hydrogen emission (Fig. 3.3). From the energy dependence of the emission cross sections at low electron impact energies (Fig. 3.4) it can be observed that at least two different excitation processes are involved in the formation of carbon $3s\ ^1P^0$, one having an onset at 24.4 ± 1 eV and another with an onset at 45 eV.

The emission from the $3s\ ^1P^0$ state is much weaker in methane and ethylene which suggests that excited carbon atoms are not formed from the various hydrocarbons in equal amounts as is the case for formation of excited hydrogen atoms.

3.3.3. Emission from molecular fragments

3.3.3.1. Introduction

The light emission from molecular fragments produced by electron impact on hydrocarbons has been studied in the case of methane and ethylene by Aarts *et al.* [3]; the results for acetylene have been presented in Section 3.2.

Apart from emission from excited atoms, diatomic fragments have also been observed: CH, C_2 and CH^+ . The $CH(A^2\Delta - X^2\Pi)$ emission cross sections have been measured for methane, ethylene, and acetylene. The results are compared in this section. Contamination or weak signals prevented the measurement of the emission cross sections for C_2 and CH^+ radiation. Only in the case of acetylene were measurements of the C_2 Mulliken system possible (see Section 3.2.).

3.3.3.2. Results

In Table 3.9 and Fig. 3.6 the cross section data for $CH(A^2\Delta - X^2\Pi)$ emission are compared for methane, ethylene and acetylene. In the case of methane and ethylene the same energy dependence and the same absolute cross sections have been found [3]. From the values of c_{em} and M_{em}^2 it was concluded that both optically forbidden and optically allowed transitions are involved in the formation of $CH(A^2\Delta)$. In the case of acetylene the emission cross sections are much larger. The rather small value of c_{em} and the positive slope in the Fano plot imply that optically allowed

TABLE 3.9.

Emission cross section data and threshold energies for $\text{CH}(A^2\Delta - X^2\Pi)$ radiation from methane, ethylene and acetylene.				
	$M_{\text{em}}^2 (\times 10^2)^a$	c_{em}	σ_{em}^b	Threshold (eV)
methane ^c	0.94 ± 0.10	15	17.0	14.6 ± 0.5
ethylene ^c	0.82 ± 0.03	14	14.6	15.2 ± 1.0
acetylene	4.90 ± 0.20	1.25	46.6	13.0 ± 1.5

^a Errors refer to the standard deviation in the slope of the Fano plot only.

^b At 100 eV and in units of 10^{-19} cm^2 .

^c Ref. 3.

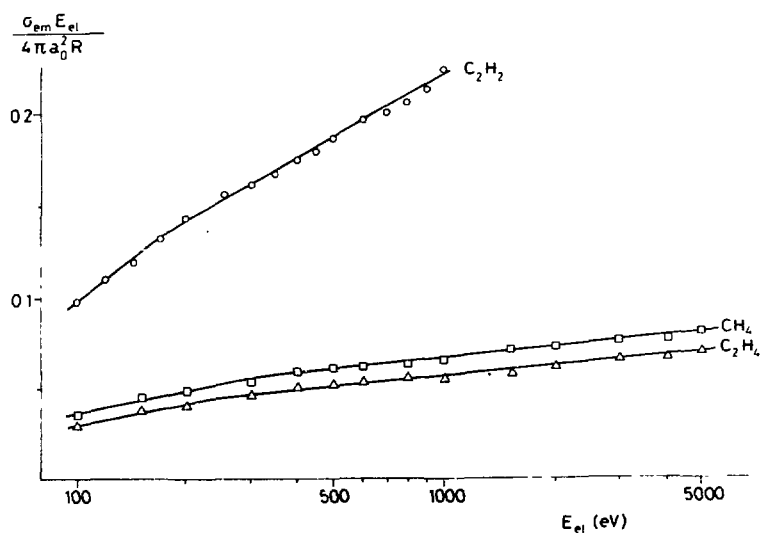


FIGURE 3.6. Emission cross sections for $\text{CH}(A^2\Delta - X^2\Pi)$ radiation presented in the form of a Fano plot for electron impact on acetylene, methane and ethylene.

transitions are more important in the dissociative excitation of acetylene into $\text{CH}(A^2\Delta)$ than in the case of methane and ethylene.

The thresholds for $\text{CH}(A^2\Delta)$ production are above the adiabatic ionization potential in all three molecules, while the lowest thresholds are too low to allow the other fragment or fragments to be ionized. Therefore, $\text{CH}(A^2\Delta)$ is at least in part formed via super-excited states of the parent molecule (see Section 1.4). Moreover, discrete structure is observed in the energy dependence of the emission cross sections (Ref. 3 and Fig. 3.2), indicating that several excited states of the hydrocarbons may be involved in the $\text{CH}(A^2\Delta)$ production.

REFERENCES

- [1] D.A. Vroom and F.J. de Heer, *J.Chem.Phys.* 50 (1969) 573.
- [2] W. Sroka, *Z.Naturforsch.* 24a (1969) 1724.
- [3] J.F.M. Aarts, C.I.M. Beenakker and F.J. de Heer, *Physica* 53 (1971) 32.
- [4] J.M. Kurepa, M.D. Tasic and V.V. Urosevic, Paper submitted to VIII ICPEAC, Beograd (1973).
- [5] R.W. Pearse and A.G. Gaydon, *The Identification of Molecular Spectra* (Chapman, London 1965).
- [6] A.R. Striganov and N.S. Sventitskii, *Tables of Spectral Lines of Neutral and Ionized Atoms* (IFI/Plenum, New York 1968).
- [7] B. Rosen, *Spectroscopic Data relative to Diatomic Molecules* (Pergamon Press, Oxford 1970).
- [8] D.R. Childs, *J.Quant.Radiat.Transfer* 4 (1964) 283.
- [9] J.E. Hesser and B.L. Lutz, *Astrophys.J.* 159 (1970) 703.
- [10] M. Carré, Thesis, University of Lyon, France (1967).
- [11] H.A. Bethe, *Ann.Physik* 5 (1930) 325.
- [12] M. Inokuti, *Rev.Mod.Phys.* 43 (1971) 297.
- [13] J.F.M. Aarts and F.J. de Heer, *Chem.Phys.Letters* 4 (1969) 116.
- [14] A.W. Weiss, *Phys.Rev.* 162 (1969) 71.
- [15] A.R. Welch and D.L. Judge, *J.Chem.Phys.* 57 (1972) 286.
- [16] C. Backx and M.J. van der Wiel, to be published.
- [17] L.G. Smith, *Phys.Rev.* 51 (1937) 263.
- [18] J.T. Tate, P.T. Smith and A.C. Vaughan, *Phys.Rev.* 48 (1935) 525.

- [19] G. Herzberg, *Electronic Spectra of Polyatomic Molecules* (Van Nostrand, Princeton 1966).
- [20] G. Herzberg, *Spectra of Diatomic Molecules* (Van Nostrand, Princeton 1950).
- [21] H. Okabe and V.H. Dibeler, *J.Chem.Phys.* 59 (1973) 2430.
- [22] C.E. Moore, *A Multiplet Table of Astrophysical Interest* (Observatory, Princeton 1945).
- [23] C.E. Moore, *An Ultraviolet Multiplet Table*, NBS Circ. 488 (U.S. Government Printing Office, Washington 1950).
- [24] D.W. Turner et al., *Molecular Photoelectron Spectroscopy* (John Wiley-Interscience, London 1970).
- [25] K. Hamrin, G. Johansson, U. Gelius, A. Fahlman, C. Nordling and K. Siegbahn, *Chem.Phys.Letters* 1 (1968) 613.
- [26] A.J. Merer and R.S. Mulliken, *Chem.Rev.* 69 (1969) 639.
- [27] R.J. Buenker, S.D. Peyerimhoff and J.L. Whitten, *J.Chem.Phys.* 46 (1967) 2029.
- [28] J.J. Thomson, *Phil.Mag.* 23 (1912) 419.
- [29] M. Gryzinski, *Phys.Rev.* 138 (1965) A305; 138 (1965) A322.
- [30] R. Fuchs and R. Taubert, *Z.Naturforsch.* 19a (1964) 1181.
- [31] M. Roussel and A. Julienne, *Int.J.Mass Spectrom. and Ion Phys.* 9 (1972) 449.
- [32] K.E. McCulloh, T.E. Sharp and H.M. Rosenstock, *J.Chem.Phys.* 42 (1964) 3501.
- [33] K. Siegbahn et al., *ESCA applied to Free Molecules* (North-Holland, Amsterdam 1969).

CHAPTER IV

A N A L Y S I S O F T H E I N T E N S I T Y D I S T R I B U T I O N O F T H E $\text{CH}(\text{A}^2\Delta - \text{X}^2\Pi)$ S P E C T R U M F R O M A C E T Y L E N E.

4.1. INTRODUCTION

In this chapter we analyse the $\text{CH}(\text{A}^2\Delta - \text{X}^2\Pi)$ spectrum produced by electron impact on acetylene. The features of this spectrum are found to be independent of the energy of the incident electrons in the range 15 - 1000 eV. The $\text{CH}(\text{A}^2\Delta - \text{X}^2\Pi)$ spectrum which covers the region 4150 - 4400 Å is built up from three overlapping bands corresponding to the 0-0, 1-1 and 2-2 vibrational transitions. An analysis of the intensities in these bands provides information about the distribution of the CH molecules over the rotational and vibrational levels in the $\text{A}^2\Delta$ state after dissociative excitation of acetylene by electron impact.

The intensity distribution in the rotational structure of the 0-0 band of the spectrum has been studied before by Brennen and Carrington [1] and by Clerc and Schmidt [2]. The former obtained excited CH radicals by the reaction of oxygen atoms with acetylene in the pressure range 0.1 to 8.5 Torr, the latter by radiolysis of methane and acetylene by an electron pulse at pressures of about 1 Torr. In these experiments the intensity distribution is obtained by an analysis of the lines in the R branch of the 0-0 band. It is found that the intensity distribution can be described by two rotational energy distributions. However, in the method of analysis used in Refs. 1 and 2 serious errors may arise from overlap of different vibrational transitions and from overlap of the various branches in the rotational structure.

In the present study the analysis is performed by two methods. In the first method the free lines in the R branch of the 0-0 band are analysed. In the other method the spectrum is compared with a spectrum simulated on the computer. Because in the calculated spectrum all transitions contributing

to the spectrum are taken into account; also lines which are not free from overlap can be analysed. The computer program is described in the appendix to this chapter.

4.2. SPECTRUM

The frequency of a rotational transition is given by:

$$\nu = \nu_0 + F'[J'] - F''[J''] \quad (1)$$

where ν_0 is the band origin and $F[J]$ is the rotational term value depending on the total angular momentum J . The single prime refers to the upper electronic state, the double prime to the lower electronic state. The total angular momentum J is the resultant of the component of the electronic angular momentum along the internuclear axis Λ , of the spin angular momentum S and of the angular momentum of nuclear rotation N . These three quantities are mutually coupled. The limiting cases of the modes of coupling are given by Hund (see Ref. 3). For large J the coupling between Λ and S is very weak in the $A^2\Delta$ and $X^2\Pi$ states of CH and therefore these states belong to Hund's case b. At low J the spin becomes gradually coupled to Λ ; a transition from Hund's case b to Hund's case a takes place.

Because we largely deal with Hund's case b, it is convenient to introduce the quantum number K . It represents the total angular momentum apart from spin. K can take the values $\Lambda, \Lambda+1, \dots$. Each rotational level belonging to a particular value of K is split into two components, one with $J=K+S$ and one with $J=K-S$. These two spin components are indicated by the subscripts

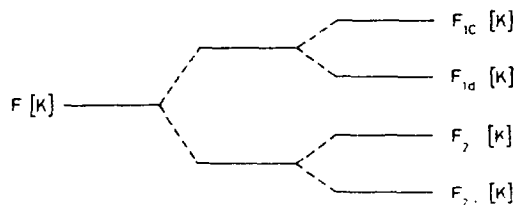


FIGURE 4.1. Schematic representation of the splitting of rotational terms.

1 and 2 respectively. An interaction between the rotation of the nuclei and the electronic angular momentum causes a further splitting called Λ -type doubling. The components of Λ -type doubling are indicated by the subscripts c and d. A schematic representation of the splitting of the rotational terms is given in Fig. 4.1.

For rotational transitions the following rigorous selection rule holds:

$$J' - J'' = -1, 0, +1$$

If $J' - J'' = K' - K'' = -1, 0, +1$, we obtain the P, Q and R branches respectively. These are called main branches. If $J' - J'' \neq K' - K''$ we obtain so called satellite branches. Furthermore, only some particular combinations of the subscripts c and d are possible, depending on the branch involved [4]. We then find 12 main branches and 8 satellite branches (see appendix). In the $\text{CH}(A^2\Delta - X^2\Pi)$ spectrum the Q branch is centered around the origin near 4310 \AA . The R branch extends to shorter wavelength and the P branch to longer wavelength from the origin.

4.3. EXPERIMENTAL

The $\text{CH}(A^2\Delta - X^2\Pi)$ spectrum is produced by dissociative excitation of acetylene by electron impact at a pressure of 10^{-2} Torr. An electron beam of 500 \mu A is used. The energy of the incident electrons is about 15 eV. Under these conditions we could analyse the rotational lines in the R branch up to $K = 20$.

We found the features of the spectrum, recorded at a resolution of 0.45 \AA , to be independent of the electron impact energy (15 - 1000 eV), the pressure ($10^{-4} - 10^{-2}$ Torr) and the electron beam intensity (0 - 500 μA).

4.4. INTENSITY RELATIONS

4.4.1. General

The intensity in emission of a transition between an upper electronic state n' with vibrational quantum number v' and rotational quantum number K' and a lower electronic state with quantum numbers n'' , v'' and K'' is given by [3,5]:

$$I_{n''v''K''}^{n'v'K'} = N_{n'v'K'} A_{n''v''K''}^{n'v'K'} \quad (2)$$

where I is the intensity in photons per second, N is the number of molecules in the initial state and A is the Einstein transition probability of spontaneous emission. If the motion of the electrons and the nuclear vibration and rotation are mutually independent, the following can be shown [5]:

$$A_{n''v''K''}^{n'v'K'} = \frac{64\pi^4 \nu^3}{3h} \frac{|R_e^{n'n''}|^2 |R_{\text{vibr}}^{v'v''}|^2 S_{K'K''}}{g_{K'}} \quad (3)$$

Here h is the Planck constant, ν the frequency of the transition and $g_{K'} = 2K' + 1$ is the degree of degeneracy of the initial state. $|R_e^{n'n''}|^2$ is proportional to the electronic transition probability. It is taken constant in our problem. The quantity $|R_{\text{vibr}}^{v'v''}|^2$ is proportional to the Franck-Condon factor $q_{v',v''}$ of the vibrational transition. $S_{K'K''}$ is the line-strength of the rotational transition, which is proportional to the square of the overlap integral of the rotational wavefunctions in the upper and lower electronic state. By combining Eqs. (2) and (3) we can write for the intensity of a rovibronic transition:

$$I_{v''K''}^{v'K'} \propto N_{v'K'} \nu^3 q_{v',v''} \frac{S_{K'K''}}{g_{K'}} \quad (4)$$

Suppose that the distribution of molecules over the rotational levels belonging to one vibronic state is described by a function $R_{v'}(K')$ such that:

$$N_{v'K'} = \frac{N_{v'}}{Q_{r,v'}} g_{K'} R_{v'}(K') \quad (5)$$

where we have introduced for normalization the rotational state sum $Q_{r,v'}$:

$$Q_{r,v'} = \sum_{K'} g_{K'} R_{v'}(K') \quad (6)$$

We then obtain from Eqs. (4) and (5):

$$I_{v''K''}^{v'K'} \propto \frac{N_{v'}}{Q_{r,v'}} \nu^3 q_{v',v''} S_{K'K''} R_{v'}(K') \quad (7)$$

From the experimentally determined spectrum we wish to deduce the distribution function $R_v(K')$ and the relative population of the vibrational states. This requires a knowledge of the Franck-Condon factors, line-strengths and frequencies.

4.4.2. Franck-Condon factors

Franck-Condon factors of the $CH(A^2\Delta - X^2\Pi)$ vibrational transitions have been calculated by Childs [6]. His calculations show that within 0.5% the Franck-Condon factors of the 0-0, 1-1 and 2-2 transitions can be put equal to unity.

4.4.3. Line-strengths

At high rotational quantum numbers the $A^2\Delta$ and $X^2\Pi$ states of CH belong to Hund's case b, while at lower K values a gradual transition to Hund's case a takes place. We have calculated the line-strengths of the rotational transitions when both states belong to case b and when both states are described by a coupling intermediate between case a and b. The relevant formulas for the line-strength calculation, taken from Kovács [5], are given in the appendix. For Hund's case b the spin-orbit coupling constant Y is put equal to zero. The numerical results are presented in Tables 4.1 and 4.2.

4.4.4. Frequencies

For almost all lines belonging to the main branches the frequency of the rotational transition is known experimentally [7]. We calculated the frequencies of all lines (see appendix). In Tables 4.3, 4.4 and 4.5 we compare these with the experimental frequencies [7]. For the stronger lines in the spectrum ($K < 20$ for the main branches) the calculated and experimental frequencies agree to within 6 cm^{-1} .

TABLE 4.1.
LINE STRENGTH FOR CH ($\Delta 2\Delta$ - $X2P$) ROTATIONAL TRANSITIONS.
K-VALUES REFER TO THE LOWER STATE; $LY=0$.

K	P1	P2	Q1	Q2	R1	R2	PQ12	QP21	QR12	RQ21
1										.000
2	.381	.267	1.867	1.200	3.800	2.000		.000	.133	.190
3			3.214	2.382	4.167	3.214	.019	.114	.119	.119
4	.833	.643	4.400	3.500	4.582	3.733	.024	.100	.100	.085
5	1.309	1.067	5.515	4.582	5.026	4.242	.024	.084	.085	.065
6	1.795	1.515	6.593	5.641	5.486	4.747	.023	.073	.073	.053
7	2.266	1.978	7.650	6.686	5.956	5.250	.022	.064	.064	.044
8	2.729	2.450	8.693	7.721	6.433	5.752	.021	.057	.057	.038
9	3.275	2.928	9.726	8.749	6.914	6.253	.019	.051	.051	.033
10	3.771	3.411	10.753	9.772	7.399	6.753	.018	.047	.047	.029
11	4.269	3.896	11.775	10.791	7.887	7.254	.017	.043	.043	.026
12	4.767	4.384	12.794	11.807	8.376	7.754	.016	.039	.039	.024
13	5.255	4.874	13.810	12.821	8.867	8.254	.015	.037	.037	.022
14	5.764	5.365	14.823	13.833	9.359	8.754	.014	.034	.034	.020
15	6.262	5.857	15.835	14.843	9.852	9.254	.013	.032	.032	.019
16	6.761	6.351	16.845	15.852	10.346	9.754	.013	.030	.030	.017
17	7.261	6.845	17.854	16.861	10.841	10.254	.012	.028	.028	.016
18	7.760	7.340	18.862	17.868	11.336	10.754	.012	.027	.027	.015
19	8.259	7.835	19.869	18.874	11.832	11.254	.011	.026	.026	.014
20	8.759	8.331	20.876	19.880	12.328	11.754	.011	.024	.024	.014
21	9.258	8.827	21.882	20.886	12.824	12.254	.010	.023	.023	.013
22	9.758	9.323	22.887	21.891	13.321	12.754	.010	.022	.022	.012
23	10.257	9.820	23.892	22.895	13.818	13.254	.009	.021	.021	.012
24	10.757	10.317	24.896	23.900	14.315	13.753	.009	.020	.020	.011
25	11.256	10.815	25.900	24.904	14.813	14.253	.009	.020	.020	.011
26	11.756	11.312	26.904	25.907	15.310	14.753	.009	.019	.019	.010
27	12.256	11.810	27.908	26.910	15.808	15.253	.008	.018	.018	.010
28	12.756	12.308	28.911	27.914	16.306	15.753	.008	.018	.018	.010
29	13.255	12.806	29.914	28.916	16.804	16.253	.008	.017	.017	.009
30	13.755	13.304	30.917	29.919	17.303	16.753	.008	.016	.016	.009
31	14.255	13.802	31.920	30.922	17.801	17.253	.007	.016	.016	.009
32	14.755	14.301	32.922	31.924	18.299	17.753	.007	.015	.015	.008
33	15.255	14.799	33.924	32.926	18.798	18.253	.007	.015	.015	.008
34	15.754	15.298	34.927	33.928	19.297	18.753	.007	.014	.014	.008
35	16.254	15.796	35.929	34.930	19.795	19.253	.007	.014	.014	.008

TABLE 4.2.

LINESTRENGTH FOR CH ($\Delta 2P$) ROTATIONAL TRANSITIONS.
K-VALUES REFER TO THE LOWER STATE; $L_Y=2$ AND $U_Y=-0.96/UBV$.

K	P1	P2	Q1	Q2	R1	R2	PQ12	QP21	QR12	RQ21
1					3.009	1.850				.000
2			1.736	1.051	3.471	2.466		.000	.734	.492
3	.371	.234	3.080	2.085	3.935	3.105	.143	.201	.466	.349
4	.820	.564	4.278	3.275	4.407	3.661	.153	.180	.339	.268
5	1.295	.990	5.406	4.402	4.886	4.199	.143	.160	.266	.216
6	1.781	1.444	6.496	5.492	5.370	4.705	.130	.143	.218	.181
7	2.272	1.912	7.562	6.559	5.857	5.215	.118	.128	.185	.156
8	2.766	2.390	8.613	7.610	6.347	5.722	.107	.116	.160	.136
9	3.262	2.872	9.653	8.651	6.838	6.227	.098	.106	.141	.121
10	3.760	3.359	10.686	9.684	7.331	6.731	.090	.097	.126	.109
11	4.258	3.848	11.713	10.712	7.825	7.234	.083	.090	.114	.099
12	4.756	4.339	12.736	11.735	8.320	7.736	.078	.084	.104	.091
13	5.255	4.832	13.755	12.754	8.815	8.238	.072	.078	.096	.084
14	5.754	5.326	14.777	13.771	9.311	8.739	.068	.073	.080	.078
15	6.253	5.820	15.787	14.786	9.807	9.240	.064	.069	.082	.072
16	6.753	6.316	16.800	15.799	10.304	9.741	.060	.065	.077	.068
17	7.252	6.811	17.811	16.810	10.801	10.242	.057	.062	.072	.064
18	7.752	7.308	18.821	17.821	11.299	10.743	.054	.059	.068	.060
19	8.252	7.805	19.830	18.830	11.797	11.243	.052	.056	.064	.057
20	8.751	8.302	20.839	19.838	12.294	11.744	.049	.054	.061	.054
21	9.251	8.799	21.846	20.846	12.793	12.244	.047	.051	.053	.052
22	9.751	9.297	22.853	21.852	13.291	12.745	.045	.049	.055	.049
23	10.251	9.795	23.859	22.859	13.789	13.245	.043	.047	.053	.047
24	10.751	10.293	24.865	23.865	14.288	13.745	.042	.045	.051	.045
25	11.250	10.791	25.870	24.870	14.786	14.246	.040	.044	.049	.043
26	11.750	11.289	26.875	25.875	15.285	14.746	.039	.042	.047	.042
27	12.250	11.788	27.880	26.879	15.784	15.246	.037	.041	.045	.040
28	12.750	12.286	28.884	27.884	16.283	15.746	.036	.039	.043	.039
29	13.250	12.785	29.888	28.887	16.782	16.246	.035	.038	.042	.037
30	13.750	13.284	30.891	29.891	17.281	16.747	.034	.037	.040	.036
31	14.250	13.783	31.895	30.895	17.780	17.247	.033	.036	.039	.035
32	14.750	14.282	32.898	31.898	18.279	17.747	.032	.035	.038	.034
33	15.250	14.781	33.901	32.901	18.778	18.247	.031	.034	.037	.033
34	15.750	15.280	34.904	33.904	19.277	18.747	.030	.033	.035	.032
35	16.250	15.779	35.907	34.907	19.777	19.247	.029	.032	.034	.031

TABLE 4.3.

CALCULATED AND EXPERIMENTAL FREQUENCIES (CM-1) FOR CH₃ (A2DELTA - X2P), 0-0, ROTATIONAL TRANSITIONS.
K-VALUES REFER TO THE LOWER STATE.

K	P1CD			P1DC			P2CD			P2DC		
	EXP.	CALC.	DIFF.	EXP.	CALC.	DIFF.	EXP.	CALC.	DIFF.	EXP.	CALC.	DIFF.
3	23088.52	23088.62	-00.10	23088.19	23088.19	-00.00	23094.44	23094.30	+00.14	23093.98	23093.87	+00.11
4	23063.39	23063.46	-00.07	23062.75	23062.74	+00.01	23067.73	23067.61	+00.12	23066.89	23066.89	-00.00
5	23038.95	23039.05	-00.10	23037.92	23037.97	-00.05	23042.29	23042.27	+00.02	23041.13	23041.19	-00.06
6	23015.42	23015.47	-00.05	23013.97	23013.96	+00.01	23018.16	23018.06	+00.10	23016.49	23016.55	-00.06
7	22992.82	22992.81	+00.01	22990.84	22990.79	+00.05	22995.11	22994.93	+00.19	22992.82	22992.91	-00.09
8	22971.08	22971.08	-00.00	22968.54	22968.49	+00.05	22972.96	22972.84	+00.12	22970.14	22970.24	-00.10
9	22950.32	22950.33	-00.01	22947.14	22947.09	+00.05	22951.90	22951.78	+00.12	22948.41	22948.54	-00.13
10	22930.62	22930.56	+00.06	22926.72	22926.60	+00.12	22931.91	22931.76	+00.15	22927.76	22927.80	-00.04
11	22911.90	22911.78	+00.12	22907.26	22907.03	+00.23	22913.02	22912.77	+00.25	22908.07	22908.02	+00.05
12	22894.13	22894.01	+00.12	22888.68	22888.39	+00.29	22895.05	22894.00	+00.28	22889.32	22889.19	+00.13
13	22877.95	22877.24	+00.31	22871.26	22870.69	+00.37	22878.21	22877.07	+00.42	22871.46	22871.31	+00.15
14	22861.86	22861.47	+00.39	22854.73	22853.91	+00.82	22862.14	22861.94	+00.56	22854.73	22854.38	+00.35
15	22847.20	22846.70	+00.50	22838.96	22838.06	+00.90	22847.11	22847.03	+00.75	22838.96	22838.39	+00.57
16	22833.50	22832.92	+00.58	22824.21	22823.13	+01.08	22833.79	22833.12	+00.67	22824.21	22823.32	+00.89
17	22820.88	22820.11	+00.77	22810.49	22809.09	+01.40	22820.88	22820.17	+00.69	22810.33	22809.17	+01.16
18	22808.95	22808.26	+00.69	22797.65	22795.95	+01.71	22808.95	22808.22	+00.73	22797.15	22795.91	+01.24
19	22798.05	22797.35	+00.70	22785.64	22783.67	+01.97	22798.05	22797.25	+00.85	22785.10	22783.52	+01.58
20	22787.78	22787.36	+00.42	22774.41	22772.24	+02.17	22787.78	22787.11	+00.67	22773.73	22771.99	+01.74
21	22778.38	22778.27	-00.11	22763.95	22761.63	+02.32	22778.38	22777.91	+00.47	22763.20	22761.28	+01.92
22	22769.83	22770.03	-00.20	22754.30	22751.82	+02.48	22769.83	22769.58	+00.25	22753.39	22751.37	+02.02
23	22761.77	22762.63	-00.86	22745.11	22742.76	+02.35	22761.77	22762.09	-00.32	22744.16	22742.22	+01.94
24	22754.30	22756.03	-01.73	22736.92	22734.43	+02.09	22754.30	22755.39	-01.09	22735.60	22733.79	+01.81
25	22747.36	22750.18	-02.82	22728.58	22726.78	+01.80	22747.36	22749.46	-02.10	22727.44	22726.06	+01.38
26	22741.09	22745.05	-03.96	22720.92	22719.78	+01.14	22740.72	22744.25	-03.53	22719.74	22718.98	+00.76
27	22734.82	22740.60	-05.78	22713.45	22713.38	-00.07	22734.82	22739.71	-05.33	22712.19	22712.49	-00.30
28	22728.58	22736.77	-08.19	22706.19	22707.53	-01.34	22727.97	22735.79	-07.82	22704.86	22706.56	-01.70
29				22698.72	22702.19	-03.47				22697.44	22701.14	-03.70
30				22691.10	22697.29	-06.19				22689.73	22696.16	-06.43
31				22683.17	22692.78	-09.61				22681.62	22691.57	-09.95
32				22674.32	22688.60	-14.28				22672.69	22687.32	-14.63
33				22664.71	22684.68	-19.97				22663.07	22683.33	-20.26
34				22654.44	22680.97	-26.53				22653.12	22679.54	-26.42

TABLE 4.4.

CALCULATED AND EXPERIMENTAL FREQUENCIES (CM⁻¹) OF CH₃ A2DELTA - X2P1, 0-0) ROTATIONAL TRANSITIONS.
K-VALUES REFER TO THE LOWER STATE.

	Q1C			Q1D			Q2C			Q2D		
K	EXP.	CALC.	DIFF.	EXP.	CALC.	DIFF.	EXP.	CALC.	DIFF.	EXP.	CALC.	DIFF.
2	23172.72	23172.64	+00.08	23172.72	23172.85	-00.13	23180.78	23180.34	+00.44	23180.78	23180.55	+00.23
3	23175.66	23175.66	+00.00	23176.04	23176.09	-00.05	23180.78	23180.83	-00.05	23181.39	23181.26	+00.13
4	23179.05	23179.07	-00.02	23179.75	23179.79	-00.04	23183.00	23182.92	+00.08	23183.74	23183.64	+00.10
5	23183.00	23183.03	-00.03	23184.15	23184.11	+00.04	23186.06	23186.05	+00.01	23187.27	23187.13	+00.14
6	23187.62	23187.59	+00.03	23189.12	23189.10	+00.02	23190.01	23190.03	-00.02	23191.64	23191.54	+00.10
7	23192.87	23192.77	+00.10	23194.83	23194.78	+00.05	23194.83	23194.76	+00.07	23196.97	23196.78	+00.19
8	23198.68	23198.56	+00.12	23201.25	23201.15	+00.10	23200.17	23200.20	-00.03	23203.01	23202.80	+00.21
9	23205.20	23204.94	+00.26	23208.37	23208.18	+00.19	23206.35	23206.30	+00.05	23209.82	23209.54	+00.28
10	23212.33	23211.90	+00.43	23216.11	23215.86	+00.25	23213.13	23213.03	+00.10	23217.39	23216.99	+00.40
11	23219.85	23219.42	+00.43	23224.53	23224.17	+00.36	23220.57	23220.33	+00.24	23225.55	23225.08	+00.47
12	23227.95	23227.45	+00.50	23233.54	23233.06	+00.48	23228.59	23228.17	+00.42	23234.38	23233.79	+00.59
13	23236.84	23235.96	+00.88	23243.12	23242.51	+00.61	23237.11	23236.52	+00.59	23243.86	23243.07	+00.79
14	23246.12	23244.91	+01.21	23253.34	23252.47	+00.87	23246.12	23245.32	+00.80	23253.88	23252.88	+01.00
15	23255.76	23254.26	+01.50	23263.96	23262.90	+01.06	23255.76	23254.53	+01.23	23264.34	23263.17	+01.17
16	23265.75	23263.97	+01.78	23275.07	23273.76	+01.31	23265.75	23264.11	+01.64	23275.33	23273.90	+01.43
17	23276.29	23273.98	+02.31	23286.63	23284.99	+01.64	23276.04	23274.00	+02.04	23286.63	23285.01	+01.62
18	23287.07	23284.23	+02.84	23298.36	23296.55	+01.81	23286.63	23284.14	+02.49	23298.36	23296.45	+01.91
19	23298.00	23294.69	+03.31	23310.40	23308.37	+02.03	23297.42	23294.48	+02.94	23310.40	23308.16	+02.24
20	23309.13	23305.27	+03.86	23322.56	23320.39	+02.17	23308.46	23304.96	+03.50	23322.56	23320.08	+02.48
21	23320.37	23315.92	+04.45	23334.83	23332.56	+02.27	23319.57	23315.52	+04.05	23334.86	23332.15	+02.71
22	23331.56	23326.58	+04.98	23347.15	23344.80	+02.35	23330.64	23326.08	+04.56	23347.15	23344.30	+02.85
23	23342.69	23337.17	+05.52	23359.51	23357.05	+02.46	23341.68	23336.58	+05.10	23359.51	23356.45	+03.06
24	23353.65	23347.63	+06.02	23371.49	23369.23	+02.26	23351.79	23346.94	+05.76	23371.24	23368.54	+02.70
25	23364.18	23357.87	+06.31	23383.17	23381.27	+01.90	23363.01	23357.10	+05.91	23382.70	23380.50	+02.20
26	23374.27	23367.81	+06.46	23394.50	23393.08	+01.42	23373.07	23366.96	+06.11	23393.53	23392.23	+01.30
27	23383.88	23377.38	+06.50	23405.14	23404.60	+00.54	23382.70	23376.45	+06.25	23404.63	23403.66	+00.97
28				23415.01	23415.73	-00.72				23414.29	23414.71	-00.42
29				23425.00	23426.37	-01.37				23422.97	23425.28	-02.31
30				23431.23	23436.45	-05.22				23430.54	23435.28	-04.74
31				23437.17	23445.87	-08.70				23436.50	23444.61	-08.11

TABLE 4.5.

CALCULATED AND EXPERIMENTAL FREQUENCIES (CM⁻¹) FOR CH₃ A2DELTA - X2P1 (0-0) ROTATIONAL TRANSITIONS.
K-VALUES REFER TO THE LOWER STATE.

K	R1CD				R2CD				R2DC			
	EXP.	CALC.	DIFF.	EXP.	CALC.	DIFF.	EXP.	CALC.	EXP.	CALC.	DIFF.	DIFF.
1	2327.95	2328.12	-00.17	2327.95	2328.05	-00.10	2327.54	2327.59	-00.05	2327.54	2327.52	+00.02
2	2328.36	2328.32	-00.04	2328.36	2328.11	+00.25	2327.58	2327.51	+00.07	2327.37	2327.29	+00.08
3	2329.10	2329.14	-00.04	2329.10	2329.19	-00.09	2327.42	2327.39	+00.03	2327.37	2327.29	+00.08
4	2329.42	2329.46	-00.04	2329.42	2329.41	+00.01	2327.42	2327.40	+00.02	2327.37	2327.29	+00.08
5	2329.76	2329.74	+00.02	2329.76	2329.66	+00.10	2327.42	2327.40	+00.02	2327.37	2327.29	+00.08
6	2330.10	2330.06	+00.04	2330.10	2330.05	+00.05	2327.42	2327.40	+00.02	2327.37	2327.29	+00.08
7	2330.44	2330.40	+00.04	2330.44	2330.39	+00.05	2327.42	2327.40	+00.02	2327.37	2327.29	+00.08
8	2330.78	2330.74	+00.04	2330.78	2330.73	+00.05	2327.42	2327.40	+00.02	2327.37	2327.29	+00.08
9	2331.12	2331.08	+00.04	2331.12	2331.07	+00.05	2327.42	2327.40	+00.02	2327.37	2327.29	+00.08
10	2331.46	2331.42	+00.04	2331.46	2331.41	+00.05	2327.42	2327.40	+00.02	2327.37	2327.29	+00.08
11	2331.80	2331.76	+00.04	2331.80	2331.75	+00.05	2327.42	2327.40	+00.02	2327.37	2327.29	+00.08
12	2332.14	2332.10	+00.04	2332.14	2332.09	+00.05	2327.42	2327.40	+00.02	2327.37	2327.29	+00.08
13	2332.48	2332.44	+00.04	2332.48	2332.43	+00.05	2327.42	2327.40	+00.02	2327.37	2327.29	+00.08
14	2332.82	2332.78	+00.04	2332.82	2332.77	+00.05	2327.42	2327.40	+00.02	2327.37	2327.29	+00.08
15	2333.16	2333.12	+00.04	2333.16	2333.11	+00.05	2327.42	2327.40	+00.02	2327.37	2327.29	+00.08
16	2333.50	2333.46	+00.04	2333.50	2333.45	+00.05	2327.42	2327.40	+00.02	2327.37	2327.29	+00.08
17	2333.84	2333.80	+00.04	2333.84	2333.79	+00.05	2327.42	2327.40	+00.02	2327.37	2327.29	+00.08
18	2334.18	2334.14	+00.04	2334.18	2334.13	+00.05	2327.42	2327.40	+00.02	2327.37	2327.29	+00.08
19	2334.52	2334.48	+00.04	2334.52	2334.47	+00.05	2327.42	2327.40	+00.02	2327.37	2327.29	+00.08
20	2334.86	2334.82	+00.04	2334.86	2334.81	+00.05	2327.42	2327.40	+00.02	2327.37	2327.29	+00.08
21	2335.20	2335.16	+00.04	2335.20	2335.15	+00.05	2327.42	2327.40	+00.02	2327.37	2327.29	+00.08
22	2335.54	2335.50	+00.04	2335.54	2335.49	+00.05	2327.42	2327.40	+00.02	2327.37	2327.29	+00.08
23	2335.88	2335.84	+00.04	2335.88	2335.83	+00.05	2327.42	2327.40	+00.02	2327.37	2327.29	+00.08
24	2336.22	2336.18	+00.04	2336.22	2336.17	+00.05	2327.42	2327.40	+00.02	2327.37	2327.29	+00.08
25	2336.56	2336.52	+00.04	2336.56	2336.51	+00.05	2327.42	2327.40	+00.02	2327.37	2327.29	+00.08
26	2336.90	2336.86	+00.04	2336.90	2336.85	+00.05	2327.42	2327.40	+00.02	2327.37	2327.29	+00.08
27	2337.24	2337.20	+00.04	2337.24	2337.19	+00.05	2327.42	2327.40	+00.02	2327.37	2327.29	+00.08
28	2337.58	2337.54	+00.04	2337.58	2337.53	+00.05	2327.42	2327.40	+00.02	2327.37	2327.29	+00.08
29	2337.92	2337.88	+00.04	2337.92	2337.87	+00.05	2327.42	2327.40	+00.02	2327.37	2327.29	+00.08
30	2338.26	2338.22	+00.04	2338.26	2338.21	+00.05	2327.42	2327.40	+00.02	2327.37	2327.29	+00.08
31	2338.60	2338.56	+00.04	2338.60	2338.55	+00.05	2327.42	2327.40	+00.02	2327.37	2327.29	+00.08
32	2338.94	2338.90	+00.04	2338.94	2338.89	+00.05	2327.42	2327.40	+00.02	2327.37	2327.29	+00.08
33	2339.28	2339.24	+00.04	2339.28	2339.23	+00.05	2327.42	2327.40	+00.02	2327.37	2327.29	+00.08
34	2339.62	2339.58	+00.04	2339.62	2339.57	+00.05	2327.42	2327.40	+00.02	2327.37	2327.29	+00.08
35	2339.96	2339.92	+00.04	2339.96	2339.91	+00.05	2327.42	2327.40	+00.02	2327.37	2327.29	+00.08

4.4.5. Distribution functions

If we deal with only one vibrational transition we obtain from Eq. (7):

$$I_{K''}^{K'} \propto \nu^3 S_{K'K''} R(K') \quad (8)$$

For free rotational lines the distribution function $R(K')$ can easily be obtained from this relation.

We investigate whether the distribution over the rotational levels can be described by a Boltzmann distribution:

$$R(K') = e^{-hcB_v K'(K'+1)/kT_v} \quad (9)$$

where $hcB_v K'(K'+1)$ is the rotational energy, c is the velocity of light in vacuum, k is the Boltzmann constant and T_v is the Boltzmann temperature. In the case of dissociative excitation the Boltzmann temperature should be considered as a distribution parameter; it does not refer to some temperature in the system. Combining Eqs. (8) and (9) we have

$$I_{K''}^{K'} \propto \nu^3 S_{K'K''} e^{-hcB_v K'(K'+1)/kT_v} \quad (10)$$

In the case of a Boltzmann distribution a plot of $\ln(I/S\nu^3)$ versus $K'(K'+1)$ gives a straight line with a slope equal to $-hcB_v/kT_v$.

4.5. RESULTS

The $\text{CH}(A^2\Delta - X^2\Pi)$ spectrum obtained in this experiment has a complex structure due to overlap of the different branches of the 0-0, 1-1 and 2-2 vibrational transitions. In the case of the 0-0 band the R branch is almost in a spectral free range at higher rotational quantum numbers ($K \geq 7$). For these lines we can apply Eq. (10). In Fig. 4.2 it can be seen that a plot of $\ln(I/S\nu^3)$ versus $K'(K'+1)$ yields a straight line. This indicates that the distribution of molecules over the higher rotational levels of the $\text{CH}(A^2\Delta, v'=0)$ state can be described by a Boltzmann distribution. From the slope of the straight line we derive $T_0 = 2700 \pm 150^\circ\text{K}$. A spectrum of the 0-0 transition computed for several values of T_0 is

shown in Fig. 4.3. It follows that the intensities in the R branch are rather sensitive to the temperature parameter.

For the 1-1 and 2-2 vibrational transitions only a small number of free lines with relatively high K are present in the R branch. Assuming a Boltzmann distribution also in the $v'=1$ and $v'=2$ states we can roughly determine the temperature parameter. However, a greater accuracy is obtained by including in the analysis also lines which are not free from overlap. This is done by simulation of the $\text{CH}(A^2\Delta - X^2\Pi, 0-0, 1-1, 2-2)$ spectrum on the computer. The intensity of each line is calculated by a relation similar to Eq. (10).

$$I_{v''K''}^{v'K'} = \alpha_{v'} v^3 S_{K'K''} e^{-E_R^{v'}/kT_{v'}} \quad (11)$$

where $\alpha_{v'}$ is the relative intensity of the vibrational transition, $E_R^{v'}$ is the rotational energy and $T_{v'}$ is the temperature parameter. Next the spectrum is convoluted by scanning a window, determined by the intensity of the lines and the dispersion and slit width of the monochromator, through the calculated

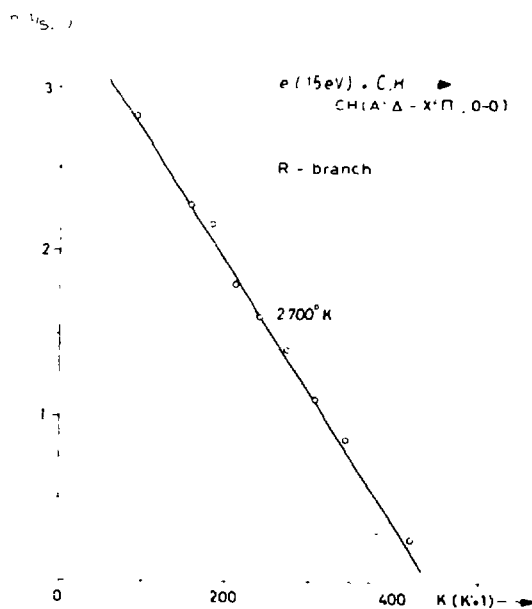
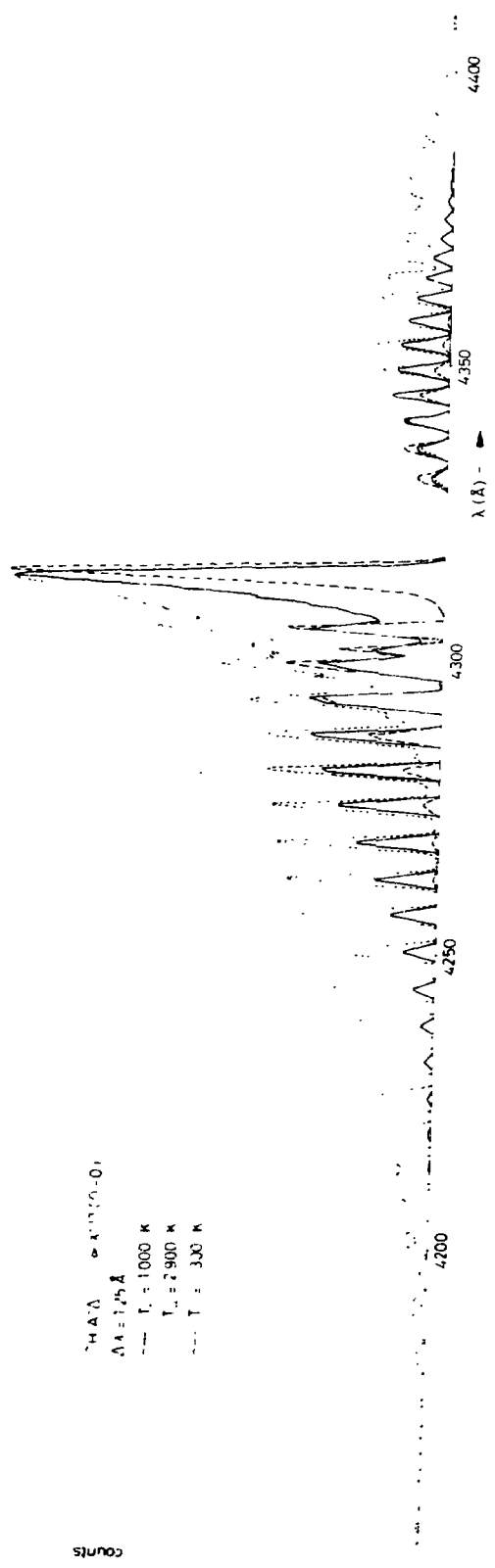


FIGURE 4.2. Plot of $\ln(I/Sv^3)$ versus $K'(K'+1)$ for $\text{CH}(A^2\Delta - X^2\Pi, 0-0)$.



$\text{CH}(A^2\Delta - X^2\Pi, 0-0)$
 $\Delta\lambda = 1.25 \text{ \AA}$
 $T_{\text{ex}} = 1000 \text{ K}$
 $T_{\text{ex}} = 2900 \text{ K}$
 $T = 330 \text{ K}$

FIGURE 4.3. Computed spectrum of the $\text{CH}(A^2\Delta - X^2\Pi, 0-0)$ transition.

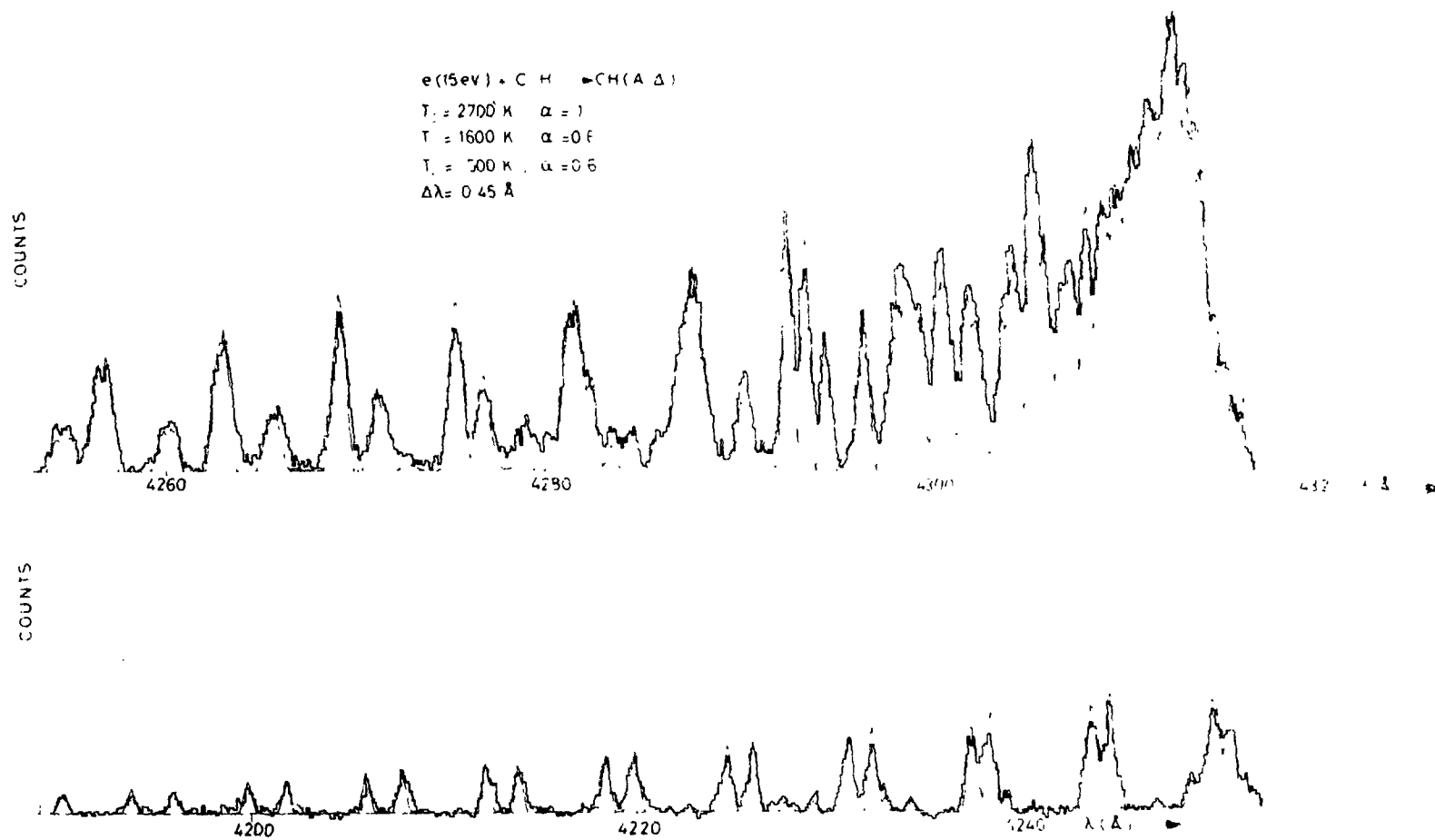


FIGURE 4.4. Comparison of the calculated and the experimental $CH(A^2\Delta - X^2\Pi)$ spectrum.

line spectrum (see appendix). After various computer scans using different values of α_v , and T_v , a good agreement between the calculated and the experimental spectrum is obtained for (Fig. 4.4):

$$\begin{aligned} T_0 &= 2700^\circ\text{K}; \alpha_0 = 1 \\ T_1 &= 1600^\circ\text{K}; \alpha_1 = 0.6 \\ T_2 &= 500^\circ\text{K}; \alpha_2 = 0.6 \end{aligned}$$

The corresponding Boltzmann distributions are shown in Fig. 4.5. Only a few discrepancies can be observed between the calculated and the experimental spectrum. These are probably due to radiation from other excited species as is the case near 4278 \AA , where N_2^+ radiation from background gas in the collision chamber is present.

Because the Franck-Condon factors of the 0-0, 1-1 and 2-2 transitions are almost equal to unity (see Section 4.4.2) we derive from Eqs. (7) and (11):

$$N_v \propto \alpha_v Q_{r,v} \quad (12)$$

The rotational state sum can be calculated from Eqs. (6) and (9) by summing

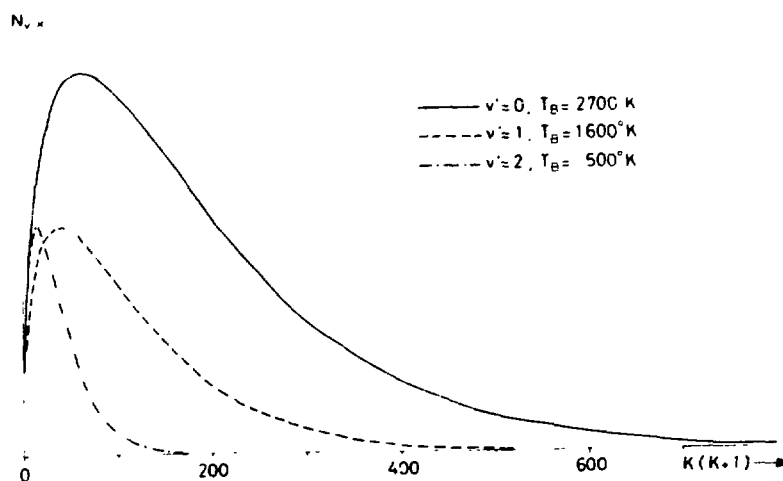


FIGURE 4.5. Boltzmann distributions over the rotational levels of the $CH(A^2\Delta, v'=0,1,2)$ states.

from $K'=2$ on. We obtain:

$$Q_{r,0} = 125.0$$

$$Q_{r,1} = 76.4$$

$$Q_{r,2} = 22.9$$

To a good approximation $Q_{r,v}$ can be put equal to kT/hcB (see Ref. 3) giving:

$$N_v \propto \alpha_v T_v \quad (13)$$

Considering the uncertainties in α_v, T_v , of 5% for $v'=0$ and 30% for $v'=1,2$, as estimated from the computer scans, we find for the relative population of the vibrational levels of the $CH(A^2\Delta)$ molecule (Eq. (12)) the following:

$$N_0 = 0.68 \pm 0.03$$

$$N_1 = 0.25 \pm 0.08$$

$$N_2 = 0.07 \pm 0.02$$

If for the population of the vibrational levels also a Boltzmann distribution is assumed then these numbers can be fitted by a temperature parameter of 3500 ± 500 °K.

4.6. DISCUSSION

Brennen and Carrington [1] and Clerc and Schmidt [2] have determined the rotational distribution function of the 0-0 band by the method of plotting $\ln(I/Sv^3)$ for the R branch versus $K'(K'+1)$ (see above). In their experiments the resolution amounts to 2 Å and 3 Å respectively. They found that the intensity distribution can be described by two Boltzmann distributions over the vibrationless $A^2\Delta$ state. One Boltzmann distribution is described by a high temperature parameter, the other by a low temperature parameter. The high Boltzmann temperature is explained as due to the direct process of the formation of $CH(A^2\Delta)$, the low temperature by collisional relaxation of excited CH radicals. From the calculated spectrum (Fig. 4.6) it follows that at wavelengths near 4300 Å the R branch is strongly contaminated by the Q branch. In that wavelength region the R branch consists of transitions involving low rotational quantum numbers. If we neglect the contamination by the Q branch, as done in Refs. 1 and 2, we find too high intensities of the R branch transitions towards lower values of K. This may give rise to an apparent deviation from the straight line in the $\ln(I/Sv^3)$ versus

$K'(K'+1)$ plot, which can erroneously be attributed to a second Boltzmann distribution with a low temperature parameter. The description of the intensity distribution in one vibrational transition by two functions should therefore be considered with some reserve.

There is no *a priori* reason to assume a Boltzmann distribution over the vibrational and rotational levels of the $\text{CH}(\text{A}^2\Delta)$ molecule formed by dissociative excitation of acetylene. Theoretical calculations of the distribution of rotational and vibrational energy after dissociative excitation have been performed by Horie *et al.* [8,9] for various molecules, but not for the splitting of acetylene into $\text{CH}(\text{A}^2\Delta)$. In their theory the excess energy, which is equal to the difference between the vertical energy and the adiabatic energy for formation of the fragments, is distributed among the vibrational, rotational and translational degrees of freedom in a statistical way. The calculated distributions depend therefore on the excess energy.

It has been shown before (Section 3.2.2) that $\text{CH}(\text{A}^2\Delta)$ is formed by several excitation processes, each process probably giving rise to a different excess energy. In addition $\text{CH}(\text{A}^2\Delta - \text{X}^2\Pi)$ spectra taken from methane, ethylene and ethane closely resemble that taken from acetylene. The excess energies

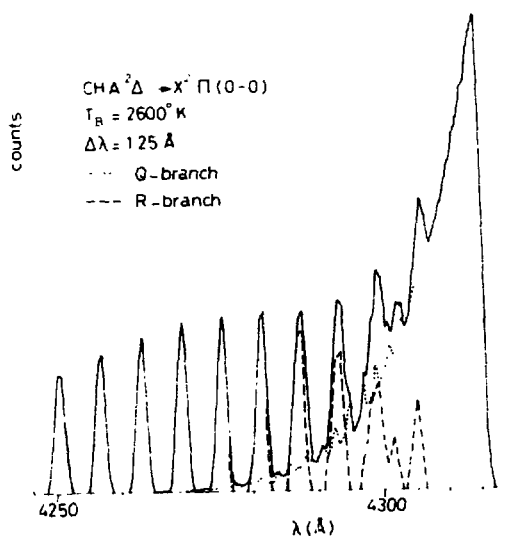


FIGURE 4.6. Part of the calculated $\text{CH}(\text{A}^2\Delta - \text{X}^2\Pi, 0-0)$ spectrum for $T_0 = 2600^\circ\text{K}$, showing the overlap of the Q and R branches.

with which the excited CH radicals are formed differ in the various molecules (see Section 3.2 and Ref. 10). Therefore, we do not think that the present results can be completely explained by the theory of Horie *et al.*¹. We intend to do further experimental and theoretical investigations on this subject.

REFERENCES

- [1] W. Brennen and T. Carrington, J.Chem.Phys. 46 (1967) 7.
- [2] M. Clerc and M. Schmidt, Far.Disc.Chem.Soc. 53 (1972) 2,7.
- [3] G. Herzberg, Spectra of Diatomic Molecules (Van Nostrand, Princeton, 1950).
- [4] R.S. Mulliken, Rev.Mod.Phys. 3 (1931) 89.
- [5] I. Kovács, Rotational Structure in the Spectra of Diatomic Molecules (Adam Hilger Ltd., London, 1969).
- [6] D.R. Childs, J.Quant.Radiat.Transfer 4 (1964) 283.
- [7] L. Gerö, Z.Phys. 118 (1941) 27.
- [8] S. Watanabe, T. Kasuga and T. Horie, Progr.Theor.Phys. 39 (1968) 564.
- [9] M. Kimura, S. Watanabe and T. Horie, J.Phys.Soc.Jap. 32 (1972) 1348.
- [10] J.F.M. Aarts, C.I.M. Beenakker and F.J. de Heer, Physica 53 (1971) 32.

A P P E N D I X

ANALYSIS OF THE INTENSITY DISTRIBUTION IN THE ROTATIONAL STRUCTURE OF THE ELECTRONIC SPECTRA OF DIATOMIC MOLECULES BY COMPUTER SIMULATION. APPLICATION TO THE $\text{CH}(A^2\Delta - X^2\Pi)$ TRANSITION.

PROGRAM SUMMARY

Title of program: ROSCOS

Catalogue number:

Program obtainable from: CPC Program Library, Queen's University of Belfast,
Northern Ireland (see application form in this issue).

Computer: El-X8; Installation: Mathematisch Centrum, Amsterdam, The Netherlands.

Operating system: MILLI.

Programming language used: ALCOL 60.

High speed storage required: 39458 words. Number of bits in a word: 27.

Is this program overlaid? No.

Number of magnetic tapes required: None.

What other peripherals are used? Card reader; Line printer; Plotter.

Number of cards in combined program and test deck: 1266.

Card punching code: MC code (IBM-29).

Keywords: Diatomic Molecules, Wavelength, Line-strengths, Intensity, Convolution, Plotting of Spectrum, Rotational Band Spectrum.

Nature of the physical problem

This program is concerned with the analysis of the intensity distribution in the rotational structure of the $\text{CH}(A^2\Delta - X^2\Pi)$ spectrum, produced by dissociative excitation of simple aliphatic hydrocarbons (CH_4 , C_2H_2 , C_2H_4 , C_2H_6) by electron impact.

Method of solution

When the resolving power of the monochromator does not allow one to separate all lines contributing to the spectrum, the intensity distribution in the rotational structure can be established by simulation of the experimental spectrum on the computer by a convolution technique. For this purpose, the wavelengths, line-strengths and intensities of the rotational transitions are calculated. Relevant formulae are given by Kovács [1]. The wavelengths, which have been determined experimentally by Gerö [2], are read in. The intensity is calculated by applying a Boltzmann distribution over the rotational levels.

Restrictions on the complexity of the problem

The program is restricted to the calculation of a $^2\Delta - ^2\Pi$ transition. It can also be applied to singlet-singlet and other doublet-doublet transitions, when relevant parts of the formulas are changed (see Ref. 1).

Typical running times

The running time depends on the number of lines to be convoluted. The test run required 225 sec for 1714 lines, including compilation, loading and syntax control.

REFERENCES

- [1] I. Kovács, Rotational Structure in the Spectra of Diatomic Molecules (Adam Hilger Ltd., London, 1969).
- [2] L. Gerö, Z.Phys. 118 (1941) 27.

LONG-WRITE-UP

1. Introduction

Methyldidyne (CH) molecules, excited into the $A^2\Delta$ state, show their presence in emission spectra by a complex band system extending from about 4150 - 4400 Å. This band system is attributed to the 0-0, 1-1 and 2-2 vibrational transitions of the $A^2\Delta - X^2\Sigma$ system. The numerous rotational lines, belonging to each vibrational transition, are not separated by most monochromators. Therefore, each peak in the spectrum is built up from several lines.

To analyse the intensity distribution over the rotational levels we used convolution rather than deconvolution, because the spectrum in the 4150 - 4400 Å region may be contaminated by emission from other excited species, like CH^+ and H, formed simultaneously in the dissociative excitation of aliphatic hydrocarbons. The ratios of the contributions of the 0-0, 1-1 and 2-2 vibrational transitions to the total spectrum and the Boltzmann temperatures are used as parameters to fit the convoluted spectrum to the experimentally determined spectrum.

2. Basic formulas

2.1. Wavelength calculation

The rotational term values of the components of a doublet state are given by:

$$F_1[J] = B_v \left[(J + \frac{1}{2})^2 - \Lambda^2 - \frac{1}{2} \sqrt{4(J + \frac{1}{2})^2 + Y(Y-4)} \Lambda^2 \right] - D_v J^4 \quad (1a)$$

$$F_2[J] = B_v \left[(J + \frac{1}{2})^2 - \Lambda^2 + \frac{1}{2} \sqrt{4(J + \frac{1}{2})^2 + Y(Y-4)} \Lambda^2 \right] - D_v (J+1)^4 \quad (1b)$$

where J is the total angular momentum, Λ represents the component of the electronic orbital angular momentum along the internuclear axis, Y is a measure of the strength of the coupling between Λ and the spin; B_v and D_v are rotational constants, depending on the vibrational quantum number v.

Except at low values of J both the $A^2\Lambda$ and $X^2\Pi$ states belong to Hund's case b [1]. In that case it is convenient to introduce the quantum number K , the total angular momentum apart from spin. Formulas 1a and 1b can then be recast in the form:

$$F_1[K] = B_V[K(K+1) - \Lambda^2] - D_V(K + \frac{1}{2})^4 + B_V(K+1)(1 - \sqrt{1 + Y(Y-4)\Lambda^2/4(K+1)^2}) + \gamma K/2 \quad (2a)$$

$$F_2[K] = B_V[K(K+1) - \Lambda^2] - D_V(K + \frac{1}{2})^4 + B_V K(1 - \sqrt{1 + Y(Y-4)\Lambda^2/4K^2}) - \gamma(K+1)/2 \quad (2b)$$

$F_1[K]$ refers to the spin component with $J=K+\frac{1}{2}$ and $F_2[K]$ to that with $J=K-\frac{1}{2}$. The term containing γ refers to the spin splitting. Each component is further splitted by Λ -type doubling:

$$F_{1c}[K] = F_1[K] + \frac{1}{2}\lambda K(K+1) \quad (3a)$$

$$F_{1d}[K] = F_1[K] - \frac{1}{2}\lambda K(K+1) \quad (3b)$$

$$F_{2c}[K] = F_2[K] + \frac{1}{2}\lambda K(K+1) \quad (3c)$$

$$F_{2d}[K] = F_2[K] - \frac{1}{2}\lambda K(K+1) \quad (3d)$$

In Fig. 4.1. a schematic representation of the splitting of rotational terms is shown.

The frequency of a rotational transition is given by:

$$\nu = \nu_0 + F'[K'] - F''[K''] \quad (4)$$

where ν_0 is the band origin. The single prime always refers to the upper state and the double prime to the lower state. The possible values of K are $\Lambda, \Lambda+1, \Lambda+2, \dots$. For rotational transitions the following rigorous selection rule holds: $J'-J'' = -1, 0, +1$. If $J'-J'' = K'-K'' = -1, 0, +1$, we obtain the *P*, *Q* and *R* branches respectively. These are called main branches. If $\Delta J \neq \Delta K$ we obtain so called satellite branches. Furthermore, only some particular combinations of the subscripts *c* and *d* are possible, depending on the branch involved [2].

Using the notation $K''=K$ we find from the selection rules the following 8 satellite branches and 12 main branches.

$$P_{Q_{1c}2d}[K] = \nu_0 + F'_{1c}[K-1] - F''_{2d}[K] \quad (5a)$$

$$P_{Q_{1d}2c}[K] = \nu_0 + F'_{1d}[K-1] - F''_{2c}[K] \quad (5b)$$

$$Q_{P_{2c}1c}[K] = \nu_0 + F'_{2c}[K] - F''_{1c}[K] \quad (5c)$$

$$Q_{P_{2d}1d}[K] = \nu_0 + F'_{2d}[K] - F''_{1d}[K] \quad (5d)$$

$$Q_{R_{1c2c}}[K] = v_o + F'_{1c}[K] - F''_{2c}[K] \quad (5e)$$

$$Q_{R_{1d2d}}[K] = v_o + F'_{1d}[K] - F''_{2d}[K] \quad (5f)$$

$$R_{Q_{2c1d}}[K] = v_o + F'_{2c}[K+1] - F''_{1d}[K] \quad (5g)$$

$$R_{Q_{2d1c}}[K] = v_o + F'_{2d}[K+1] - F''_{1c}[K] \quad (5h)$$

$$P_{1cd}[K] = v_o + F'_{1c}[K-1] - F''_{1d}[K] \quad (5i)$$

$$P_{1dc}[K] = v_o + F'_{1d}[K-1] - F''_{1c}[K] \quad (5k)$$

$$P_{2cd}[K] = v_o + F'_{2c}[K-1] - F''_{2d}[K] \quad (5l)$$

$$P_{2dc}[K] = v_o + F'_{2d}[K-1] - F''_{2c}[K] \quad (5m)$$

$$Q_{1c}[K] = v_o + F'_{1c}[K] - F''_{1c}[K] \quad (5n)$$

$$Q_{1d}[K] = v_o + F'_{1d}[K] - F''_{1d}[K] \quad (5o)$$

$$Q_{2c}[K] = v_o + F'_{2c}[K] - F''_{2c}[K] \quad (5p)$$

$$Q_{2d}[K] = v_o + F'_{2d}[K] - F''_{2d}[K] \quad (5q)$$

$$R_{1cd}[K] = v_o + F'_{1c}[K+1] - F''_{1d}[K] \quad (5r)$$

$$R_{1dc}[K] = v_o + F'_{1d}[K+1] - F''_{1c}[K] \quad (5s)$$

$$R_{2cd}[K] = v_o + F'_{2c}[K+1] - F''_{2d}[K] \quad (5t)$$

$$R_{2dc}[K] = v_o + F'_{2d}[K+1] - F''_{2c}[K] \quad (5u)$$

The constants used in the calculations are given in Table 4.6.

2.2. Line-strength calculation

In the notation $K''=K$ the line-strengths or Hönl-London factors for the rotational transitions are given by the following formulae [3]:

$$S(P_1)[K] = \frac{(K-\Lambda''-1)(K-\Lambda'')}{8(K+\frac{1}{2})C'^{-}[K]C''^{-}[K+1]} \{u'^{-}[K]u''^{-}[K+1]+4(K-\Lambda''+1)(K+\Lambda''+1)\}^2 \quad (6a)$$

$$S(P_2)[K] = \frac{(K-\Lambda''-2)(K-\Lambda''-1)}{8(K-\frac{1}{2})C'^{+}[K-1]C''^{+}[K]} \{u'^{+}[K-1]u''^{+}[K]+4(K-\Lambda'')(K+\Lambda'')\}^2 \quad (6b)$$

$$S(Q_1)[K] = \frac{(K-\Lambda'')(K+1)(K+\Lambda''+2)}{4(K+\frac{1}{2})(K+3/2)C'^{-}[K+1]C''^{-}[K+1]} \{u'^{-}[K+1]u''^{-}[K+1]+4(K-\Lambda''+1)(K+\Lambda''+1)\}^2 \quad (6c)$$

$$S(Q_2)[K] = \frac{(K-\Lambda''-1)K(K+\Lambda''+1)}{4(K-\frac{1}{2})(K+\frac{1}{2})C'^{+}[K]C''^{+}[K]} \{u'^{+}[K]u''^{+}[K]+4(K-\Lambda'')(K+\Lambda'')\}^2 \quad (6d)$$

$$S(R_1)[K] = \frac{(K+\Lambda''+2)(K+\Lambda''+3)}{8(K+3/2)C''-[K+2]C''-[K+1]} \{u'^-[K+2]u''-[K+1]+4(K-\Lambda''+1)(K+\Lambda''+1)\}^2 \quad (6e)$$

$$S(R_2)[K] = \frac{(K+\Lambda''+1)(K+\Lambda''+2)}{8(K+1/2)C''+[K+1]C''+[K]} \{u'^+[K+1]u''+[K]+4(K-\Lambda'')(K+\Lambda'')\}^2 \quad (6f)$$

$$S(P_{12})[K] = \frac{(K-\Lambda''-1)(K+\Lambda''+1)}{4(K-1/2)(K+1/2)C''-[K]C''+[K]} \{u'^-[K]u''+[K]-4(K-\Lambda'')(K+\Lambda'')\}^2 \quad (6g)$$

$$S(Q_{21})[K] = \frac{(K-\Lambda''-1)(K-\Lambda'')}{8(K+1/2)C''+[K]C''-[K+1]} \{u'^+[K]u''-[K+1]-4(K-\Lambda''+1)(K+\Lambda''+1)\}^2 \quad (6h)$$

$$S(Q_{12})[K] = \frac{(K+\Lambda''+1)(K+\Lambda''+2)}{8(K+1/2)C''-[K+1]C''+[K]} \{u'^-[K+1]u''+[K]-4(K-\Lambda'')(K+\Lambda'')\}^2 \quad (6i)$$

$$S(R_{21})[K] = \frac{(K-\Lambda'')(K+1)(K+\Lambda''+2)}{4(K+1/2)(K+3/2)C''+[K+1]C''-[K+1]} \{u'^+[K+1]u''-[K+1]-4(K-\Lambda''+1)(K+\Lambda''+1)\}^2 \quad (6k)$$

Furthermore we have

$$u'^+[K] = \sqrt{Y'(Y'-4)\Lambda'^2+4K^2} + \Lambda'(Y'-2) \quad (7a)$$

$$u'^-[K] = \sqrt{Y'(Y'-4)\Lambda'^2+4K^2} - \Lambda'(Y'-2) \quad (7b)$$

$$u''+[K] = \sqrt{Y''(Y''-4)\Lambda''^2+4K^2} + \Lambda''(Y''-2) \quad (7c)$$

$$u''-[K] = \sqrt{Y''(Y''-4)\Lambda''^2+4K^2} - \Lambda''(Y''-2) \quad (7d)$$

and

$$C'^+[K] = \frac{1}{2}\{u'^+[K]^2+4(K^2-\Lambda'^2)\} \quad (8a)$$

$$C'^-[K] = \frac{1}{2}\{u'^-[K]^2+4(K^2-\Lambda'^2)\} \quad (8b)$$

$$C''+[K] = \frac{1}{2}\{u''+[K]^2+4(K^2-\Lambda''^2)\} \quad (8c)$$

$$C''-[K] = \frac{1}{2}\{u''-[K]^2+4(K^2-\Lambda''^2)\} \quad (8d)$$

The line-strengths of the $O_2[2]$ and $P_2[3]$ transitions have been calculated using the case b formulas given by Mulliken [2]. The two components of Λ -type doubling are given an equal line-strength.

2.3. Intensity calculation

Employing a Boltzmann distribution over the rotational levels, the intensity $I_{K'K''}$ of a rotational line is given by:

$$I_{K'K''} = \nu_{K'K''}^3 S_{K'K''} e^{-hcF'[K']/kT} \quad (9)$$

These calculations are done for the 0-0, 1-1 and 2-2 vibrational transitions. The ratio of the contributions of these transitions to the total spectrum and the Boltzmann temperature are used as parameters to fit the calculated spectrum to the experimentally determined spectrum.

3. Program description

The operations are accompanied by detailed comments in the program itself. The parameters and functions in the formulas have the following program names:

B_v : BV	u^+ : UPLS
D_v : DV	u^- : UMN
Y : Y	C^+ : CPLS
γ : GMM	C^- : CMN
Λ : LMBD	

These are preceded by the symbol L or U, which indicates whether the parameter or function refers to the lower or upper state respectively.

Example:

$u^+ = u^+$ for the lower state;

program name: LUPLS

The program has four important tasks:

- frequency calculation,
- line-strength calculation,
- intensity calculation,
- output.

After some preliminary runs on the computer we found out that the values of the constants D_v were not known with sufficient accuracy. By a trial and error method a value of D_0 was established which allowed a better agreement between the calculated and experimentally determined frequencies of Gerö [4]. An impression as to the quality of the frequency calculation can be obtained from Tables 4.3, 4.4 and 4.5. Only for the main branches are experimental frequencies known. These are read in, while the frequencies of the weaker satellite branches are calculated.

The parameters for the intensity calculation are the Boltzmann temperature (TEMP) and the relative population of the vibrational levels (INTRATIO).

TABLE 4.6

Values of the constants used in the calculations of the line-strength,
frequency and intensity.

Constant		Ref.
ν_o 0-0	= 23217.56 cm^{-1}	4,5,6
ν_o 1-1	= 23222.3 cm^{-1}	4,5,6
ν_o 2-2	= 23159.6 cm^{-1}	4,5,6
$B_{v''=0}$	= 14.190 cm^{-1}	4
$B_{v''=1}$	= 13.655 cm^{-1}	4
$B_{v''=2}$	= 13.122 cm^{-1}	4
$B_{v'=0}$	= 14.577 cm^{-1}	4
$B_{v'=1}$	= 13.907 cm^{-1}	4
$B_{v'=2}$	= 13.182 cm^{-1}	4
$D_{v''=0}$	= $1.432 \times 10^{-3} \text{ cm}^{-1}$	4
$D_{v''=1}$	= $1.39 \times 10^{-3} \text{ cm}^{-1}$	4
$D_{v''=2}$	= $1.39 \times 10^{-3} \text{ cm}^{-1}$	4
$D_{v'=0}$	= $1.564 \times 10^{-3} \text{ cm}^{-1}$	4
$D_{v'=1}$	= $1.58 \times 10^{-3} \text{ cm}^{-1}$	4
$D_{v'=2}$	= $1.65 \times 10^{-3} \text{ cm}^{-1}$	4
γ'	= 0.021 cm^{-1}	4
γ''	= -0.016 cm^{-1}	4
Y''	= $6.96/B_{v'}$	2
Y'	= 2.0	2
Λ''	= 2	1
Λ'	= 1	1
λ''	= 0 cm^{-1}	2
λ'	= 0.036 cm^{-1}	2

These are read in. The quantum sensitivity of the monochromator as a function of wavelength (EFF) is taken into account.

The output consists of two parts:

- a table of the lines used for the convolution of the spectrum via the line printer. These lines have the following properties:
 - a) the wavelength lies in the desired interval,
 - b) the intensity is larger than .01% of the intensity of the strongest line in the interval.
- a simulated spectrum via the plotter. This spectrum is formed from the 'ideal' line spectrum by scanning a window through this line spectrum. In the present case this window is a triangle, completely determined by the intensity of the lines and the slit width and dispersion of the monochromator.

4. Test run

Input desk for TEST RUN

K-VALUES AND FREQUENCIES

RELATIVE INTENSITY OF THE
VIBRATIONAL TRANSITIONS,
3 NUMBERS

TEMPERATURES,
3 NUMBERS

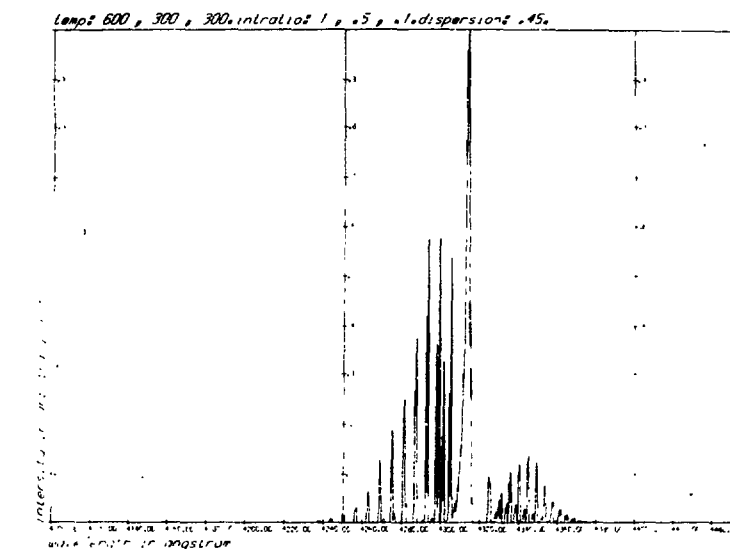
PROGRAM VARIABLES
EXPLANATION IN PROGRAM -
COMMENTS

WAVELENGTH	FREQUENCY	K	LINE NO	LINE STRENGTH	INTENSITY	NAME OF LINE
4310.11	23201.25	8	1005	+.1160+-0	+.6857+-11	Qp2D1C CH 0-0
4310.12	23201.25	8	344	+.8613+-1	+.5092+-13	Q1D CH 0-0
4310.19	23200.84	3	512	+.8651+-1	+.9272+-11	Q2C CH 1-1
4310.31	23200.17	8	529	+.7610+-1	+.2649+-12	Q2D CH 1-1
4310.31	23200.17	8	456	+.7610+-1	+.4498+-13	Q2C CH 0-0
4310.33	23200.10	8	1039	+.1600+-0	+.9459+-11	QR1C2C CH 0-0
4310.39	23199.74	9	376	+.9653+-1	+.1035+-12	Q1C CH 1-1
4310.43	23199.52	8	1345	+.1603+-0	+.5585+-10	QR1D2D CH 1-1
4310.59	23198.68	3	118	+.8613+-1	+.5090+-13	Q1C CH 0-0
4310.59	23198.66	8	971	+.1160+-0	+.6855+-11	Qp2C1D CH 0-0
4310.66	23196.31	8	392	+.8613+-1	+.2949+-12	Q1D CH 1-1
4310.69	23198.14	8	127	+.1622+-0	+.4045+-10	Qp2D1C CH 1-1
4310.77	23197.70	2	1646	+.4940+-0	+.1826+-12	Qp2D1C CH 2-2
4310.81	23197.48	2	1681	+.4340+-0	+.1854+-12	Qp2D1C CH 2-2
4310.84	23197.31	2	691	+.3470+-1	+.1310+-13	Q1C CH 2-2
4310.84	23197.31	2	722	+.3470+-1	+.1310+-13	Q1D CH 2-2
4310.84	23197.31	2	511	+.7610+-1	+.2648+-12	Q2C CH 1-1
4310.91	23196.97	7	480	+.6559+-1	+.6726+-13	Q2D CH 0-0
4310.92	23196.93	3	131	+.1603+-0	+.5683+-10	QR1C2C CH 1-1
4310.93	23196.57	7	1072	+.1846+-0	+.1894+-12	QR1D2D CH 0-0
4311.03	23194.30	7	528	+.6559+-1	+.6530+-12	Q2D CH 1-1
4311.11	23195.88	8	374	+.8613+-1	+.2948+-12	Q1C CH 1-1
4311.15	23195.68	7	1346	+.6500+-0	+.8444+-11	QR1D2D CH 1-1
4311.17	23195.55	3	243	+.1622+-0	+.4044+-10	Qp2D1C CH 1-1
4311.28	23194.99	7	1008	+.1381+-0	+.1313+-12	Qp2D1C CH 0-0
4311.31	23194.83	7	343	+.7562+-1	+.7566+-13	Q1D CH 0-0
4311.31	23194.83	7	454	+.6559+-1	+.6724+-13	Q2C CH 0-0
4311.36	23194.56	7	1038	+.1846+-0	+.1894+-12	QR1C2C CH 0-0
4311.42	23194.19	7	391	+.7562+-1	+.7534+-12	Q2D CH 1-1
4311.42	23194.19	7	510	+.6559+-1	+.6528+-12	Q2C CH 1-1
4311.43	23194.17	7	1276	+.1333+-0	+.1277+-11	Qp2D1C CH 1-1
4311.52	23193.66	7	1320	+.1850+-0	+.1843+-11	QR1C2C CH 1-1
4311.65	23192.97	7	970	+.1381+-0	+.1312+-12	Qp2C1D CH 0-0
4311.67	23192.87	6	527	+.5492+-1	+.1763+-13	Q2D CH 1-1
4311.67	23192.87	7	317	+.7562+-1	+.7756+-13	Q1C CH 0-0
4311.76	23192.41	7	373	+.7562+-1	+.7532+-12	Q1C CH 1-1
4311.78	23192.28	6	1343	+.2685+-0	+.5487+-11	QR1D2D CH 1-1
4311.80	23192.15	6	1242	+.1293+-0	+.1277+-11	Qp2C1D CH 1-1
4311.90	23191.64	6	470	+.5492+-1	+.9332+-13	Q2D CH 0-0
4311.90	23191.64	6	500	+.5492+-1	+.1375+-13	Q2C CH 1-1
4311.99	23191.21	6	1071	+.2680+-0	+.3628+-12	QR1D2D CH 0-0
4312.06	23190.76	6	1309	+.2685+-0	+.5494+-11	QR1C2C CH 1-1
4312.09	23190.58	6	1275	+.1428+-0	+.3576+-11	Qp2D1C CH 1-1
4312.10	23190.56	5	526	+.4402+-1	+.2437+-13	Q2D CH 1-1
4312.10	23190.56	6	390	+.6495+-1	+.1629+-13	Q1D CH 1-1

WAVELENGTH	FREQUENCY	K	LINE NO	LINE STRENGTH	INTENSITY	NAME OF LINE
4312.20	23190.01	6	453	+.5492** 1	+.9130**13	Q2C
4312.26	23189.70	6	1037	+.2180** 0	+.3627**12	QR1C2C
4312.31	23180.43	6	1003	+.1426** 0	+.2370**12	QR2D1C
4312.32	23179.38	5	1342	+.2663** 0	+.1477**12	QR1C2D
4312.37	23189.12	6	342	+.6496** 1	+.1081**14	Q1D
4312.37	23189.12	6	372	+.6495** 1	+.1629**13	Q1C
4312.37	23189.12	1	854	+.1848** 1	+.1011**13	R2UC
4312.37	23189.12	1	879	+.1848** 1	+.1011**13	R2CD
4312.37	23189.12	5	508	+.4402** 1	+.2436**13	Q2C
4312.38	23189.07	6	1243	+.1428** 0	+.3575**11	QR2C1D
4312.52	23188.30	5	1308	+.2663** 0	+.1177**12	QR1C2C
4312.53	23188.26	4	525	+.3275** 1	+.3515**13	Q2D
4312.59	23187.92	6	900	+.1426** 0	+.2369**12	QR2C1D
4312.65	23187.62	6	316	+.6496** 1	+.1080**14	Q1C
4312.68	23187.42	5	1274	+.1603** 0	+.8870**11	QR2D1C
4312.71	23187.27	5	389	+.5405** 1	+.2098**13	Q1D
4312.71	23187.27	5	478	+.4022** 1	+.1109**14	Q2D
4312.71	23187.27	4	507	+.3275** 1	+.3515**13	Q2C
4312.75	23187.05	4	1341	+.3398** 0	+.3660**12	QR1D2D
4312.83	23186.65	5	1070	+.2658** 0	+.3701**12	QR1D2D
4312.83	23186.34	5	1240	+.1603** 0	+.8869**11	QR2C1D
4312.89	23186.33	4	1307	+.3398** 0	+.3629**12	QR1C2C
4312.94	23186.06	3	523	+.1451** 1	+.2854**13	Q2D
4312.94	23186.06	2	524	+.2085** 1	+.3804**13	Q2D
4312.94	23186.06	5	371	+.5405** 1	+.2998**13	Q1C
4312.94	23186.06	5	452	+.4402** 1	+.1109**14	Q2C
4312.94	23186.06	2	505	+.1051** 1	+.2854**13	Q2C
4312.94	23186.06	3	506	+.2085** 1	+.3804**13	Q2C
4313.03	23185.57	3	1036	+.2658** 0	+.6700**12	QR1C2C
4313.05	23185.44	3	1340	+.4667** 0	+.8556**12	QR1D2D
4313.13	23185.00	3	1306	+.4667** 0	+.8556**12	QR1C2C
4313.14	23184.98	2	1339	+.7346** 0	+.2009**13	QR1D2D
4313.18	23184.76	2	1205	+.7346** 0	+.2009**13	QR1C2C
4313.19	23184.69	4	1273	+.1808** 0	+.1940**12	QR2D1C
4313.21	23184.59	5	1002	+.1600** 0	+.4030**12	QR2D1C
4313.29	23184.15	5	341	+.5406** 1	+.1363**14	Q1C
4313.29	23184.15	4	388	+.4277** 1	+.4604**14	Q1D
4313.32	23183.97	4	1277	+.1800** 0	+.1939**12	QR2C1D
4313.37	23183.74	4	370	+.4277** 1	+.4604**14	Q1C
4313.37	23183.74	4	477	+.3275** 1	+.1157**14	Q2D
4313.41	23183.51	5	908	+.1600** 0	+.4039**12	QR2C1D
4313.51	23183.00	5	315	+.5406** 1	+.1363**14	Q1C
4313.51	23183.00	4	451	+.3275** 1	+.1167**14	Q2C
4313.51	23182.96	4	1009	+.3392** 0	+.1311**13	QR1D2D
4313.62	23182.40	3	1272	+.2011** 0	+.3668**12	QR2D1C

WAVELENGTH	FREQUENCY	K	LINE NO	LINE STRENGTH	INTENSITY	NAME OF LINE	
4313.65	23182.24	4	1034	+3792 _m -0	+121 _m +13	GR1C2C	C-0-0
4313.70	23181.97	3	1234	+2011 _m -0	+3658 _m +12	GR2C1D	C-1-1
4313.74	23181.72	3	387	+3379 _m +1	+3642 _m +13	Q1C	C-1-1
4313.81	23181.39	3	369	+3379 _m +1	+3642 _m +13	Q1C	C-1-1
4313.81	23181.39	3	476	+2785 _m +1	+9813 _m +13	Q2C	C-0-0
4313.92	23180.78	2	449	+1051 _m +1	+6091 _m +13	Q2C	C-0-0
4313.92	23180.78	3	450	+2095 _m +1	+9813 _m +13	Q2C	C-0-0
4313.92	23180.78	2	475	+1051 _m +1	+6091 _m +13	Q2D	C-0-0
4313.97	23180.48	4	1061	+1405 _m -0	+6429 _m +12	GR1D1C	C-0-0
4314.01	23180.27	3	1068	+4459 _m -0	+219 _m +13	GR1D2D	C-0-0
4314.09	23179.84	3	1064	+4659 _m -0	+219 _m +13	GR1C3C	C-0-0
4314.11	23179.76	4	967	+1915 _m -0	+5470 _m +12	GR2C1D	C-0-0
4314.11	23179.75	4	340	+4378 _m +1	+526 _m +14	Q1D	C-0-0
4314.24	23179.05	2	1067	+7135 _m -0	+4266 _m +13	GR1D2D	C-0-0
4314.24	23179.05	4	514	+4278 _m +1	+526 _m +14	Q1C	C-0-0
4314.24	23179.05	2	1063	+1735 _m +1	+4113 _m +13	Q1C	C-1-1
4314.24	23179.05	2	386	+1735 _m +1	+4743 _m +13	Q1D	C-1-1
4314.28	23178.84	2	1137	+7135 _m -0	+4266 _m +13	GR1C2C	C-0-0
4314.61	23177.08	3	1061	+2709 _m -0	+9448 _m +12	GR2D1*	C-0-0
4314.69	23176.64	3	755	+2709 _m -0	+9448 _m +12	GR2C1D	C-0-0
4314.80	23176.04	3	339	+3080 _m +1	+1452 _m +14	Q1D	C-0-0
4314.87	23175.60	3	317	+3080 _m +1	+1452 _m +14	Q1C	C-0-0

SCALING FACTOR ON PLOT: +.5875_m+14



REFERENCES

- [1] G. Herzberg, Spectra of Diatomic Molecules (Van Nostrand, Princeton, 1950).
- [2] R.S. Mulliken, Rev.Mod.Phys. 3 (1931) 89. In the formulas for the line-strength of the R_1 and R_2 branches (p.126) a factor $(K+1)$ and $(K-1)$ has been omitted in the numerator.
- [3] I. Kovács, Rotational Structure in the Spectra of Diatomic Molecules (Adam Hilger Ltd., London, 1969).
- [4] L. Gerö, Z.Phys. 118 (1941) 27.
- [5] Ref. 1, p.518.
- [6] R.H. Garstang, Proc.Phys.Soc. 82 (1963) 545.

CHAPTER V

D I S S O C I A T I V E E X C I T A T I O N O F W A T E R.

5.1. INTRODUCTION

Several investigations on the dissociative excitation of water by electron impact have been made by studying the emission of light. Vroom and de Heer [1] measured absolute cross sections for Lyman α and Balmer α , β , γ and δ emission. Böse and Sroka [2] determined appearance potentials and cross sections for excited fragments, which emit light in the wavelength region 500 - 1250 Å. Lawrence [3] studied $O(3p^3P - 3s^3S^o)$ and $O(3p^5P - 3s^5S^o)$ emission. Radiation from the excited OH radical has been investigated by Hayakawa [4], by Sushanin and Kishko [5] and by Tsurubuchi *et al.* [6]. The latter two studied also Balmer emission. The dissociative excitation of water by electron impact has been reviewed by Olivero, Stagat and Green [7].

In the above mentioned studies large discrepancies appear both in the absolute values of the emission cross sections and in their energy dependence. In addition only in a few cases have thresholds for emission been measured. We started therefore a new study on the formation of excited fragments which radiate between 1850 and 9000 Å and which arise due to electrons with energies from 0 - 1000 eV. The thresholds and emission cross sections of various excited fragments are determined. A mechanism of their formation is discussed.

5.2. EXPERIMENTAL

The apparatus and experimental procedure to evaluate emission cross sections have been described in Chapter II. An error discussion is also given there. For Balmer and oxygen emission the energy scale has been calibrated against the He 4713 Å line, which has a known threshold at

23.5 eV [8], and the He 7065 Å line, which has a threshold at 22.6 eV [8]. The threshold for $\text{OH}(A^2\Sigma^+ - X^2\Pi)$ emission has been determined with respect to that for $\text{N}_2(C^3\Pi_u - B^3\Pi_g, 0-0)$ radiation, which is calculated to be 11.03 eV [9].

5.3. SPECTRUM

In the wavelength region 1850 - 9000 Å radiation from various excited fragments could be identified [9,10,11] (Table 5.1). For reasons of intensity and overlap with other band systems the cross section and threshold measurements were confined to $\text{OH}(A^2\Sigma^+ - X^2\Pi, 0-0, 1-1, 2-2)$, Balmer α , β , γ and δ , $\text{OI}(3p^3P - 3s^3S^0)$ and $\text{OI}(3p^5P - 3s^5S^0)$ radiation.

5.4. $\text{OH}(A^2\Sigma^+ - X^2\Pi)$ EMISSION

Radiation of the hydroxyl radical from the $A^2\Sigma^+$ state to the $X^2\Pi$ ground state is by far the strongest feature in the emission spectrum produced by electron impact on water. It shows its presence by a complex band system with a bandhead at 3064 Å, extending from 3060 - 3500 Å. This wavelength region includes the $\Delta v = 0$ sequence. The emission cross sections of this band system have been determined by an adding-up procedure (see Section

TABLE 5.1.

Emission observed by electron impact on water.		
$\lambda(\text{\AA})$	Transition	Name
2810 - 2950	$\text{OH } A^2\Sigma^+ \rightarrow X^2\Pi, 1-0, 2-1, 3-2$	3064 Å system
3060 - 3500	$\text{OH } A^2\Sigma^+ \rightarrow X^2\Pi, 0-0, 1-1, 2-2$	
4102	$\text{H } n=6 \rightarrow n=2$	Balmer δ
4340	$\text{H } n=5 \rightarrow n=2$	Balmer γ
4861	$\text{H } n=4 \rightarrow n=2$	Balmer β
6563	$\text{H } n=3 \rightarrow n=2$	Balmer α
7774	$\text{OI } 3p^5P \rightarrow 3s^5S^0$	
8447	$\text{OI } 3p^3P \rightarrow 3s^3S^0$	

2.5). This introduces an extra error of 5% in addition to an error of 15% from uncertainties in the gas pressure, electron beam intensity and quantum sensitivity of the optical equipment. The emission cross sections are collected in Table 5.2.

The 3064 Å system of OH has also been investigated by Hayakawa [4], by Sushanin and Kishko [5] and by Tsurubuchi *et al.* [6]. The first measured the energy dependence of the emission cross sections from 20 - 335 eV with a simple triode set-up. The other groups used a crossed beam method and measured absolute emission cross sections in the energy range 0 - 70 eV and 20 - 400 eV respectively. In Figure 5.1 the results on the energy dependence are compared by normalization of the maximum value of the emission cross section at unity in each experiment. From threshold to maximum our results agree with those of Sushanin and Kishko [5] and at energies above 100 eV with those of Hayakawa [4], but otherwise the agreement is poor. The discrepancies may be due to an insufficient suppression of secondary electrons and the use of too high electron beam currents, giving rise to a poor energy definition, in the experiments of Ref. 4, 5 and 6. The absolute emission cross sections, measured in a crossed beam

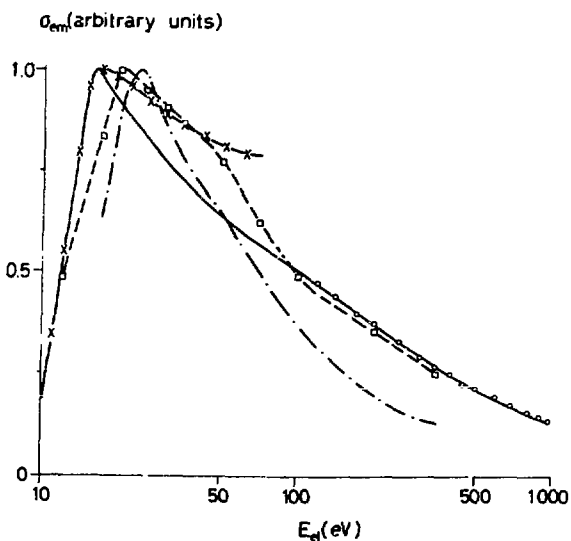


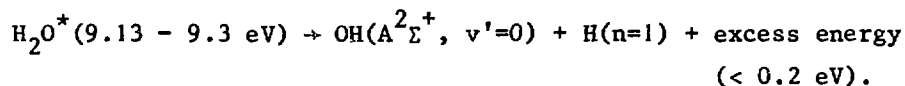
FIGURE 5.1. Energy dependence of the OH($A^2\Sigma^+ - X^2\Pi$) emission cross sections. -o-o-o-: present; -□-□-: Hayakawa [4]; -.-.-.-: Tsurubuchi *et al.* [6]; -x-x-x-: Sushanin and Kishko [5].

TABLE 5.2.

Emission cross sections in units of 10^{-19} cm^2 for electron impact on water.				
$E_{e1} \text{ (eV)}$	$\text{OH}(\text{A}^2\Sigma^+ \rightarrow \text{X}^2\Pi)$ 3064 Å	$\text{H}(n=4 \rightarrow 2)$ 4861 Å	$\text{OI}(\text{P}^2 \rightarrow \text{S}^0)$ 8447 Å	$\text{OI}(\text{P}^5 \rightarrow \text{S}^0)$ 7774 Å
40	66.3	3.06	1.40	0.945
50	60.3	4.04	1.88	1.16
60	56.6	5.25	2.30	1.29
70	53.5	5.89	2.54	1.33
80	50.8	6.25	2.70	1.32
90	48.3	6.40	2.80	1.28
100	46.4	6.41	2.86	1.26
120	43.2	6.13	2.87	1.17
140	40.0	5.83	2.59	1.02
170	36.4	5.22	2.53	0.804
200	33.9	4.86	2.32	0.734
250	29.7	4.18	1.90	0.540
300	26.6	3.68	1.67	0.461
350	24.0	3.27	1.45	0.425
400	22.4	2.92	1.30	0.362
450	20.6	2.62	1.13	0.347
500	19.6	2.39	1.05	0.282
600	17.9	2.05	0.892	0.244
700	15.8	1.82	0.784	0.172
800	14.9	1.61	0.680	0.170
900	13.1	1.47	0.586	0.160
1000	12.1	1.38	0.532	0.135

set-up, differ from the present results. At 300 eV Tsurubuchi *et al.* [6] determined a value of $(7.1 \pm 3.5) \times 10^{-18} \text{ cm}^2$, to be compared with our value of $(2.66 \pm 0.50) \times 10^{-18} \text{ cm}^2$; Sushanin and Kishko [5] found a maximum value of $4.1 \times 10^{-19} \text{ cm}^2$, which is about 20 times lower than our result.

We found the threshold for $\text{OH}(A^2\Sigma^+)$ at $9.0 \pm 0.3 \text{ eV}$, which is close to the value of 9.5 eV determined by Sushanin and Kishko. The minimum energy required to produce the OH fragment in the vibrationless and rotationless $A^2\Sigma^+$ state is calculated to be 9.13 eV [9]. The threshold corresponds therefore with excited states of water in the 9.13 - 9.3 eV range. It can be seen from Table 5.3 that these states dissociate by:



The energy dependence of the emission cross sections shows that these excited states of water are both singlet and triplet states. At high energies the Fano plot for $\text{OH}(A^2\Sigma^+)$ yields a straight line (Fig. 5.2).

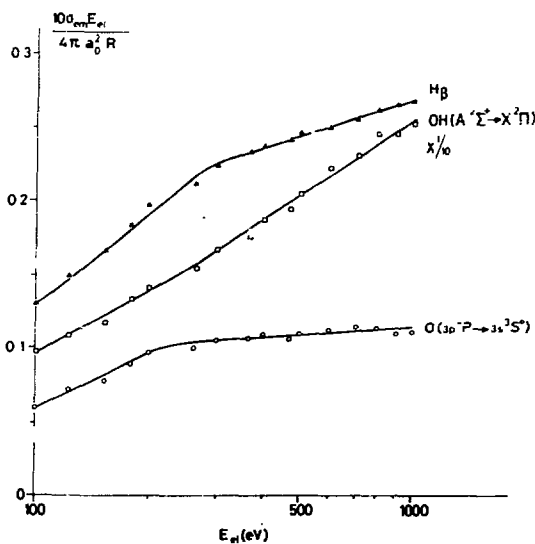


FIGURE 5.2. Emission cross sections presented in the form of a Fano plot.

TABLE 5.3.

Calculated minimum energies ^{a,b)} for formation of excited fragments by dissociative excitation of water	
Dissociation products	E(eV)
$H_2O(\tilde{X}^1 A_1) \rightarrow H(n=1) + OH(A^2 \Sigma^+)$	9.1
$\rightarrow H(n=3) + OH(X^2 \Pi)$	17.2
$\rightarrow H(n=4) + OH(X^2 \Pi)$	17.8
$\rightarrow H(n=5) + OH(X^2 \Pi)$	18.1
$\rightarrow H(n=3) + OH(A^2 \Sigma^+)$	21.2
$\rightarrow O(3p^3 P) + H_2(X^1 \Sigma_g^+)$	15.9
$\rightarrow O(3p^3 P) + H(n=1) + H(n=1)$	20.4
$\rightarrow O(3p^5 P) + H_2(X^1 \Sigma_g^+)$	15.7
$\rightarrow O(3p^5 P) + H(n=1) + H(n=1)$	20.2
$\rightarrow O(2p^4^3 P) + H(n=1) + H(n=3)$	21.5

a) $D(H-OH) = 5.11$ eV [12], $D(O-H) = 4.35$ eV [13], $D(H-H) = 4.48$ eV [13].

b) Excitation energies have been taken from Refs. 8, 10 and 13.

TABLE 5.4.

Transition	M_{em}^2 ^{a)}	c_{em}
H_α	$(1.41 \pm 0.12) \times 10^{-2}$	946
H_β	$(2.84 \pm 0.10) \times 10^{-3}$	151
H_γ	$(1.36 \pm 0.06) \times 10^{-3}$	38.4
H_δ	$(5.19 \pm 0.30) \times 10^{-4}$	24.1
$OH(3064 \text{ \AA})$	$(7.72 \pm 0.44) \times 10^{-2}$	0.387
$OI(3p^3 P \rightarrow 3s^3 S^0)$	$(1.03 \pm 0.31) \times 10^{-3}$	24500

a) Errors refer to the standard deviation in the slope of the Fano plot only.

The small value of c_{em} and the positive slope of this plot (Table 5.4) give evidence for optically allowed excitation processes leading to $\text{OH}(A^2\Sigma^+)$. At low electron impact energies (Fig. 5.3) the energy dependence of the $\text{OH}(3064 \text{ \AA})$ emission cross sections is characterized by a steep increase of the cross section for a few eV above the threshold, followed by a slow decrease. Such a behaviour is not expected for an optically allowed excitation process, in which case the maximum value of the cross section is reached at much higher energies. A maximum close to the threshold is, however, typical for an electron exchange process. For such a process the cross section decreases rapidly after having reached the maximum [14,15]. The energy dependence of the emission cross section near threshold is therefore interpreted as a superposition of an excitation process to triplet and singlet states, which then dissociate into $\text{OH}(A^2\Sigma^+)$. Because of the rapid decrease of the excitation cross section in the case of an electron exchange process with increasing energy of the incident electrons, the high energy results reflect only the excitation to the singlet manifold.

The contribution from both optically allowed excitation processes and electron exchange processes to the $\text{OH}(A^2\Sigma^+)$ yield is also suggested by photofluorescence measurements of Beyer and Welge [16], who found $\text{OH}(A^2\Sigma^+)$

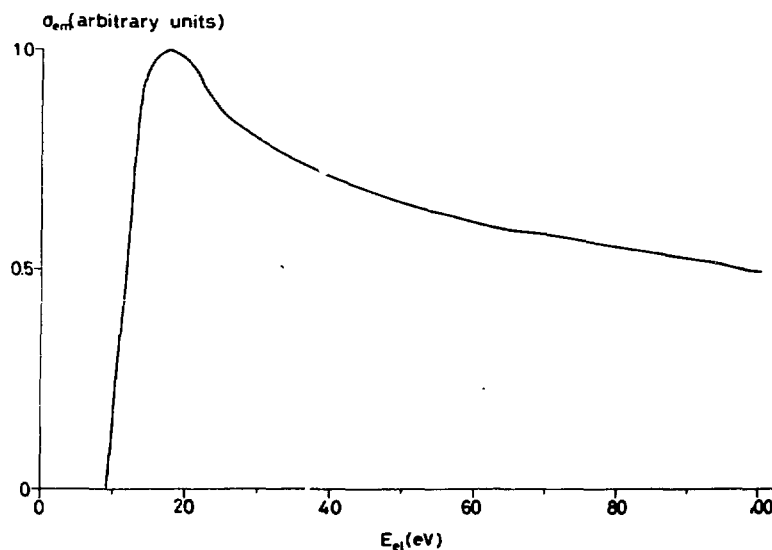


FIGURE 5.3. Energy dependence of the $\text{OH}(A^2\Sigma^+ - X^2\Pi)$ emission cross sections below 100 eV.

emission after excitation of water by photoabsorption from 1360 - 850 Å (9.2 - 14.7 eV) and by measurements of Clyne *et al.* [17], who observed $\text{OH}(\text{A}^2\Sigma^+ - \text{X}^2\Pi)$ emission after excitation of water by metastable argon atoms in the $^3\text{P}_0$ and $^3\text{P}_2$ states, which have an energy of 11.54 and 11.82 eV respectively. In addition the presence of more than one excitation process leading to excited hydroxyl radicals is suggested by an analysis of the intensity distribution in the rotational structure of the $\text{A}^2\Sigma^+ - \text{X}^2\Pi$ spectrum. This shows that some rotational states are preferably populated at low electron impact energies [18].

We cannot conclude from our measurements whether the threshold for $\text{OH}(\text{A}^2\Sigma^+)$ corresponds to a singlet or triplet state of water. According to correlation rules [19,20] these states should have B_2 or A_1 symmetry in C_{2v} . Theoretical calculations [21-24] give evidence for a $^1\text{A}_1$ and a $^3\text{A}_1$ state of water in the threshold region. These states arise from the promotion of a $3a_1$ electron to the $4a_1$ orbital:

$$(1a_1)^2(2a_1)^2(1b_2)^2(3a_1)^2(1b_1)^2 \tilde{\text{X}}^1\text{A}_1 \rightarrow$$

$$(1a_1)^2(2a_1)^2(1b_2)^2(3a_1)(1b_1)^2(4a_1) ^1,^3\text{A}_1$$

The long progression of diffuse bands, extending from 1411 - 1256 Å (8.79 - 9.87 eV), in the photoabsorption spectrum [25] has been attributed by Herzberg [12] to the $^1\text{A}_1$ state. The photofluorescence measurements of Beyer and Welge (see above) give evidence that this state dissociates into $\text{OH}(\text{A}^2\Sigma^+)$ immediately above the dissociation limit. Some experimental indication that triplet states may be present in the 9.13 - 9.3 eV region has been obtained from trapped electron measurements by Schulz [26] and by Knoop [27].

5.5. BALMER EMISSION

5.5.1. Results

The emission cross sections for Balmer β radiation are collected in Table 5.2. For the Balmer α , γ and δ line the emission cross section was

only determined at 100, 200, 500 and 800 eV. At these energies we found the same energy dependence for all Balmer lines within 4%. Therefore in Table 5.5 we give for these lines the emission cross sections relative to the Balmer β emission cross section. An error discussion is given in Section 2.5. For the Balmer β , γ and δ lines the error in the emission cross sections is estimated to be 10%. An error of 15% arises in the Balmer α emission cross section.

TABLE 5.5.

Balmer emission cross sections relative to the absolute emission cross section for Balmer β radiation at 300 eV					
	H_{α}	H_{β}	H_{γ}	H_{δ}	$\sigma_{em}(H_{\beta})$
present	5.17	1.00	0.37	0.14	$3.68 \times 10^{-19} \text{ cm}^2$
ref. 1	5.85	1.00	0.44	0.17	$5.11 \times 10^{-19} \text{ cm}^2$
ref. 6	10	1.00	0.6	0.2	$4.2 \times 10^{-18} \text{ cm}^2$

The energy dependence of the Balmer emission cross sections has also been determined by Vroom and de Heer [1], by Hayakawa [4] and by Tsurubuchi *et al.* [6]. In Fig. 5.4 we compare the results for Balmer β by normalization of the maximum value of the emission cross section at unity in each experiment. Above 100 eV the present results agree with those measured by Vroom and de Heer [1] within 4%, but towards lower energies their relative emission cross sections gradually deviate to larger values. Hayakawa [4] found the maximum value of the Balmer β cross section at almost the same energy as in this experiment, but the cross section falls off slower. This might be due to an incomplete collection of the primary electrons at the Faraday cage in Hayakawa's experiment. The agreement with the results of Tsurubuchi *et al.* [6], obtained in a cross beam experiment, is rather poor.

Absolute emission cross sections for Balmer radiation have also been measured by Vroom and de Heer [1] and by Tsurubuchi *et al.* [6]. For the Balmer α , γ and δ line they also found a similar energy dependence as for

the Balmer β line between 0 and 1000 eV (Fig. 5.4). Therefore we compare the absolute emission cross sections only for the Balmer β line and present the cross sections of the other Balmer lines relative to the Balmer β line (Table 5.5). Within the stated errors the present results for the ratios agree with those measured by Vroom and de Heer. Their absolute values are about 40% higher than in this experiment. This might be due to the fact that in the experiment of Vroom and de Heer the pressure could actually be higher than calculated from the temperature of the cold bath in which a wide-mouth pipe containing the water sample was placed. Small heat leaks may cause a somewhat higher pressure in the pipe than in the heat bath and this establishes a higher pressure than calculated from the temperature of the bath. With the MKS Baratron manometer, used in this experiment, the pressure can be determined more accurately. The agreement with the results of Tsurubuchi *et al.* is also poor as to the absolute values of the emission cross sections. At 300 eV their value of $\sigma_{em}(H_\beta)$ is one order of magnitude larger than our cross section. In Fig. 5.2 we give the Balmer β cross section data in the form of a Fano plot. Since we found the same

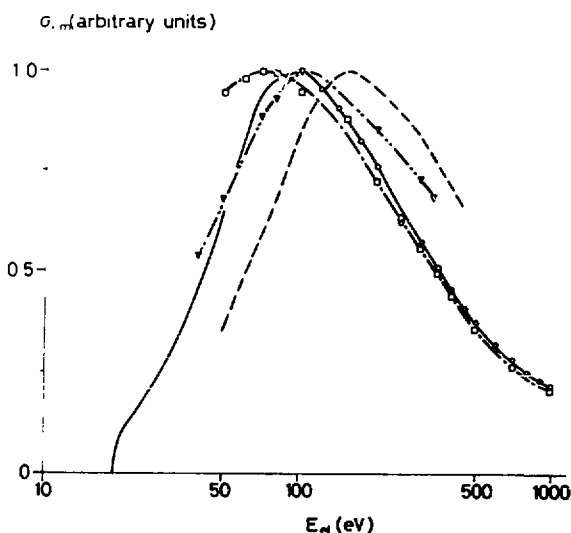
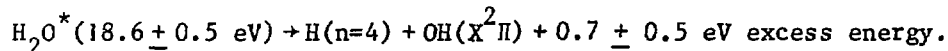


FIGURE 5.4. Energy dependence of the Balmer β emission cross sections. -o-o-: present; -. \square -. \square -: Vroom and de Heer [1]; —: Tsurubuchi *et al.* [6]; - ∇ -. - ∇ -: Hayakawa [4].

energy dependence between 100 and 1000 eV as Vroom and de Heer, we determined the value of M_{em}^2 and c_{em} from the Fano plot obtained by normalization of their cross section data, which extend to 6 keV, on the present absolute emission cross section at 100 eV. These values of M_{em}^2 and c_{em} are shown in Table 5.4. The positive slope in the Fano plot and the large value of c_{em} indicate that excited hydrogen atoms ($n \geq 3$) are formed both by optically allowed and symmetry forbidden excitation processes in the water molecule.

The Balmer β emission cross sections below 100 eV are depicted in Fig. 5.5. For the measured Balmer lines two onsets for emission are observed, one around 19 eV and one around 26 eV. The onset energies are collected in Table 5.6 and compared with the results of Böse and Sroka [2] for the corresponding Lyman emissions. Within the experimental errors the threshold values are in agreement with each other. Considering the calculated minimum energies for production of Balmer β radiation, $H(n=4)$ in Table 5.3, we conclude that near the first onset of about 18.6 eV all $H(n=4)$ radiation is formed as a result of the dissociation process:



This excess energy is released as kinetic energy of both fragments and as

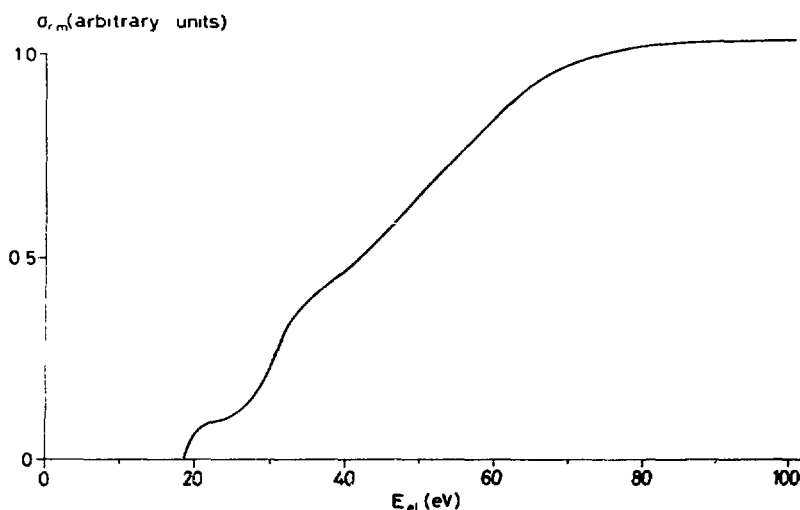


FIGURE 5.5. Energy dependence of the Balmer β emission cross sections below 100 eV.

vibrational and rotational energy of the OH fragment. Similar processes occur at the first onset for formation of H in other excited states. At the second onset the formation of excited hydrogen atoms can be accompanied both by the formation of a ground state oxygen atom and a ground state hydrogen atom or by formation of OH in the $A^2\Sigma^+$ state. The relative unimportance of the latter process is indicated by the fact that the energy dependence of the $OH(A^2\Sigma^+)$ emission cross section does not show an onset for $OH(A^2\Sigma^+ - X^2\Pi)$ emission at the onsets for Balmer radiation.

TABLE 5.6.

Measured onset energies for formation of excited fragments by dissociative excitation of water		
Fragment	Measured onset (eV)	
	Present	Ref. 2
H(n=3)	18.5 ± 0.5	18.0 ± 0.5
	26.8 ± 1.5	25.5 ± 0.8
H(n=4)	18.6 ± 0.5	18.8 ± 0.5
		26.8 ± 0.8
H(n=5)	19.1 ± 0.5	18.9 ± 0.6
		26.4 ± 0.8
OH($A^2\Sigma^+$)	9.0 ± 0.3	
O(3p 3P)	17.3 ± 1.5	
	24.5 ± 2.0	
O(3p 5P)	17.6 ± 1.5	
	23.1 ± 2.0	

5.5.2. Discussion

The first threshold for production of $H(n \geq 3)$ has been found in this experiment to be about 19 eV. At this energy the remaining fragment cannot be ionized and hence the excited hydrogen atoms can only originate from states of the neutral molecule. Since these states are above the first ionization potential of water (12.62 eV) [12], they are called super-excited states (see Section 1.4). The dependence of the Balmer emission cross sections on the energy of the incident electrons shows that electron exchange processes are not important in the formation of excited hydrogen atoms and hence we conclude that these super-excited states are predominantly singlet states. In principle these states can be formed by one-electron transitions in the molecule or by simultaneous excitation of several electrons. The latter mechanism, which is believed to be less probable, will be discussed later on. A qualitative estimate of the singlet states of water formed by one-electron transitions can be obtained by means of a comparison of molecular orbital energies.

Excited states of the water molecule are generated by promoting an electron from an occupied orbital to higher unoccupied orbitals. Because, at least around the ground state equilibrium distance, these orbitals have an appreciable Rydberg character, they give rise to a Rydberg series of electronic states whose limit corresponds to complete removal of the electron, i.e. to an ionization limit for the molecule. Since the Rydberg orbitals have a non-bonding character the potential energy surfaces of the Rydberg states have the same shape as the surface of the corresponding ion state. The energies of the Rydberg states can be found to a good approximation from the Rydberg formula:

$$E_n = A - R/(n-\delta)^2,$$

where A is the energy of the ion, R the Rydberg energy, n the principal quantum number of the Rydberg orbital and δ the quantum defect. For molecules built-up from atoms of the first period δ ranges from 0 to 1.2 [12]. Substituting also $n \geq 3$ yields values of E_n which range from A to a few eV below A .

Ionization energies, according to Koopman's theorem equal to minus the orbital energies, have been measured in photoelectron spectroscopy. The spectrum consists of bands at 539.7 eV and 32.2 eV as measured by

Siegbahn *et al.* [28] and bands which extend between 17.2 - 20.3 eV, 13.7 - 16.3 eV and 12.6 - 13.5 eV as measured by Turner *et al.* [29]. These bands correspond to states of the H_2O^+ ion, which are obtained by removal of a $1a_1$, $2a_1$, $1b_2$, $3a_1$ and $1b_1$ electron from water respectively. Considering the energies of the states of H_2O^+ and the Rydberg formula we conclude that only Rydberg states converging to the third ionization limit, i.e. the $\tilde{\text{B}}^2\text{B}_2$ state of H_2O^+ , come into consideration for the production of Balmer emission near the first threshold around 19 eV. Some diffuse bands have been assigned in the absorption spectrum of water to these Rydberg states [30]. The $\tilde{\text{B}}^2\text{B}_2$ state of the ion is a bound state. However, the vibrational structure in the third band of the photoelectron spectrum shows a broadening above 18.1 eV, which is attributed to predissociation into $\text{H} + \text{OH}^+$ by a repulsive $^4\text{B}_1$ doubly excited state of the ion with the electronic configuration:

$$(1a_1)^2(2a_1)^2(1b_2)^2(3a_1)(1b_1)(4a_1)$$

The first threshold for H^+ production has been measured by Appell and Durup [32] to be 18.7 ± 0.5 eV. They explained the formation of protons by a crossing of the $\tilde{\text{B}}^2\text{B}_2$ state with one of the two $^2\text{B}_1$ states of the aforementioned configuration, indicating a second predissociation channel of the $\tilde{\text{B}}^2\text{B}_2$ state. Because of the similarity of the $\tilde{\text{B}}^2\text{B}_2$ state and the corresponding Rydberg states of the neutral molecule we suggest a similar mechanism for the predissociation into $\text{H}(n \geq 3) + \text{OH}(X^2\Pi)$: predissociation of the bound Rydberg states by repulsive doubly excited states with electronic configuration:

$$(1a_1)^2(2a_1)^2(1b_2)^2(3a_1)(1b_1)(4a_1)(nR)$$

Lyman emission from excited hydrogen atoms, $\text{H}(n=2)$, has been observed in the photofluorescence measurements of Beyer and Welge [16] in the photon energy range 15.30 - 20.66 eV. If the same mechanism as for $\text{H}(n \geq 3)$ is also responsible for $\text{H}(n=2)$ production, then the process for H^* production near threshold explains at least part of the optically allowed character of the Fano plot.

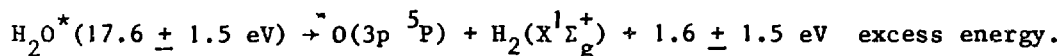
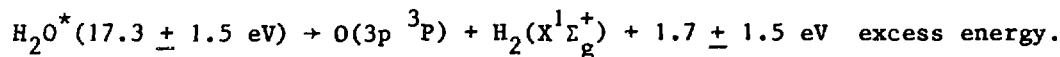
There is no indication that the Balmer radiation near the first threshold is due to direct dissociation of doubly excited states. Their energies can be estimated from recent calculations on excited states of H_2O^+ by Leclerc *et al.* [33]. According to their calculations the lowest doubly excited ion states have the configuration:

$$(1a_1)^2(2a_1)^2(1b_2)^2(3a_1)(1b_1)(4a_1)$$

These states are unstable with respect to dissociation. The resulting doublet states have calculated vertical excitation energies of 25.5 eV and 27.6 eV and similarly the quartet state has 24.6 eV. The lowest doubly excited singlet state of H_2O has probably the same configuration but now with two electrons in the $4a_1$ orbital. Applying the Rydberg formula with $A = 25.5$ eV we estimate the energy of this state to be 21.3 eV. This is much higher than the first onset for Balmer radiation. However, direct dissociation processes of doubly excited states might explain the second onset near 26 eV in the Balmer radiation. We exclude the possibility that states formed by simultaneous excitation of more than two electrons are involved in the production of excited hydrogen atoms. Such states have a high excitation energy and a very small excitation cross section.

5.6. OXYGEN EMISSION

Electron impact on water produces also excited oxygen atoms of which the $3p\ ^3P - 3s\ ^3S^0$ and $3p\ ^5P - 3s\ ^5S^0$ multiplet transitions around 8447 Å and 7774 Å respectively could be detected in our wavelength region. The emission cross sections for these transitions are collected in Table 5.2. They have also been measured by Lawrence [3] in the case of 8447 Å radiation. At 100 eV his value agrees with ours within the errors of 20% in both experiments. The energy dependence is compared in Fig. 5.6. In Fig. 5.2 we give the $3p\ ^3P - 3s\ ^3S^0$ emission cross sections in the form of a Fano plot. The small positive value of M_{em}^2 and the large value of c_{em} (Table 5.4) indicate that both optically allowed and symmetry forbidden transitions are involved in the formation of $O(3p\ ^3P)$. An accurate determination of the Fano plot for 7774 Å radiation was not possible because of the weak light signal at higher energies. It indicates, however, that the major part of $O(3p\ ^5P)$ is formed by symmetry forbidden excitation processes. For the region below 100 eV the emission cross sections of the $3p\ ^3P - 3s\ ^3S^0$ transition are depicted in Fig. 5.7 and of the $3p\ ^5P - 3s\ ^5S^0$ transition in Fig. 5.8. The values of the onsets for emission are given in Table 5.6. By a comparison with calculated minimum excitation energies (Table 5.3) the processes which can occur near the onsets may be derived. For reasons of energy the observed onsets near 18 eV can only correspond with the processes:



At the second onset dissociation into two ground state hydrogen atoms may occur. The energy dependence of the emission cross sections does not suggest that both excited oxygen atoms are formed by the same sort of excitation process in the water molecule (Figs. 5.7 and 5.8).

The energy dependence of the $\text{O}(8447 \text{ \AA})$ and Balmer emission cross sections and the threshold energies are quite similar. This might indicate that near the first threshold $\text{O}(3p^3P)$ is formed by a mechanism analogous to that for $\text{H}(n \geq 3)$, namely by predissociation of Rydberg states converging to the \tilde{B}^2B_2 ion state. Because near threshold the fragments produced by dissociative excitation can only be $\text{H}_2(X^1\Sigma_g^+)$ and $\text{O}(3p^3P)$ the predissociating state should be a triplet state with A_2 , B_1 or B_2 symmetry according to correlation rules. The second onset for $\text{O}(3p^3P - 3s^3S^0)$ radiation can be interpreted again as direct dissociation of a doubly excited state.

The slow increase of the $\text{O}(3p^5P)$ emission cross section shows that a small

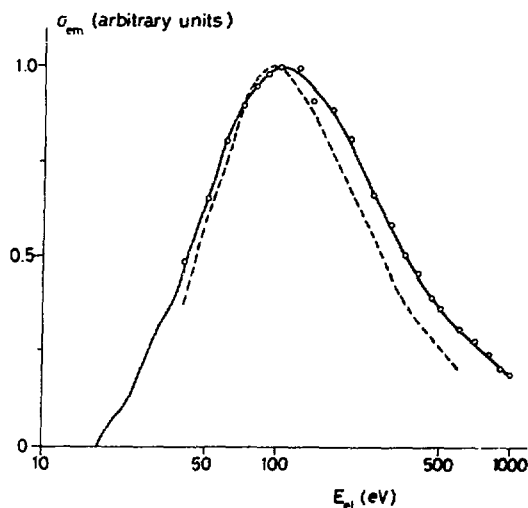


FIGURE 5.6. Energy dependence of the $\text{O}(3p^3P - 3s^3S^0)$ emission cross sections. —○—: present; ---: Lawrence [3].

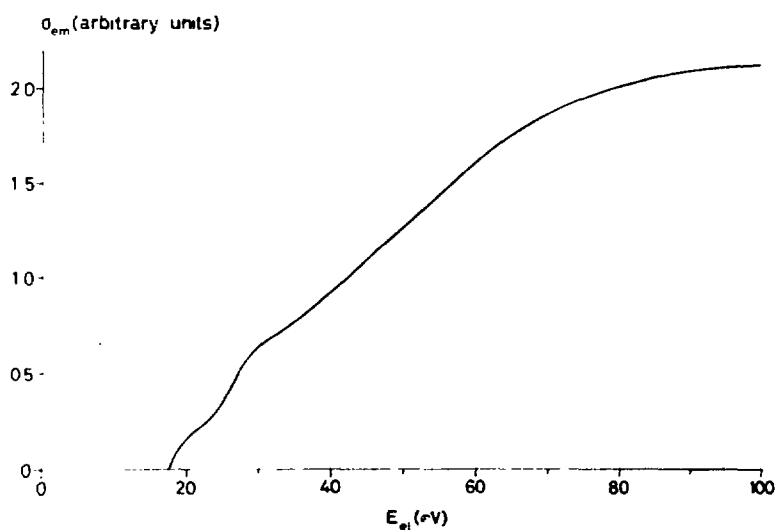


FIGURE 5.7. Energy dependence of the $O(3p\ ^3P - 3s\ ^3S^0)$ emission cross sections below 100 eV.

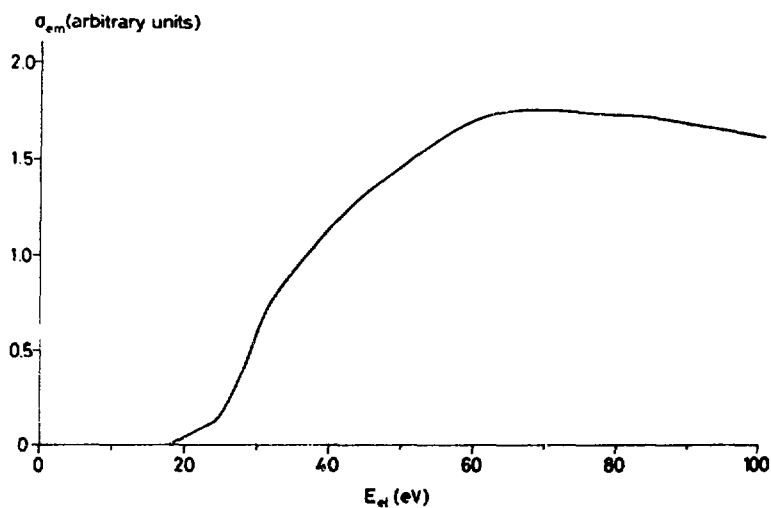


FIGURE 5.8. Energy dependence of the $O(3p\ ^5P - 3s\ ^5S^0)$ emission cross sections below 100 eV.

part of the excited quintet atoms are formed near the first threshold, which is in the 16 - 19 eV region. At that energy the dissociation of water can only take place into $H_2(^1\Sigma_g^+)$ and $O(3p^5P)$. Therefore at the first threshold quintet oxygen atoms originate from quintet states of the water molecule. Such a state can be reached either by direct excitation or by predissociation of singlet or triplet states of the water molecule. Direct excitation can be excluded because excitation to such a state would require simultaneous excitation and exchange of two electrons, which is an improbable process. In addition doubly excited states are not expected below 20 eV (see Section 5.5.2.). Therefore, we suggest that near the first threshold quintet oxygen atoms are produced by a spin-forbidden predissociation of singlet and triplet states of water in the 16 - 19 eV region. These states can be Rydberg states converging to the second or third ionization potential.

Most of the $O(3p^5P)$ atoms are formed from molecular states at the second onset of 23 ± 2 eV. At that energy only doubly excited states of the neutral water molecule can be formed. The dissociation of these states into $O(3p^5P)$ can be accompanied by formation of two hydrogen atoms in the ground state. According to correlation rules the doubly excited states of water from which these fragments occur can be triplet states as well as quintet states.

REFERENCES

- [1] D.A. Vroom and F.J. de Heer, J.Chem.Phys. 50 (1969) 1883.
- [2] N. Böse and W. Sroka, Z.Naturforsch. 28a (1973) 22.
- [3] G.M. Lawrence, Phys.Rev. A 2 (1970) 397.
- [4] G. Hayakawa, Proc.Phys.Math.Soc.Jap. 26 (1944) 78.
- [5] I.V. Sushanin and S.M. Kishko, Opt.& Spectr. 30 (1971) 315.
- [6] S. Tsurubuchi, T. Iwai and T. Horie, J.Phys.Soc.Japan 36 (1974) 537.
- [7] J.J. Olivero, R.W. Stagat and A.E.S. Green, J. Geophys.Res. 27 (1972) 4797.
- [8] C.E. Moore, A Multiplet Table of Astrophysical Interest (Observatory, Princeton, 1945).
- [9] B. Rosen, Spectroscopic Data relative to Diatomic Molecules (Pergamon Press, Oxford, 1970).
- [10] A.R. Striganov and N.S. Sventitskii, Tables of Spectral Lines of Neutral and Ionized Atoms (IFI/Plenum, New York, 1968).

- [11] R.W. Pearse and A.G. Gaydon, *The Identification of Molecular Spectra* (Chapman, London, 1965).
- [12] G. Herzberg, *Electronic Spectra of Polyatomic Molecules* (Van Nostrand, Princeton, 1966).
- [13] G. Herzberg, *Spectra of Diatomic Molecules* (Van Nostrand, Princeton, 1950).
- [14] J.F.M. Aarts and F.J. de Heer, *Chem.Phys.Letters* 4 (1969) 116.
- [15] V.I. Ochkur, *Soviet Phys. JETP* 18 (1964) 503.
- [16] K.D. Beyer and K.H. Welge, *Z.Naturforschg.* 22a (1967) 1161.
- [17] M.A.A. Clyne, J.A. Coxon, D.W. Setser and D.H. Stedman, *Trans.Far.Soc.* 65 (1969) 1177.
- [18] G.R. Möhlmann, to be published.
- [19] F. Fiquet-Fayard, *J.Chim.Phys.* 54 (1957) 274.
- [20] K.E. Shuler, *J.Chem.Phys.* 21 (1953) 624.
- [21] C.R. Claydon, G.A. Segal and H.S. Taylor, *J.Chem.Phys.* 54 (1971) 3799.
- [22] W.J. Hunt and W.A. Goddard, *Chem.Phys.Letters* 3 (1969) 414.
- [23] W.J. Hunt, T.H. Dunning and W.A. Goddard, *Chem.Phys.Letters* 3 (1969) 606.
- [24] J.A. Horsley and W.H. Fink, *J.Chem.Phys.* 50 (1969) 750.
- [25] K. Watanabe and M. Zelikoff, *J.Opt.Soc.Amer.* 43 (1953) 753.
- [26] G.J. Schulz, *J.Chem.Phys.* 33 (1960) 1661.
- [27] F.W.E. Knoop, Thesis, University of Leiden (1972).
- [28] K. Siegbahn *et al.*, *ESCA applied to Free Molecules* (North-Holland, Amsterdam, 1969).
- [29] D.W. Turner *et al.*, *Molecular Photoelectron Spectroscopy* (John Wiley-Interscience, London 1970).
- [30] D.H. Katayama, R.E. Huffman and C.L. O'Bryan, *J.Chem.Phys.* 59 (1973) 4309.
- [31] F. Fiquet-Fayard and P.M. Guyon, *Mol.Phys.* 11 (1966) 17.
- [32] J. Appell and J. Durup, *Int.J.Mass Spectrom.Ion Phys.*, 10 (1972/73) 247.
- [33] J.C. Leclerc, J.A. Horsley and J.C. Lorquet, to be published.

CHAPTER VI

${}^1B_{2u} \rightarrow {}^1A_{1g}$ FLUORESCENCE FROM BENZENE. I.

The ${}^1B_{2u} \rightarrow {}^1A_{1g}$ fluorescence resulting from electron impact (30-1000 eV) on benzene has been studied in the pressure range $10^{-4} - 2 \times 10^{-3}$ Torr. The fluorescence spectrum is compared with the spectrum obtained by other methods. The energy dependence of the absolute emission cross section indicates a small probability for internal conversion from higher singlet states to the ${}^1B_{2u}$ state.

6.1. INTRODUCTION

Impact of electrons on benzene results in light emission from fragments (H, C and CH) as well as from the molecule (${}^1B_{2u} \rightarrow {}^1A_{1g}$ fluorescence). In this chapter the discussion will be restricted to the fluorescence of the benzene molecule excited by monoenergetic electrons in the range 30-1000 eV. Because the pressure ($p < 2 \times 10^{-3}$ Torr) is such that the time between two hard sphere collisions is much longer than the lifetime of the lowest excited singlet state (${}^1B_{2u}$ state), our data refer to isolated molecules.

In the case of high energy electrons the excitation mechanism is known to be similar to that of irradiation by "white" light [1], covering a wide range of photon energies, which are not easily available from conventional light sources.

6.2. EXPERIMENTAL

The apparatus has been described before [2]. Basically it consists of an electron gun which produces an electron beam of variable energy and of a collision chamber. With a monochromator one observes the light emission produced by the impact of electrons.

Benzene (Baker Analyzed Reagent), dried over sodium and next repeatedly degassed at -40°C and -196°C to remove water and air, was admitted into the collision chamber via an all metal variable leak. The pressure was measured by a capacitance manometer (MKS Baratron). The electron beam was produced by a directly heated Rhenium filament, resulting in an energy spread of 2 eV. All measurements were done in a region where the light signal is proportional to the beam current and the gas pressure ($I < 100 \mu\text{A}$ and $p < 2 \times 10^{-3}$ Torr).

6.3. FLUORESCENCE SPECTRUM

The ${}^1\text{B}_{2u} \rightarrow {}^1\text{A}_{1g}$ fluorescence spectrum, which results from the impact of electrons on benzene, is depicted in Fig. 6.1. It is independent of the energy of the incident electrons. The energy level diagram of the benzene molecule is depicted in Fig. 6.2.

To describe the spectrum we adopt the notation suggested by Callomon, Dunn and Mills [3]. Transitions between vibronic levels are indicated by a capital number, which refers to the fundamental involved, followed by a superscript and a subscript indicating the number of quanta of that

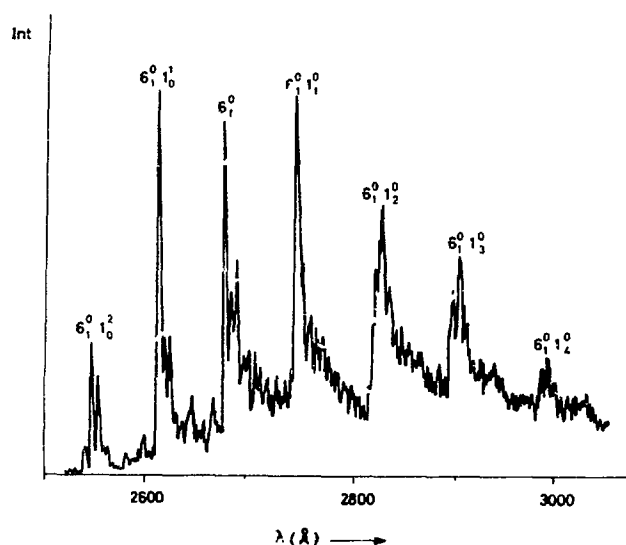


FIGURE 6.1. ${}^1\text{B}_{2u} \rightarrow {}^1\text{A}_{1g}$ fluorescence resulting from impact of 100 eV electrons on benzene. The optical resolution amounts 1.5 Å.

fundamental excited in the upper and lower state respectively. The numbering of the fundamentals is that of Wilson, Decius and Cross [4]. A comparison with other notations is also made in Ref. 3. The main features in this spectrum are explained as vibronic transitions involving the e_{2g} ring vibration ν_6 , the totally symmetric breathing vibration ν_1 and the e_{2u} ring vibration ν_{16} (see Ref. 5).

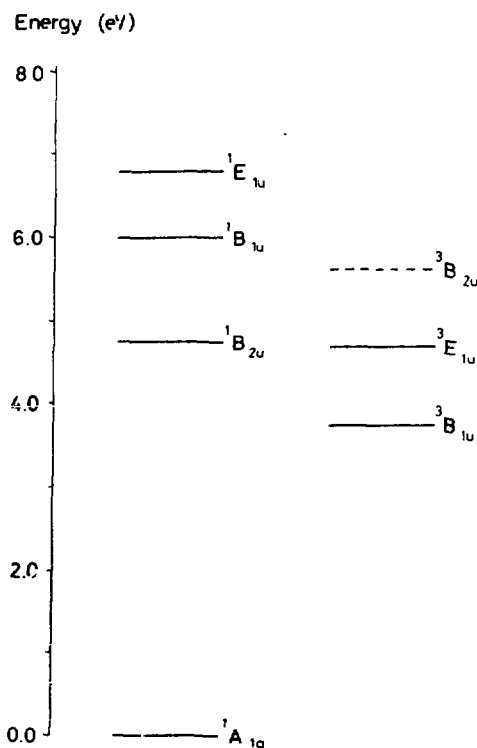


FIGURE 6.2. Energy levels of benzene.

At pressures larger than about 5 Torr vibrational relaxation by collisions establishes a thermal distribution before fluorescence takes place. Consequently, emission from several low lying vibrational levels is observed, giving rise to a complicated spectrum which is independent of the mode of excitation (equilibrated fluorescence) [6,7]. At lower pressures, where the time between two successive collisions of a benzene molecule is of the same order or longer than the lifetime of the $^1B_{2u}$ state, no thermal

distribution will be obtained. However, in the case of electron impact all vibronic levels below the impact energy can be excited simultaneously. Therefore, we expect that the fluorescence spectrum might be as complicated as the equilibrated fluorescence spectrum, while in addition emission might be observed from vibrational levels which are not populated in a 300°K Boltzmann distribution. Comparison of our spectrum with the equilibrated fluorescence spectrum [6] shows indeed additional vibronic bands, viz. $6_1^{0,1}1_0$ and $6_1^{0,2}1_0$. These bands are also found in a discharge spectrum [6,8] and in the fluorescence spectrum obtained when benzene is excited by metastable argon atoms, having an energy of about 11.6 eV [9]. However, in those experiments the intensity of the $6_1^{0,1}1_0$ and $6_1^{0,2}1_0$ bands is somewhat less due to the higher pressures used.

6.4. EMISSION CROSS SECTIONS

The absolute emission cross sections σ_{em} for ${}^1B_{2u} \rightarrow {}^1A_{1g}$ fluorescence in the energy range 30 - 1000 eV are collected in Table 6.1. At these energies the ${}^1B_{2u}$ state can be populated both by direct excitation by electrons and by internal conversion from other states excited simultaneously. Because at high energies spin exchange processes are of minor importance, intersystem crossing from the triplet manifold to the ${}^1B_{2u}$ state can be disregarded. Moreover, experiment [10] and theoretical calculations [11,12] show that excitation to the lowest excited $\pi \rightarrow \pi^*$ states, namely ${}^1B_{2u}$, ${}^1B_{1u}$ and ${}^1E_{1u}$, is more important than excitation to other states. We therefore restrict ourselves to internal conversion from the ${}^1B_{1u}$ and ${}^1E_{1u}$ states to the ${}^1B_{2u}$ state.

The ${}^1B_{2u}$ emission cross section can be written in terms of excitation cross sections as:

$$\sigma_{em}({}^1B_{2u}) = \phi_1 \sigma_{exc}({}^1B_{2u}) + \phi_2 \sigma_{exc}({}^1B_{1u}) + \phi_3 \sigma_{exc}({}^1E_{1u}) \quad (1)$$

where ϕ is the fluorescence yield, the indices 1, 2 and 3 referring to the ${}^1B_{2u}$, ${}^1B_{1u}$ and ${}^1E_{1u}$ states respectively.

According to the Bethe theory [13,14] the excitation cross section of these states can at sufficiently high energies be expressed as:

$$\sigma_{exc}^n = \frac{4\pi a_o^2 R}{E_{el}} M_n^2 \ln \frac{c_n E_{el}}{R} \quad (2)$$

where n represents the excited state, a_0 is the Bohr radius, R is the Rydberg constant, E_{el} is the energy of the incident electrons and c_n is a constant. M_n^2 is related to the optical oscillator strength f_n and the excitation energy E_n of the excited state n by:

$$M_n^2 = f_n R/E_n \quad (3)$$

Substituting Eq. (2) into (1) gives:

$$\sigma_{em}(^1B_{2u}) = \frac{4\pi a_0^2 R}{E_{el}} M_{em}^2 \ln \frac{c_{em} E_{el}}{R} \quad (4)$$

where

$$M_{em}^2 = \phi_1 M_1^2 + \phi_2 M_2^2 + \phi_3 M_3^2 \quad (5)$$

and

$$\ln c_{em} = (\phi_1 M_1^2 \ln c_1 + \phi_2 M_2^2 \ln c_2 + \phi_3 M_3^2 \ln c_3) / M_{em}^2.$$

Plotting $\sigma_{em}(^1B_{2u}) E_{el} / 4\pi a_0^2 R$ versus $\ln E_{el}$ gives a straight line at sufficiently high energies with a slope equal to M_{em}^2 . In Fig. 6.3. the emission cross sections are presented in such a so called Fano plot. From

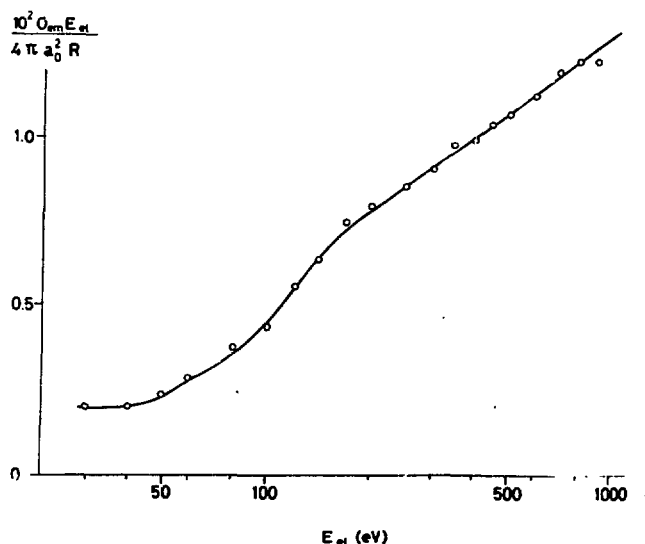


FIGURE 6.3. Emission cross sections of $^1B_{2u} \rightarrow ^1A_{1g}$ fluorescence presented in a Fano plot.

TABLE 6.1.

Emission cross sections for ${}^1B_{2u} \rightarrow {}^1A_{1g}$ fluorescence in units of 10^{-19} cm^2 .			
$E_{el} \text{ (eV)}$	σ_{em}	$E_{el} \text{ (eV)}$	σ_{em}
30	3.09	300	1.44
40	2.37	350	1.34
50	2.29	400	1.19
60	2.29	450	1.11
80	2.26	500	1.3
100	2.09	600	0.900
120	2.22	700	0.816
140	2.18	800	0.733
170	2.11	900	0.649
200	1.90	1000	0.649
250	1.63		

TABLE 6.2.

Transition energies and oscillator strengths in benzene.			
	$E_n \text{ (eV)}$	f_n	M_n^2
${}^1B_{2u}$	4.9 ^a	0.00147 ^c	0.0041
${}^1B_{1u}$	6.2 ^b	0.094 ^a	0.21
${}^1E_{1u}$	6.9 ^b	0.88 ^a	1.73

^a Ref. 21.^b Ref. 22.^c Ref. 23, 24 and 25.

the linear part of it one obtains $M_{em}^2 = 3.23 \times 10^{-3}$ and $c_{em} = 0.764$. The error in M_{em}^2 , deduced from the standard deviation in the slope (5%) and the uncertainty in the emission cross section (25%), is mainly determined by systematic errors in the determination of the quantum yield of the optical equipment (see Section 2.5). Hence it follows that $4.20 \times 10^{-3} > M_{em}^2 > 2.26 \times 10^{-3}$.

The values of M_n^2 are tabulated in Table 6.2. From the facts that the fluorescence yield for excitation into the $^1B_{2u}$ state is about 0.3 [15, 16, 17] and that the region below Parmenter's threshold [18] carries about 70% of the $^1B_{2u}$ oscillator strength [19], we estimate $\phi_1 = 0.21$. From formula (5) it is then derived that $3.34 \times 10^{-3} > \phi_2 M_2^2 + \phi_3 M_3^2 > 1.4 \times 10^{-3}$. Hence it follows that excitation to the $^1B_{1u}$ and $^1E_{1u}$ state contributes to the value of M_{em}^2 and therefore we conclude that the fluorescence spectrum obtained in this experiment is partially due to internal conversion from these states. If we assume $\phi_2 \approx \phi_3$, we find $2 \times 10^{-3} > \phi_2$, $\phi_3 > 7 \times 10^{-4}$. So measurements indicate a small probability for internal conversion from higher singlet states. This finding is in agreement with recent results of Gregory *et al.* [20], who found fluorescence of benzene when it is excited in the vapour phase into the $^1E_{1u}$ state by the mercury line ($\lambda = 1849 \text{ \AA}$).

REFERENCES

- [1] R.L. Platzman, *The Vortex* 23 (1962) 372.
- [2] Chapter II of this thesis.
- [3] J.H. Callomon, T.M. Dunn and I.M. Mills, *Phil.Trans.Roy.Soc.(London)* A 259 (1966) 499.
- [4] E.B. Wilson, J.C. Decius and P.C. Cross, *Molecular Vibrations* (McGraw-Hill, New York, 1955).
- [5] A review is given by G. Herzberg, *Molecular Spectra and Molecular Structure* (Van Nostrand, Princeton, 1966).
- [6] H.F. Kemper and M. Stockburger, *J.Chem.Phys.* 53 (1970) 268.
- [7] C.W. Lawson, F. Hirayama and S. Lipsky, *J.Chem.Phys.* 51 (1969) 1590.
- [8] S. Leach, *J.Chim.Phys.* 51 (1955) 556.
- [9] H.J. de Jong, *Chem.Phys.Letters* 15 (1972) 414.
- [10] A. Skerbele and E.N. Lassettre, *J.Chem.Phys.* 42 (1965) 395.

- [11] M. Matsuzawa, J.Phys.Soc.Japan, 18 (1963) 1473.
- [12] F.H. Read and G.L. Whiterod, Proc.Phys.Soc. 85 (1965) 71.
- [13] H.A. Bethe, Ann.Physik 5 (1930) 325.
- [14] M. Inokuti, Rev.Mod.Phys. 43 (1971) 297.
- [15] E.M. Anderson and G.M. Kistiakowsky, J.Chem.Phys. 48 (1968) 4787.
- [16] K.G. Spears and S.A. Rice, J.Chem.Phys. 55 (1971) 5561.
- [17] C.S. Parmenter and M.W. Schuyler, Chem.Phys.Letters 6 (1970) 339.
- [18] C.S. Parmenter and M.W. Schuyler, 20^e Réunion de la Société de Chimie Physique, J.Chim.Phys. 66 (1969) 92.
- [19] T. Kakitani, J.Phys.Soc. Japan 29 (1970) 1562.
- [20] T.A. Gregory, F. Hirayama and S. Lipsky, J.Chem.Phys. 58 (1973) 4697.
- [21] S.P. McGlynn, T. Azumi and M. Kinoshita, Molecular Spectroscopy of the Triplet State (Prentice Hall, Englewood Cliffs, 1969).
- [22] J.P. Doering, J.Chem.Phys. 51 (1969) 2866.
- [23] D.S. McClure, J.Chem.Phys. 17 (1949) 905.
- [24] J.R. Platt *et al.*, Systematics of Electronic Spectra of Conjugated Molecules: A Source Book. (John Wiley & Sons, New York, 1964).
See paper no. 10 by H.B. Klevens and J.R. Platt.
- [25] S.J. Stickler has recently attempted to measure the absorption oscillator strength of benzene vapour. The results seem to give a value slightly lower than the literature value of 0.00147.
(Private communication.)

CHAPTER VII

$^1B_{2u} - ^1A_{1g}$ FLUORESCENCE FROM BENZENE. II.

The $^1B_{2u} - ^1A_{1g}$ fluorescence of benzene resulting from the impact of low energy electrons (0 - 30 eV) has been studied in the pressure range $10^{-4} - 2 \times 10^{-3}$ Torr. It is found that the apparent emission cross section near threshold varies linearly with the pressure. A reaction scheme explaining this behaviour is given. From the absolute value of the apparent emission cross section it follows that excitation of the $^3E_{1u}$ state is by far dominant over excitation of the $^1B_{2u}$ state at low electron impact energies.

7.1. INTRODUCTION

The $^1B_{2u} - ^1A_{1g}$ fluorescence of benzene excited by mono-energetic electrons in the range 0 - 30 eV shows features which differ from those found by excitation with high energy electrons [1]. These features may be correlated with the occurrence of optically forbidden transitions. Particularly electron exchange processes are highly probable at low electron impact energies.

In this investigation the electron beam is produced by an electron gun with an oxide cathode. The energy spread of the electrons is about 0.3 eV. In order to avoid space charge effects beam currents of less than 10 μ A have been used.

7.2. RESULTS

The energy dependence of the apparent emission cross section for $^1B_{2u} - ^1A_{1g}$ fluorescence is presented in Fig. 7.1 at two different benzene

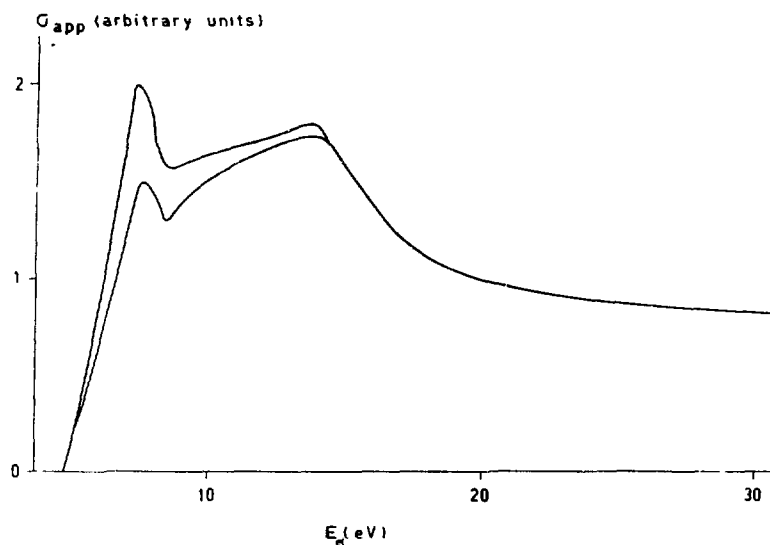


FIGURE 7.1. Energy dependence of the emission cross section for ${}^1B_{2u} - {}^1A_{1g}$ fluorescence. The upper curve has been obtained at a pressure of 1.50×10^{-3} Torr, the lower curve at 0.68×10^{-3} Torr.

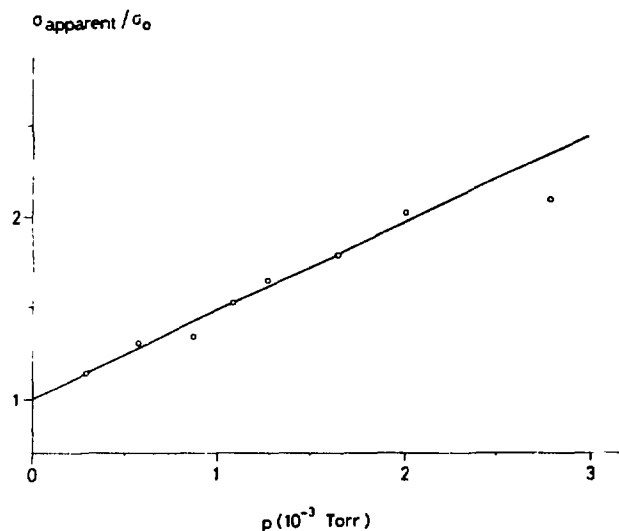


FIGURE 7.2. Plot of the apparent emission cross section at 7.3 eV divided by the emission cross section extrapolated to pressure zero.

pressures. The apparent emission cross section σ_{app} has near the onset a maximum at 7.3 eV electron impact energy. At this value of the energy σ_{app} is a linear function of the pressure (Fig. 7.2). At higher impact energies this pressure dependence disappears. No dependence of σ_{app} on the intensity of the electron beam is found. Therefore, we write the apparent emission cross section near threshold as:

$$\sigma_{\text{app}}(^1B_{2u}) = \sigma_o(^1B_{2u}) + \sigma_p(^1B_{2u}) \quad (1)$$

where σ_o is the emission cross section extrapolated to zero pressure and

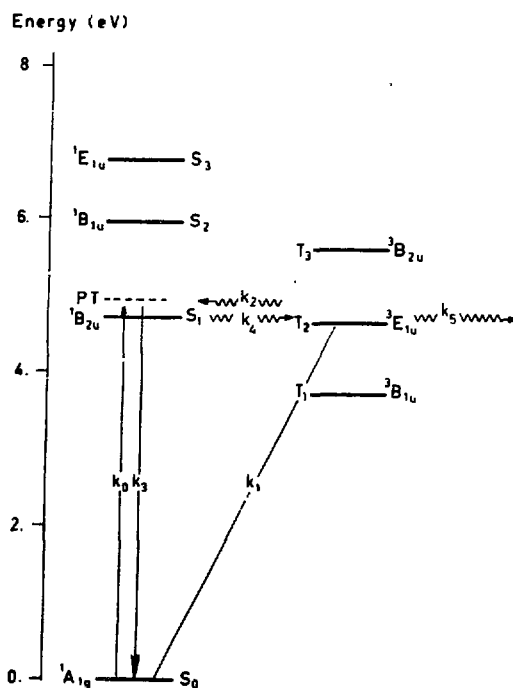


FIGURE 7.3. Reaction scheme. The rate constants have the following meaning: k_0 : excitation to the $1B_{2u}$ state; k_1 : excitation to the $3B_{1u}$ state; k_2 : collision induced energy transfer to the $1B_{2u}$ state from the $3E_{1u}$ state; k_3 : fluorescence from the $1B_{2u}$ state; k_4 : intersystem crossing; k_5 : unimolecular decay of the $3E_{1u}$ state. PT: Parmenter's threshold.

σ_p is the cross section introduced by a pressure dependent process. From the absolute values of the emission cross section [1] it follows that at 7.3 eV $\sigma_o(^1B_{2u}) = 4.8 \times 10^{-19} \text{ cm}^2$ and $\sigma(^1B_{2u}) = 2.5 \times 10^{-16} \text{ cm}^2$, the latter value being obtained by linear extrapolation to 1 Torr.

7.3. DISCUSSION

It is well known that at low electron impact energies there is a preference for triplet states to be excited [2,3,4]. The excitation cross section for such an electron exchange process has a maximum at a few eV above the threshold, in contrast to processes not involving electron exchange where the maximum cross section is at much higher energies. The existence of a pressure effect, only observed at low impact energies, suggests that the $^1B_{2u}$ state is excited in two ways, namely directly and also by energy transfer from triplet states induced by collisions with ground state molecules. Of the relevant triplet states $^3B_{1u}$, $^3E_{1u}$ and $^3B_{2u}$ the second excited triplet state $^3E_{1u}$ is approximately degenerate with the $^1B_{2u}$ state. For that reason mainly this state will be involved in the energy transfer process.

We therefore consider the following processes to be relevant in the population of the $^1B_{2u}$ state by low energy electron impact (see Fig. 7.3):

- a) direct excitation of the $^1B_{2u}$ state by electron impact (k_o),
- b) direct excitation of the $^3E_{1u}$ state by electron impact (k_1), followed by energy transfer from that state to the $^1B_{2u}$ state by collisions with ground state molecules (k_2).

The $^1B_{2u}$ state is depopulated by:

- c) fluorescence to the ground state (k_3),
- d) intersystem crossing to the triplet manifold (k_4).

Furthermore we introduce a rate constant k_5 which accounts for unimolecular decay of the $^3E_{1u}$ state.

The decay rates of the $^1B_{2u}$ and $^3E_{1u}$ states can now be expressed in terms of rate constants:

$$\frac{dS_1}{dt} = k_o S_o + k_2 S_o T_2 - k_3 S_1 - k_4 S_1 \quad (2)$$

$$\frac{dT_2}{dt} = k_1 S_o - k_2 S_o T_2 + k_4 S_1 - k_5 T_2 \quad (3)$$

Here S_0 , S_1 and T_2 denote the density of benzene molecules in the ground state, $^1B_{2u}$ state and $^3E_{1u}$ state respectively. In this reaction scheme we have not taken into account internal conversion from the $^1B_{2u}$ state to the ground state and intersystem crossing from the triplet manifold to the $^1B_{2u}$ state. The former process is only of minor importance compared to fluorescence (see for instance Refs. 5 and 6). The latter process is not considered, because intersystem crossing from the $^1B_{2u}$ state to the triplet manifold is known to be an irreversible process (see for instance Ref. 7). We do not consider internal conversion from singlet states above Parmenter's threshold [8]. It will be shown below that this process is not important at low electron impact energies.

Under stationary conditions it follows from Eqs. 2 and 3 by eliminating T_2 :

$$k_3 S_1 = k_0 S_0 + \frac{k_2 S_0}{k_2 S_0 + k_5} k_1 S_0 - \frac{k_5}{k_2 S_0 + k_5} k_4 S_1 \quad (4)$$

The rate constants k_3 and k_4 are related to the fluorescence quantum yield ϕ_1 of the $^1B_{2u}$ state, which can be obtained from photofluorescence measurements:

$$\phi_1 = \frac{k_3}{k_3 + k_4} \quad (5)$$

For the region below Parmenter's threshold ϕ_1 is about 0.3 [9,10,11]. Combining Eqs. (4) and (5) we find:

$$k_3 S_1 = \frac{(k_2 S_0 + k_5) k_0 S_0 + k_2 S_0 k_1 S_0}{k_2 S_0 + k_5 / \phi_1} \quad (6)$$

Because of the proportionality of rate constants and cross sections this equation can be rewritten as:

$$\sigma_{app}(^1B_{2u}) = \frac{(k_2 S_0 + k_5) \sigma_{exc}(^1B_{2u}) + k_2 S_0 \sigma_{exc}(^3E_{1u})}{k_2 S_0 + k_5 / \phi_1} \quad (7)$$

It follows that a linear pressure dependence is only found if in our pressure region $k_2 S_0 \ll k_5 / \phi_1$. Under this condition we obtain from Eq. (7):

$$\sigma_{app}(^1B_{2u}) = \phi_1 \sigma_{exc}(^1B_{2u}) + \frac{\phi_1 k_2 S_0}{k_5} \sigma_{exc}(^3E_{1u}) \quad (8)$$

The first term on the right hand side of Eq. (8) refers to direct excitation of the ${}^1B_{2u}$ state, the second term to the formation of that state by collisions between molecules in the ground state and molecules in the ${}^3E_{1u}$ state. This term, proportional to the pressure, is only important at low impact energies. Comparing Eqs. (1) and (8) we can write:

$$\sigma_o({}^1B_{2u}) = \phi_1 \sigma_{exc}({}^1B_{2u}) \quad (9)$$

$$\sigma_p({}^1B_{2u}) = \frac{k_2 S_o}{k_5} \phi_1 \sigma_{exc}({}^3E_{1u}) \quad (10)$$

In the derivation of Eqs. (9) and (10) internal conversion from singlet states above Parmenter's threshold has been omitted (see Section 6.4). This process contributes to the pressure independent part of the emission cross section. Within the singlet manifold mainly the ${}^1E_{1u}$ state is excited, even at low electron impact energies [3]. Therefore, the contribution of internal conversion to $\sigma_o({}^1B_{2u})$ can be put equal to a good approximation to $\phi_3 \sigma_{exc}({}^1E_{1u})$, where $\sigma_{exc}({}^1E_{1u})$ is the excitation cross section of the ${}^1E_{1u}$ state and ϕ_3 is the fluorescence quantum yield after excitation into that state. An estimate of the latter quantity has been made in Section 6.4. The excitation cross section of the ${}^1E_{1u}$ state has been measured by Brongersma [2] for impact energies up to 8 eV. From these data we calculate the possible contribution of internal conversion from the ${}^1E_{1u}$ state to the ${}^1B_{2u} - {}^1A_{1g}$ emission cross section at 7.3 eV impact energy to be $(0.7 \pm 0.4) \times 10^{-19} \text{ cm}^2$. This value is much smaller than our emission cross section $\sigma_o({}^1B_{2u})$ of $(4.8 \pm 1.6) \times 10^{-19} \text{ cm}^2$ determined also at 7.3 eV; it indicates the relative unimportance of internal conversion near the threshold energy. Using $\phi_1 = 0.3$ we derive from Eq. (9):

$$\sigma_{exc}({}^1B_{2u}) = 1.6 \times 10^{-18} \text{ cm}^2 \text{ at 7.3 eV.}$$

The uncertainty in this excitation cross section is as high as 60% due to the neglect of internal conversion and the uncertainty in $\sigma_o({}^1B_{2u})$.

In electron impact spectra [2,3,12,13] the approximately degenerate ${}^1B_{2u}$ and ${}^3E_{1u}$ states give rise to a single broad band at 4.7 eV. The excitation cross section of this band is equal to the sum of $\sigma_{exc}({}^1B_{2u})$

and $\sigma_{\text{exc}}(^3E_{1u})$. Knoop [3] measured the relative excitation cross section of this band from threshold to about 9 eV. We can bring his data to an absolute scale by normalization on the absolute value as determined by Brongersma [2] in the electron impact energy range 4.7 - 5.7 eV. It is found:

$$\sigma_{\text{exc}}(^1B_{2u}) + \sigma_{\text{exc}}(^3E_{1u}) = (1.5 \pm 0.5) \times 10^{-16} \text{ cm}^2 \text{ at } 7.3 \text{ eV.}$$

Our much smaller value of $\sigma_{\text{exc}}(^1B_{2u})$ suggests therefore that the 4.7 eV band in the electron impact experiments can be almost exclusively attributed to excitation of the $^3E_{1u}$ state. This supports Knoop's [3] assignment of this band. In addition Knoop found a maximum of the excitation cross section of the $^3E_{1u}$ state at 7.3 eV. At that energy we observed the strongest pressure dependence in the apparent emission cross section of the $^1B_{2u}$ state. The latter observation supports our assumption of the involvement of the $^3E_{1u}$ state in the energy transfer process. The large value of $\sigma_{\text{exc}}(^3E_{1u})$ is consistent with theoretical calculations by Matsuzawa [14], which lead to a value of $0.9 \times 10^{-16} \text{ cm}^2$ at 10 eV electron impact energy.

From $\sigma_{\text{exc}}(^3E_{1u})$ and σ_p (see Section 7.2) we derive from Eq. (10):

$$k_2 S_0 / k_5 = 8.3 \pm 3.3 \text{ at } 1 \text{ Torr.}$$

The rate constant k_2 is related to the effective collision cross section of the energy transfer process and k_5 to the unimolecular decay of the triplet state. We do not make any attempt to interpret the ratio of k_2 and k_5 . Neither rate constant is not known; moreover, k_5 might represent intramolecular processes in the benzene molecule as well as diffusion of excited benzene molecules out of the viewing region of the monochromator.

REFERENCES

- [1] Chapter VI of this thesis.
- [2] H.H. Brongersma, Thesis, University of Leiden (1968).
- [3] F.W.E. Knoop, Thesis, University of Leiden (1972).
- [4] R.N. Compton, R.H. Huebner, P.W. Reinhardt and L.G. Christophorou, J.Chem.Phys. 48 (1968) 901.

- [5] G.W. Robinson, J.Chem.Phys. 47 (1967) 1967.
- [6] J.B. Birks, Photophysics of Aromatic Molecules (Wiley-Interscience, London, 1970).
- [7] K.F. Freed, Topics Current Chem. 31 (1972) 105.
- [8] C.S. Parmenter and M.W. Schuyler, 20^e Réunion de la Société de Chimie Physique, J.Chim.Phys. 66 (1969) 92.
- [9] G.B. Kistiakowsky and C.S. Parmenter, J.Chem.Phys. 42 (1965) 2942.
- [10] C.S. Parmenter and A.H. White, J.Chem.Phys. 50 (1969) 1631.
- [11] K.G. Spears and S.A. Rice, J.Chem.Phys. 55 (1971) 5561.
- [12] J.P. Doering, J.Chem.Phys. 51 (1969) 2866.
- [13] E.N. Lassettre, A. Skerbele, M.A. Dillon and K.J. Ross, J.Chem.Phys. 48 (1968) 5066.
- [14] M. Matsuzawa, J.Chem.Phys. 51 (1969) 4705, *ibid* 52 (1970) 5976.

CHAPTER VIII

D I S S O C I A T I V E E X C I T A T I O N O F B E N Z E N E

8.1. INTRODUCTION

In the wavelength region 1850 - 9000 Å radiation from H and CH fragments is observed as a result of the dissociative excitation of benzene by electron impact. The Balmer series of hydrogen and the $A^2\Delta - X^2\Pi$ transition of CH can be identified. For these transitions emission cross sections and thresholds have been determined. A weak emission from the carbon fragments ($3s\ ^1P^o - 2p^2\ ^1D$, 1931 Å and $3s\ ^1P^o - 2p^2\ ^1S$, 2479 Å) could also be detected.

8.2. BALMER EMISSION OF HYDROGEN

We have determined the emission cross sections for the Balmer α , β , γ and δ lines. It is found that they all have the same energy dependence as a function of the electron impact energy. Therefore, we give in Table 8.1 the Balmer emission cross sections at one electron impact energy and in Table 8.2 the energy dependence for one Balmer line, namely H_β . A discussion of the errors in the absolute emission cross sections is given in Section 2.5. For the Balmer β , γ and δ lines the error in the emission cross sections is estimated to be 10%. An error of 15% arises in the Balmer α emission cross sections.

Cross sections for Balmer emission from benzene have also been measured by Vroom and de Heer [1]. The ratios of the emission cross sections for the different Balmer lines, as given in Table 8.1, are within 10% in agreement with their results. However, the absolute value of the emission cross sections is lower than measured previously [1]. This difference may be caused by the fact that in the latter study a McLeod manometer is used for the measurement of the pressure. This procedure may give too low values

TABLE 8.1.

Emission cross sections for Balmer radiation in units of 10^{-19} cm^2 at 100 eV electron impact energy			
$\sigma_{\text{em}}(\text{H}_{\alpha})$	$\sigma_{\text{em}}(\text{H}_{\beta})$	$\sigma_{\text{em}}(\text{H}_{\gamma})$	$\sigma_{\text{em}}(\text{H}_{\delta})$
16.8	3.35	1.47	0.91

TABLE 8.2.

Emission cross sections for Balmer β radiation from H and for $\text{A}^2\Delta - \text{X}^2\Pi$ radiation from CH fragments in units of 10^{-19} cm^2 .		
$E_{\text{el}}(\text{eV})$	$\text{CH}(\text{A}^2\Delta - \text{X}^2\Pi)$	$\text{H}(n=4 - 2)$
30	4.17	0.23
40	5.40	0.63
50	5.68	1.43
60	6.35	2.19
80	7.01	2.97
100	6.80	3.35
120	6.94	3.32
140	6.87	3.28
170	6.09	3.05
200	5.60	2.68
250	4.62	2.24
300	3.86	1.81
350	3.28	1.51
400	2.91	1.30
450	2.61	1.10
500	2.27	0.973
600	2.01	0.795
700	1.63	0.657
800	1.41	0.564
900	1.21	0.492
1000	1.17	0.442

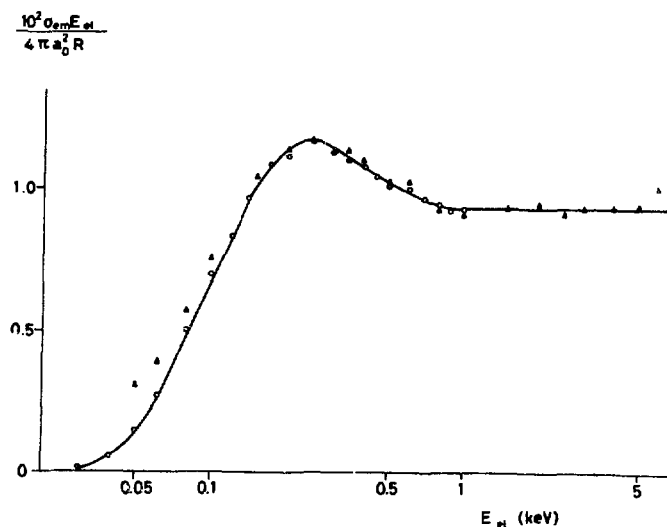


FIGURE 8.1. Emission cross sections for Balmer β radiation presented in the form of a Fano plot: Δ , Vroom and de Heer [1]; O , present work.

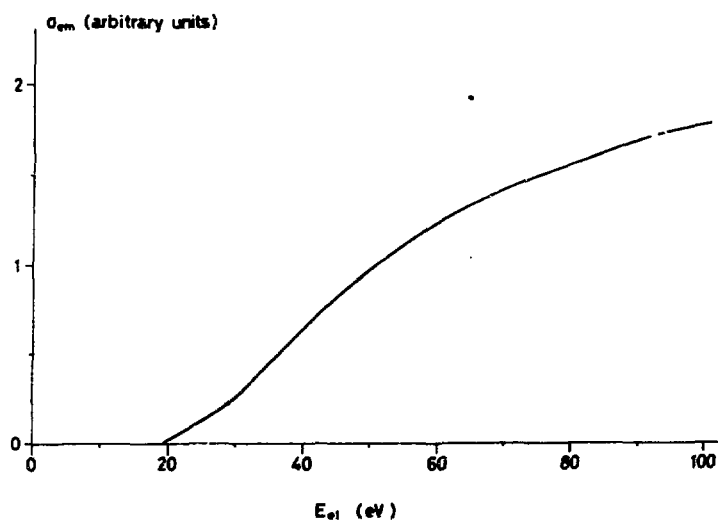
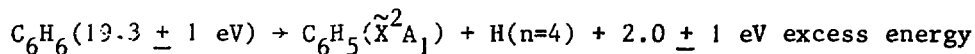


FIGURE 8.2. Energy dependence below 100 eV of the emission cross sections for Balmer β radiation.

for the pressure in the case of condensable vapours and hence too high emission cross sections. The Baratron capacitance manometer, used in the present work, enables a more accurate pressure measurement (see Section 2.5).

At high energies the values of $\sigma_{em} E_{el}$ approach a constant value (Fig. 8.1) as has been found before [1]. This indicates that optically forbidden excitation processes dominate in the formation of excited hydrogen atoms. At energies above 200 eV the emission cross sections have the same energy dependence within 3% as measured by Vroom and de Heer [1]. At lower energies their values of J_{em} become relatively higher than ours, as is also found in the case of Balmer emission from water (see Section 5.5.1).

The threshold behaviour of the H_{β} emission cross sections is shown in Fig. 8.2. From the absence of structure it is concluded that one or only a few optically forbidden states of the benzene molecule are involved in the formation of excited hydrogen atoms. The onset for Balmer β emission is found at 19.3 ± 1 eV. From this, the process which is involved in the formation of Balmer radiation may be derived. Taking for the dissociation energy of the C-H bond a value of 4.6 eV [2] and for the excitation energy of $H(n=4)$ a value of 12.69 eV [3], it follows from the energy balance and the absence of structure in the threshold behaviour that the process



plays an important role in the formation of excited hydrogen atoms.

Another possibility is that the phenyl radical is formed in the \tilde{A}^2B_1 state, which has an excitation energy of 2.35 eV [4]. However, we cannot obtain evidence for this process, because we did not find emission from the phenyl radical.

Contrary to the Balmer emission cross section data of methane, ethylene and acetylene the benzene $\sigma_{em} E_{el}$ values show a maximum at 250 eV which is not present in the case of aliphatic hydrocarbons (Fig. 8.1); the emission cross sections in the asymptotic region are 50% lower than those for the aliphatic hydrocarbons (see Section 3.3). Sufficiently accurate experimental and theoretical data on orbital energies [5] are not available to decide whether these differences can be justified.

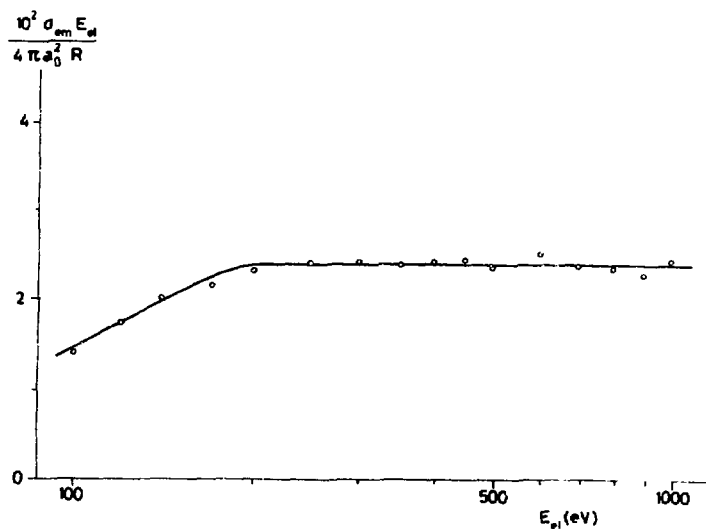


FIGURE 8.3. Emission cross sections for $\text{CH}(A^2\Delta - X^2\Pi)$ radiation presented in the form of a Fano plot.

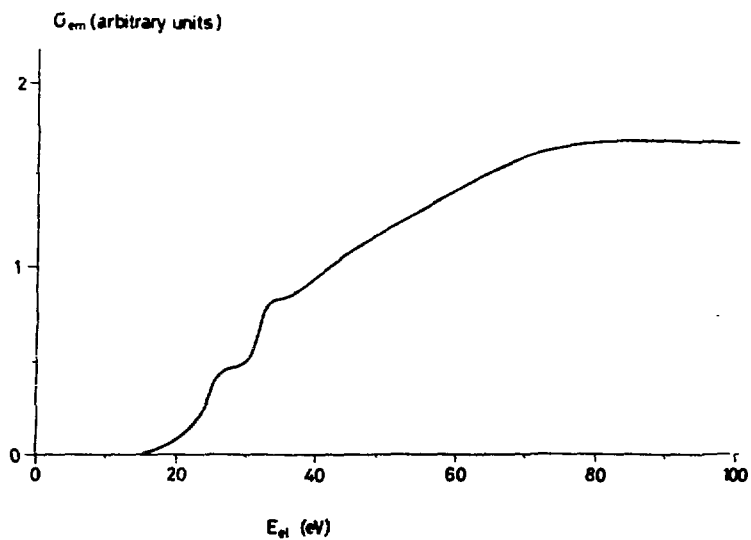


FIGURE 8.4. Energy dependence below 100 eV of the emission cross sections for $\text{CH}(A^2\Delta - X^2\Pi)$ radiation.

8.3. $\text{CH}(\text{A}^2\Delta - \text{X}^2\Pi)$ EMISSION

Since the $\text{A}^2\Delta$ state of CH decays only to the $\text{X}^2\Pi$ ground state and since cascade to the $\text{A}^2\Delta$ state from higher states is not possible (because either radiation from these states to the $\text{A}^2\Delta$ state is optically forbidden or these states are repulsive [6]), the emission cross sections are equal to the total cross sections for production of $\text{CH}(\text{A}^2\Delta)$. The emission cross sections are collected in Table 8.2. Besides errors of 10% due to uncertainties in quantum yield, pressure and electron beam intensity additional errors of 30% arise in the CH cross section data due to a continuous background under the 4314 Å system and the use of the 'adding up' procedure [7]. The results are also presented in a Fano plot (Fig. 8.3). The zero slope of the straight line portion indicates that - contrary to the aliphatic hydrocarbons (Section 3.3) - the formation of $\text{CH}(\text{A}^2\Delta)$ mainly proceeds by optically forbidden processes in the benzene molecule.

The threshold for $\text{CH}(\text{A}^2\Delta)$ is observed at 15.0 ± 1 eV (Fig. 8.4). A second threshold is found at 29 ± 1 eV. It is not possible to derive the processes which may be involved, because the relevant dissociation energies are not known.

REFERENCES

- [1] D.A. Vroom and F.J. de Heer, J.Chem.Phys. 50 (1969) 573.
- [2] D.D. Wagman *et al.*, Selected Values of Chemical Thermodynamic Properties, NBS Techn.Note 270-3 (U.S. Government Printing Office, Washington, 1968).
- [3] C.E. Moore, A Multiplet Table of Astrophysical Interest (Observatory, Princeton, 1945).
- [4] G. Herzberg, Electronic Spectra of Polyatomic Molecules (Van Nostrand, Princeton, 1966).
- [5] D.W. Turner *et al.*, Molecular Photoelectron Spectroscopy (John Wiley-Interscience, London, 1970).
- [6] G. Herzberg, Spectra of Diatomic Molecules (Van Nostrand, Princeton, 1950).
- [7] J.F.M. Aarts, C.I.M. Beenakker and F.J. de Heer, Physica 53 (1971) 32.

SUMMARY

The work described in this thesis deals with the measurement of the intensities in the spectrum (1850 - 9000 Å), produced by bombardment of molecular gases (acetylene, methane, ethylene, ethane, water and benzene) by a beam of mono-energetic electrons (0 - 1000 eV). For a large part the spectrum consists of fluorescence from excited fragments formed by dissociative excitation. The results are expressed in terms of cross sections for emission of photons of a particular wavelength. These emission cross sections are a measure of the chance that a collision between ^{an} electron and a molecule gives rise to the emission of a photon of specified kind.

At high energies of the incident electrons the cross sections can be analysed by means of the Bethe theory. This allows a classification of the excitation processes which precede the emission of the photon into optically-allowed and symmetry-forbidden. Measurements at low electron impact energies give information about the occurrence of spin-forbidden excitation processes; also the threshold energy for formation of excited molecules can be determined.

In Chapter I a brief introduction to the measurements is given. The application of the Bethe theory for dissociative excitation processes is ^{explained} ~~also shown there~~. A description of the apparatus is given in Chapter II.

Chapter III deals with the dissociative excitation of simple aliphatic hydrocarbons: acetylene, methane, ethylene and ethane. It turns out that for these molecules excited hydrogen atoms are formed by symmetry-forbidden excitation processes; the various hydrocarbons have an equal cross section for formation of these atoms. This can be explained by assuming that they arise from highly excited Rydberg states of the hydrocarbon. CH radicals in the $A^2\Delta$ state are formed by optically-allowed excitation processes. In the case of acetylene the cross section for formation of $CH(A^2\Delta)$ is particularly high.

In Chapter IV the intensity distribution in the $CH(A^2\Delta - X^2\Pi)$ spectrum, produced by dissociative excitation of acetylene, is analysed. This spectrum is built-up from three overlapping bands, namely the 0-0, 1-1 and 2-2 bands. The intensity distribution in the rotational structure of the 0-0 band can be determined by an analysis of the free rotational lines of the R branch. However, this procedure is not possible for the other bands because in that case the rotational transitions cannot be resolved. Therefore, the intensity

distribution in the 1-1 and 2-2 bands has been determined by means of a spectrum simulated on the computer. In that way the overlap of the various rotational and vibrational transitions is taken into account. The simulation program is described in the appendix to Chapter IV. It turns out that the distribution of molecules over the rotational levels can be described in a fairly good way by assuming one Boltzmann distribution for each vibrational level. This result is in contrast to work published by others, which did not take into account the overlap of transitions.

In Chapter V the results for the water molecule are given. These are compared with those obtained by other groups. The formation of excited hydrogen atoms is shown to proceed by predissociation of highly excited Rydberg states. The strong emission from the excited hydroxyl radical originates from excitation of both singlet and triplet states of the water molecule.

In Chapters VI and VII measurements on the ${}^1B_{2u} - {}^1A_{1g}$ fluorescence spectrum of benzene are presented. An analysis of the intensity of this spectrum shows a contribution by internal conversion from higher singlet states to the ${}^1B_{2u}$ state. At low electron impact energies the formation of molecules in excited triplet states is an important process. From experiment follows that these molecules can populate the ${}^1B_{2u}$ state by collisions with ground state benzene molecules. Chapter VIII deals with the dissociative excitation of benzene.

SAMENVATTING

Het in dit proefschrift beschreven onderzoek heeft betrekking op intensiteitsmetingen van het spectrum ($1850 - 9000 \text{ \AA}$), dat ontstaat bij bombardement van moleculaire gassen (acetyleen, methaan, ethyleen, ethaan, water en benzeen) door een bundel mono-energetische electronen van variabele energie ($0 - 1000 \text{ eV}$). Het spectrum bestaat voor een belangrijk deel uit fluorescentie van aangeslagen brokstukken, die zijn ontstaan door dissociatieve excitatie. De resultaten worden uitgedrukt in werkzame doorsneden voor emissie van fotonen van een bepaalde golflengte. Deze emissie doorsneden zijn een maat voor de kans dat een botsing tussen een electron en een molecuul aanleiding geeft tot het uitzenden van een bepaald soort foton.

Bij hoge energieën van de invallende electronen worden de werkzame doorsneden geanalyseerd met behulp van de theorie van Bethe. Hiermee kunnen de aanslag-processen, die het uitzenden van het foton voorafgaan, worden ingedeeld in optisch-toegestaan en symmetrie-verboden. Metingen bij lage energieën geven aanwijzingen over de rol van spin-verboden aanslagprocessen en maken een bepaling van de drempelenergie voor vorming van aangeslagen moleculen mogelijk.

Hoofdstuk I geeft een korte inleiding tot de in dit proefschrift beschreven metingen en laat zien hoe de theorie van Bethe kan worden toegepast voor dissociatieve aanslagprocessen. Een beschrijving van het apparaat wordt gegeven in Hoofdstuk II.

Hoofdstuk III gaat over de dissociatieve aanslag van eenvoudige alifatische koolwaterstoffen: acetyleen, methaan, ethyleen en ethaan. Het blijkt dat bij deze moleculen aangeslagen waterstofatomen worden gevormd door symmetrie-verboden aanslagprocessen; in de verschillende koolwaterstoffen is de werkzame doorsnede voor de vorming van deze atomen gelijk. Dit kan worden verklaard door aan te nemen dat ze ontstaan vanuit hoog-aangeslagen Rydberg toestanden van het koolwaterstof. CH radicalen in de $A^2\Delta$ toestand blijken gevormd te worden door optisch toegestane aanslagprocessen. Acetyleen heeft een bijzonder grote werkzame doorsnede voor $\text{CH}(A^2\Delta)$ vorming.

In Hoofdstuk IV wordt de intensiteitsverdeling in het $\text{CH}(A^2\Delta - X^2\Pi)$ spectrum geanalyseerd, dat gevormd wordt door dissociatieve aanslag van acetyleen. Dit spectrum is opgebouwd uit drie elkaar overlappende banden: de 0-0, 1-1 en 2-2 band. De intensiteitsverdeling in de rotatiestructuur van de 0-0 band kan worden bepaald door de vrije rotatielijnen in de R-tak te

analyseren. Dit is echter niet mogelijk voor de andere banden, daar hiervan vrijwel alle rotatie-overgangen niet spectraal opgelost kunnen worden. De intensiteitsverdeling in 1-1 en 2-2 banden is daarom bepaald aan de hand van een spectrum gesimuleerd op de computer, waarbij de overlap van de verschillende rotatie- en vibratie-overgangen in rekening wordt gebracht. Het simulatieprogramma is beschreven in het aanhangsel bij Hoofdstuk IV. Het blijkt nu dat de verdeling over de rotatieniveaus vrij goed beschreven kan worden door één Boltzmann verdeling over elk vibratieniveau aan te nemen. Dit is in tegenstelling tot door anderen gepubliceerd werk, waar geen rekening is gehouden met de overlap van banden.

Hoofdstuk V vermeldt de resultaten van metingen aan water. Deze worden vergeleken met die van andere groepen. De vorming van aangeslagen waterstof-atomen gaat door predissociatie van hoog-energetische Rydbergtoestanden. De sterke emissie van het aangeslagen hydroxylradicaal blijkt zijn oorsprong te vinden in de aanslag van zowel singulet als triplet toestanden van het watermolecuul.

In de Hoofdstukken VI en VII worden metingen gepresenteerd, die verricht zijn aan het ${}^1B_{2u} - {}^1A_{1g}$ fluorescentiespectrum van benzeen. Een analyse van de intensiteit van dit spectrum wijst op een bijdrage van "internal conversion" van hogere singulet toestanden naar de ${}^1B_{2u}$ toestand. Bij lage elektronen-energieën blijken in belangrijke mate moleculen in aangeslagen triplet toestanden te worden gevormd. Uit het experiment blijkt dat deze door botsingen met benzeen moleculen in de grondtoestand de ${}^1B_{2u}$ toestand kunnen bevolken. In Hoofdstuk VIII wordt de dissociatieve aanslag van benzeen besproken.

CURRICULUM VITAE

Na het behalen van het diploma gymnasium β aan het St. Bonaventura Lyceum te Leiden begon ik in september 1966 met de studie aan de Rijksuniversiteit te Leiden. Het kandidaatsexamen in de schei- en natuurkunde met bijvak wiskunde (letter S3) legde ik in mei 1969 af. Mijn studie werd voortgezet op de Afdeling Theoretische Organische Chemie van Professor Dr. L.J. Oosterhoff. Hier werkte ik onder de leiding van Dr. J.F.M. Aarts aan een onderzoek van de lichtemissie van moleculen na aanslag door botsingen met electronen. Dit onderzoek werd verricht op het F.O.M.-Instituut voor Atoom- en Molecuulfysica te Amsterdam in de groep botsingsfysica, die geleid wordt door Dr. F.J. de Heer. Het doctoraalexamen in de theoretische organische chemie met bijvakken theoretische natuurkunde en wiskunde legde ik in februari 1971 af. Hierna begon ik onder de leiding van Dr. F.J. de Heer met het onderzoek, dat resulteerde in dit proefschrift. Alle experimenten, die daarin beschreven zijn, werden op het F.O.M.-Instituut verricht.

Van november 1970 tot april 1971 was ik als kandidaat-assistent verbonden aan de Afdeling Theoretische Organische Chemie. Hierna was ik als wetenschappelijk medewerker in dienst van Z.W.O. (S.O.N.). Sedert mei 1974 ben ik verbonden aan het Natuurkundig Laboratorium van de N.V. Philips' Gloeilampenfabrieken te Eindhoven.

De totstandkoming van dit proefschrift is het resultaat van een samenwerking tussen de Afdeling Theoretische Organische Chemie van de Rijksuniversiteit te Leiden en het F.O.M.-Instituut voor Atoom- en Molecuulfysica te Amsterdam.

De directeur van het F.O.M.-Instituut, Prof.Dr. J. Kistemaker, ben ik bijzonder erkentelijk voor de gastvrijheid, die hij mij vele jaren heeft verleend. Alle medewerkers van dit Instituut wil ik danken voor hun bijdrage tot een optimaal werkklimaat. Mijn bijzondere dank gaat uit naar mijn groepsleider, Dr. F.J. de Heer. Sterk meelevend met dit onderzoek heeft hij door vele stimulerende en verhelderende discussies een belangrijke bijdrage geleverd bij het tot stand komen van de bereikte resultaten. De heer Drs. R.Ch. Baas heeft een groot gedeelte van de computerprogramma's geschreven. Zonder zijn effectieve hulp was een belangwekkende uitbreiding van dit onderzoek niet mogelijk geweest. Voorts dank ik de heren H.J. Luyken, R.J. Kersting en J.J. van Zeeland voor hun technische steun. De vakkkundige

hulp van de medewerkers van de rekenkundige dienst, de electronische afdeling, het vacuümtechnisch laboratorium en de instrumentmakerij heb ik zeer gewaardeerd.

In de persoon van Prof.Dr. L.J. Oosterhoff dank ik alle medewerkers van de Afdeling Theoretische Organische Chemie. Dr. J.J.C. Mulder ben ik zeer erkentelijk voor het kritisch doorlezen van het manuscript. Bijzonder veel dank ben ik ook verschuldigd aan Dr. J.F.M. Aarts. Hij was steeds een onmisbare discussiepartner, ook bij het doorlezen van het manuscript. De heer J.W. Bakker heeft op bekwame wijze het onderzoek voortdurend technisch bijgestaan. De heren Drs. G.R. Möhlmann, H.B. Krop en Drs. P.J.F. Verbeek dank ik voor hun aandeel in de metingen. De stimulerende discussies met Mevr.Drs. J.A. v.d. Hart-v.d. Hoek, Dr. R.A. van Santen en Dr. F.W.E. Knoop heb ik zeer op prijs gesteld.

Voorts dank ik Mevr. C.J. Kōke-van der Veer voor het typen van het manuscript, Mevr. M.M. Turksma-Cabanas voor het tekenen van de figuren, de heren F.L. Monterie en Th. van Dijk voor het fotografisch werk en de heer H.A. Okhuizen voor het drukken van dit proefschrift. Prof.Dr. R. Kelly corrigeerde het Engels taalgebruik.

De Directie van de N.V. Philips' Gloeilampenfabrieken ben ik zeer erkentelijk voor de medewerking bij het voltooiën van dit proefschrift.

